HHS Public Access

Author manuscript

Compr Physiol. Author manuscript; available in PMC 2017 September 15.

Published in final edited form as:

Compr Physiol. ; 6(4): 1743–1780. doi:10.1002/cphy.c150048.

Heart Valve Biomechanics and Underlying Mechanobiology

Salma Ayoub[1], **Giovanni Ferrari**[2], **Robert C. Gorman**[2], **Joseph H. Gorman III**[2], **Frederick J. Schoen**[3], and **Michael S. Sacks**[*,1]

[1]Center for Cardiovascular Simulation, Institute for Computational Engineering and Sciences, Department of Biomedical Engineering, The University of Texas at Austin, Austin, USA

[2]Gorman Cardiovascular Research Group, University of Pennsylvania, Philadelphia, USA

[3]Department of Pathology, Brigham and Women's Hospital, Boston, Massachusetts, USA

Abstract

Heart valves control unidirectional blood flow within the heart during the cardiac cycle. They have a remarkable ability to withstand the demanding mechanical environment of the heart, achieving lifetime durability by processes involving the ongoing remodeling of the extracellular matrix. The focus of this review is on *heart valve functional physiology*, with insights into the link between disease-induced alterations in valve geometry, tissue stress, and the subsequent cell mechanobiological responses and tissue remodeling. We begin with an overview of the fundamentals of heart valve physiology and the characteristics and functions of valve interstitial cells (VICs). We then provide an overview of current experimental and computational approaches that connect VIC mechanobiological response to organ- and tissue-level deformations and improve our understanding of the underlying functional physiology of heart valves. We conclude with a summary of future trends and offer an outlook for the future of heart valve mechanobiology, specifically, multiscale modeling approaches, and the potential directions and possible challenges of research development.

Introduction

Heart valves are complex multilayered structures that serve to prevent retrograde flow in the right and left ventricles by their opening and closing motion caused by differential blood pressure on each side. The heart has four valves, two atrioventricular: the mitral valve (MV) and tricuspid valve (TV), and two semilunar: the aortic valve (AV) and pulmonary valve (PV). Although they function as simple check valves that control the unidirectional flow of blood during the cardiac cycle, they are in fact complex structures that are uniquely adapted to withstand demanding mechanical and hemodynamic environments unlike any other found in the body. Their unique structure and shape enables them to maximize flow rate while minimizing flow resistance. With every heartbeat, valve leaflets experience three distinct tissue stress states: tension (closed valve to prevent retrograde flow), flexure (opening and closing motion), and shear stress (due to blood flow) (165). The duty cycle of heart valves highlights their remarkable ability to withstand mechanical demands. The MV, for example,

*Correspondence to msacks35@gmail.com.

opens in ~50 ms and remains open for ~600 ms during diastole, closes in ~50 ms and remains closed for ~300 ms during systolic ejection (215). Each heart valve opens and closes more than 40 million times per year, demonstrating the valves' ability to function in a demanding environment by consistently remodeling and repairing its functionally adapted extracellular matrix (ECM), which consists of collagen, elastic fibers, proteoglycans, and glycosaminoglycans.

ECM and collagen in particular play a vital role in the function and durability of heart valves. As in all soft tissues, the valvular ECM is a dynamic environment with fibrous proteins being continuously degraded and replaced. The ECM provides structural and functional characteristics to valve tissue that include cell support, mechanical integrity, and biological signaling (98). Altered mechanical forces due to age (5,239,240), disease, or pathology (200,202,203) are associated with phenotypic changes of valve interstitial cells (VICs). To fully understand valve behavior and tissue remodeling during pathophysiological alterations in mechanical loading, it is necessary to gain insight into VIC mechanobiology and link it to tissue- and organ-level mechanical stimuli (Figs. 1 and 2). Despite its clinical importance and relevance, the interrelation between organ level stresses and cellular responses remains relatively unexplored, with most computational models focusing on tissue level stresses only. Investigating HV biomechanics with a multiscale approach will answer important questions on the biological impact that mechanical stimuli have at the organ, tissue, and cellular scales. Thus, the focus of this review is on *heart valve biomechanics and the underlying mechanobiology*, specifically the link between disease-induced and surgically induced alterations in valve geometry and the VIC mechanobiological response that leads to tissue remodeling and in the long term, valve tissue homeostatic state.

Abbreviations used throughout this article can be found in Table 1.

Heart Valve Functional Physiology

Heart valve structure and function

The average adult heart beats at approximately 60 beats per minute. To maintain unidirectional blood flow in this dynamic environment, heart valves must open and close more than 100,000 times a day (253). The structure-function relationship between the valve cells and the surrounding ECM enables heart valves to function and maintain a homeostatic state in different hemodynamic and biomechanical environments. All heart valves have similar functional demands; yet, their structures are very different and distinct. The atrioventricular valves (AVVs) separate the atria from the ventricles and prevent retrograde flow from the ventricles into the atria. The MV is located on the right side of the heart and has two leaflets, whereas the TV is on the right side and has two leaflets. AVV also have external supporting chordae tendineae that attach the underside of the valve leaflets to the papillary muscles within the ventricle (8). The semilunar valves (SLVs) separate the ventricles from the great arteries and prohibit reverse blood flow into the ventricles. The SLV consist of the aortic and PVs, which are on the left and right sides of the heart, respectively. Each SLV has three leaflets, also known as cusps. Unlike the AVV, SLV lack external support, though the AV has a unique supporting structure within the aortic root, known as the fibrous annulus, which holds it in place (150).

The coordinated movement of the different structures of heart valves enables them to maintain unidirectional blood flow during the cardiac cycle and function as control valves in the heart. HVs must open and close at least 3×10^9 times in a lifetime, highlighting their complex and multimodal biomechanical function. The high atrial pressure that exists in diastole causes the papillary muscles to relax and results in the opening of the AVV, which then allow blood to flow from the atrium to the ventricle. The sudden increase in ventricular pressure leads to AV valve closure, which is caused by chordal tension, and maintains AVV leaflets closed and coapted to prevent the backflow of blood into the atria. Ventricular contraction leads to the opening of the SLVs. The pressure changes that occur from systole to diastole throughout the cardiac cycle expose heart valves to a variety of forces and a constant change in hemodynamics. Heart valves must have the necessary biomechanical properties to withstand and function efficiently in the complex mechanical environment described earlier. Heart valve leaflets develop and maintain an intricate and highly organized connective tissue system that allows them to do so (253).

Heart valves are multilayered structures of specialized ECM with interspersed differentiated VICs, all surrounded by an outer layer of valve endothelial cells. The AV, for example, consists of three histologically distinct layers, whereas the MV has four (Figs. 2 and 3). The fibrosa layer, which is located on the ventricular side of AVV and the atrial side of SLV, is composed of circumferentially aligned collagen fibers that provide the leaflets with the necessary tensile strength to open and transmit forces during coaptation while closed. The spongiosa layer is situated adjacent to the fibrosa and though it contains some collagen, its main constituents are the hydrophilic glycosaminoglycans and proteoglycans, which give the valve its compressive properties and allow it to absorb high forces during coaptation. The ventricularis and atrialis are the layers that are adjacent to blood flow in AVV and SLV, respectively. These layers are rich in radially oriented elastin fibers and facilitate the closure movement by extending the valve leaflet as it opens and recoils when it closes. The annulus and chordae tendineae of the AVV and the connection between the leaflets and the surrounding myocardium in the SLV provide additional support.

Valve cells, which consist of endothelial and interstitial cells, play a major role in maintaining homeostatic state that is necessary for heart valve function. Collectively, VICs and the ECM provide heart valve leaflets with the necessary biomechanical properties to open and close during the cardiac cycle. This important structure-function relationship facilitates normal heart valve functional physiology. Both VICs and leaflet ECM interact with a peripheral layer of valve endothelial cells. These cells maintain valve homeostasis in the embryo and throughout adult life by responding and adjusting to the different hemodynamic environments (253).

Developmental origin of heart valves

Endocardial cushion formation—During embryonic development, the heart is the first organ to function. The first step in heart valve development is endocardial cushion formation, a process during which the myocardial and endocardial cell layers of the primitive vertebrate heart tube are separated by specialized ECM, known as cardiac jelly (187, 188). Endocardial cushion formation begins after the end of rightward looping and is

mediated by cellular activities, such as adhesion, signaling, migration, secretion, replication, differentiation, and apoptosis (188). The first indication of valve development is the formation of endocardial cushions in the outflow tract (OFT) and atrioventricular canal regions of the primitive heart tube (111). Myocardial cells localized within the atrioventricular canal and OFT regions increase ECM biosynthesis, particularly proteoglycan and glycosaminoglycan deposition, ultimately giving rise to cardiac jelly "swellings" (253). Once formed, the endocardial cushions become populated by not only myocardial cells but also valve precursor cells through an epithelial-mesenchymal transition (EMT), which invade the underlying cardiac jelly and proliferate to populate endocardial cushions. These cells undergo directed growth and remodeling to enable the cushion structures to serve as physical barriers that drive unidirectional blood flow in the primitive heart tube and later, to form the valvular structures and membranous septa of the mature heart (188). A total of four endocardial cushions form in the atrioventricular canal: the superior, inferior, left, and right lateral cushions; whereas only two form in the OFT: the proximal and distal cushions (156). The septation of the OFT and fusion of the AV canal cushions leads to the formation of valve primordial which correspond to the distinct leaflets of the four valves. The thinning and elongation of the valve primordial and the remodeling of the ECM into layers rich in elastin, fibrillar collagen, and proteoglycans characterize valve leaflet formation (111).

Valvular precursor cells—Heart valve cells in the developing embryo originate from multiple sources. The major cell provider is, however, the endothelial cell lineage, which plays an essential role throughout heart valve development. The endothelial cells that surround valve leaflets form a continuous epithelial cell layer with the endocardium (9). The endocardial and myocardial precursors of the OFT arise from the secondary heart field (276). Lineage tracing analysis with *Tie2cre;ROSA26R* mice has shown that the majority of mesenchymal cells that form the AV and OFT endocardial cushions and later give rise to the mature valve structures are derived from endothelial cells (62,144,233). Extensive cell mapping has revealed that VICs in mature AVV are not only derived from Ti2-Cre expressing endothelial cells (62, 144) but also other alternative sources. Chick-quail chimera studies in avian embryos highlighted the existence and important contributions of epicardium-derived cells in developing AVV (87, 233). In mice however, there is little contribution of epicardially derived cells in AVV as indicated by *Wilms Tumor 1 (WT1)-Cre* lineage analysis (301). Wnt1-Cre lineage tracing studies have shown that there is a significant number of neural crest-derived cells in the developing OFT endocardial cushions (62,117,233). Cells of neural crest origin also exist in mature SLV and are concentrated in individual cusps of the PV and AV (172). Although lineage-tracing studies indicate that the majority of VICs arise from endothelially derived progenitors, there is increasing evidence that specific subpopulations arise from distinct embryonic sources. It is not known, however, if these diverse embryonic origins give rise to different VIC subpopulations with specific contributions to valvular structure and function (111).

Valvulogenesis regulation—Signaling pathways play a critical role in endocardial cushion induction and EMT. The initial induction of EMT in the OFT and the AV canal requires BMP2 signaling from the myocardium to the endocardium (152). Both canonical

Wnt and transforming growth factor (TGF)-beta signaling are required for EMT and the proliferation of mesenchymal endocardial cushion cells (116,142,188). In the endocardium, Notch signaling regulates the repression of endothelial cell gene expression and is required for EMT (273). Endocardial cushion mesenchymal cells express Twist1 and Msx transcription factors, which are characteristic of mesenchymal progenitor cells (48,296). These cells are highly proliferative and express many of the genes of mesenchymal cell types that are involved in both development and regeneration as well as tumor metastasis. Twist1 and Tbx20 are transcription factors that promote cell proliferation, migration, and primitive ECM gene expression in the endocardial cushions—they are all downregulated during valve remodeling (36,228).

Several key events occur at the end of endocardial cushion formation. Endothelial cells stop undergoing EMT and form an uninterrupted endothelium lining that is strengthened by cell-cell contact (188). The individual endocardial cushions in the atrioventricular canal region fuse and elongate into MV and TV primordial, whereas those of the OFT region form the primitive aortic and pulmonary structures (144). The cells in these developing valvular structures continue to proliferate and undergo remodeling. This said, much less is known about the regulation of remodeling, especially with respect to VECs, since most of the recent studies have been focused on VIC remodeling (253). VICs begin to downregulate and lose mesenchyme genes, including Twist1, Tbx20, Msx1, and Msx2, and start expressing differentiated lineage markers that are characteristic of chondrocyte and tendon cells (36, 115, 143, 146, 169). The transition from endocar-dial cushion formation to heart valve remodeling requires the transcription factor NFATc, which promotes the expression of the ECM remodeling enzyme cathepsin K (49, 61, 206). Several key studies have highlighted the striking similarities that exist between connective tissue, such as cartilage, tendon, and bone, and the developing valve (146). These include but are not limited to signaling molecules, transcription factors, and structural proteins. Some examples include BMP2 signaling, which activates both the Sox9 transcription factor and aggrecan gene expression in cartilage and valve progenitors, and FGF4, which activates Scleraxis and tenascin in developing tendons and remodeling valves (143, 300). Studies on mature avian hearts have revealed compartmentalization of gene localization, in which cartilaginous genes such as Sox9 are localized in the maturing valve leaflets, whereas the tendon-associated genes (i.e., Scleraxis) are in the supporting structures (143). This distinction however, was not made in the smaller mouse valve. In this case, both Sox9 and Scleraxis were highly expressed throughout the valve leaflets as well as the supporting structures (138,145).

The ECM of the valves also undergoes extensive changes during valve remodeling, which include the degradation of the primitive cardiac jelly by matrix metalloproteinases (MMPs) and the deposition of collagen and proteoglycans to form the spongiosa and fibrosa layers (64,200). Wnt signaling is active in the developing valves and early bone formation and is critical for the expression of genes that are characteristic of the collagen-rich fibrosa layer (7). The initiation of valve leaflet stratification is affected by the hemodynamics and the biomechanical forces acting on the valve, the elastin fibers and thus, the atrialis/ventricularis layers, will not be deposited until late postnatal stages when the valves becomes stratified (111). An important feature of late embryonic valve development is the reduced cell proliferation. After birth, little if any cell proliferation occurs (5,111). Cellular processes and

transcriptional pathways and networks play a key role in the regulation of heart valve maturation. However, the influence of mechanical flow is just as important in mediating valve cellular function throughout development and maturation.

Heart Valve Disease and Clinical Relevance

Overview of heart valve disease

More than five million people are diagnosed with heart valve disease in the United States (US) each year (89, 175), with approximately 95,000 annual valve replacement surgeries, and 20,000 deaths per year (148). Although valve disease can occur in any of the four valves, diseases of the AV and MV are the most common. Diseased heart valves are characterized by disruption in ECM layer stratification, VIC disarray, and VEC denunadion (111). These structural disruptions have an effect on the function of heart valves and cause them to become stenotic, restricting the one-way flow of blood, and/or regurgitant, allowing blood to flow backward. Various conditions can cause regurgitation and stenosis including but not limited to degenerative valve disease, calcification, and myocardial infarction (MI).

Heart valve defects are clinically diagnosed at birth or become apparent later in life. About 2% of live births have a congenital heart disease, these include bicuspid AVs, isolated anomalous lobar pulmonary veins, or a silent patent ductus arteriosis (113). Bicuspid AV disease, which is characterized by the presence of two instead of the normal three leaflets, is the most common congenital heart defect among the adult population with a reported incidence of 1% to 2% (113,253). These valves are highly susceptible to calcification due to the osteoblast-like VIC phenotype and matrix mineralization (205). The pathological disruption of the AV's normal structure leads to calcification causing the tissue to become thicker and stiffer, ultimately leading to a decreased orifice area and thus, stenosis. The resulting abnormal biomechanics cause lifelong valvular dysfunction, which will ultimately require surgical valve replacement. Other congenital heart valve defects, such as MV prolapse, are not apparent at birth and remain latent until late adulthood. The increased deposition of collagen and proteoglycans and the resulting biomechanical weakening of the valvular leaflet tissue characterize MVP, which affects more than 2% of the American population and leads to regurgitation, ultimately causing prolapse into the left atrium.

Mitral regurgitation, defined as the abnormal reversal of blood flow from the left ventricle to the left atrium, can be caused by the dysfunction or modifications in any part of the MV apparatus (i.e., annulus, chordae, leaflets, papillary muscles, left atrial wall, or ventricular myocardium). In the United States, nearly 40,000 patients undergo MV repair or replacement each year due to MR (89,199). In the past, replacement of the valve with a bioprosthetic or mechanical valve was the procedure of choice. However, both types of replacements have disadvantages that include a limited lifespan for bioprosthetic valves and complications caused by anticoagulant therapies associated with mechanical valves (199). As a result, cardiac surgeons have gradually shifted their focus to MV repair, mainly ring annuloplasty, which restores normal annular size, shape, and function by facilitating more natural leaflet motion and coaptation (33, 34). Despite the benefits of MV repair, recent studies have indicated that the long-term durability of this procedure is less than previously thought (2,71,73,84). Patients undergoing MV repair for myxomatous disease had a 10% to

16% recurrence rate of MR that required reoperation within 10 years of surgery (73,85). Patients with ischemic MR, caused by systolic traction on the mitral leaflets secondary to ventricular distortion (38), had a 30% recurrence rate at 6 months postsurgery, which increased to 60% after 3 to 5 years (161). More recently, Goldstein et al. have reported findings from a 2-year randomized trial that compares MV repair with MV replacement in more than 251 patients with severe ischemic MR (90). Echocardiographic and clinical outcomes data showed no significant differences in the left ventricular end-systolic volume index, survival, or adverse events at 1 year postsurgery. This said the rate of recurrence of moderate or severe MR was significantly higher in the repair group than in the replacement group (58.8% vs. 3.8%), leading to more heart-failure-related adverse events (24% vs. 15.2%) and clinical admissions. Repair failure, caused by excessive tissue stress that result in the disruption of the suture lines in both leaflets and the annulus (83), suggest that this method can be improved upon. Moreover, these findings suggest that baseline clinical or echocardiographic data can be used as predictors for MR recurrence and for selecting the patients that will benefit from MV repair instead of replacement. Recent work by Bouma et al. showed that preoperative three-dimensional echocardiography combined with a novel valve-modeling algorithm could be used to predict ischemic MR recurrence 6 months after repair (25). The results highlight that although preoperative annular geometry was the same in all IMR patients, the degree of leaflet tethering was higher in patients that had a recurrent IMR 6 months postsurgery (tethering index of 3.91 vs. 2.90 in patients without MR recurrence). More importantly, the use of multivariate logistic regression analysis highlighted the preoperative P3 tethering angle as a strong independent predictor of IMR recurrence after undersized ring annuloplasty, whereby 29.9° is the optimal cutoff for prediction. The combination of imaging and computational techniques, such as the ones demonstrated in the work by Bouma et al., can provide surgeons with unique tools that will allow them to perform detailed patient-specific preoperative analyses—such analyses can complement intraoperative valve analytic techniques and inform surgical repair outcome.

Calcified aortic valve disease (CAVD) is a slow, progressive, multifactorial disorder that is more common with age, without being an inevitable consequence of aging (16, 76, 77, 129, 274). Initial phases of the disease include mild thickening of the valve, whereas more advanced stages are associated with impaired leaflet motion, valve tissue adaptation, and resistance to blood flow (82, 96, 189, 193). These conditions are known as aortic valve sclerosis (AVSc) and calcific aortic valve stenosis (CAVS), respectively. Many cardiovascular conditions, such as MI, chronic heart failure, and severe CAVS exhibit AVSc as one of the major hallmarks of the condition in the presence of other major cardiovascular risk factors (16, 77, 129, 183, 210). AVSc affects a large portion of the population: 25% to 30% of patients over the age of 65 and up to 40% over the age of 75 are diagnosed with AVSc. Although it causes significant thickening of the AV leaflets, there is little to no change in the mechanical properties of the valve in AVSc, making the disease relatively asymptomatic. Recent statistics have shown that within 10 years of their initial diagnosis, 10% of AVSc patients reach a state of severe CAVs that requires immediate AV replacement once symptoms emerge (82). Despite its clinical prevalence, a limited number of studies have investigated the active cellular process underlying the progression of this disease. In addition, specimens from, subclinical AV diseases are generally not available to investigators

since these valves are not surgically replaced until moderate to severe stenosis occurs. We now understand that AS is just the end-stage of a disease that progresses from the microscopic early changes of AVSc to, in a subset of patients, asymptomatic and then symptomatic AS (4, 129, 183). Once AVSc is detected (Fig. 4), there is an increased risk of cardiovascular events, as shown by deviation of the survival curve (purple line in Fig. 4) from the expected event-free survival (light blue line in Fig. 4). In early AS, when mild symptoms begin to present, survival rates deviates much more than expected and decline dramatically with the onset of severe symptomatic AS. Over the last decade, several clinical trials, mostly extensions of atherosclerosis-related studies, have been performed to halt the progression of CAVD with randomized studies showing substantial equivalence between treatments and placebo (19, 51, 170, 186, 212). Cardiovascular risk factors initiate atherosclerosis-like mechanisms that promote valvular lesions and lead to CAVD. Oxidative stress leads to transcriptional upregulation of specific pathways (i.e., Wnt/β-catenin, Runx2/Cbfa1, and Msx2) that promote osteochondrogenic matrix remodeling and activate myofibroblast transdifferentiation into osteogenic phenotype (185). This said, calcium deposition can occur through several noncellular mechanisms, including but not limited to epitaxial calcification and osteopontin (185). These recent pathological findings have provided important mechanistic insight into the human disease progression and have strengthened the paradigm that CAVD is not necessarily due to a degenerative process in which calcium accumulates and protrudes along the aortic surface, but rather a variety of mechanisms, one of which being relatively similar to the atherosclerosis mechanism (185, 204). To affect the progression of the disease, we need to understand both subclinical and symptomatic stages so we can measure targeted therapy before AS proceeds to advanced stages. In all of these disease states, it is important to link organ-level and tissue-level stresses to cell response and ultimately, to VIC mechanotransduction, to fully understand the function and homeostatic response of heart valves to altered local tissue stress.

A Multiscale Approach to Understanding Heart Valve Biomechanical Functional Physiology

Organ-level hemodynamics

The surrounding hemodynamic environment controls the mechanisms that ensure proper HV function. Understanding the interactions between HVs and their local hemodynamic environment is critical to understand normal valve function and shed light on disease progression. Despite their profoundly different anatomical and functional characteristics, all four HVs function to facilitate the unidirectional flow of blood while maximizing flow rate and minimizing flow resistance. Although the effects of valve size and effective orifice area have a profound impact on the specific flow behaviors, for the purposes of this review, we choose to focus on general behaviors common to valve function and use the AV as an example to represent the hemodynamics of all four HVs.

Semilunar valve hemodynamics—In healthy individuals, the AV opens during ventricular contraction, also known as systole, and closes during ventricular relaxation, diastole, with blood flowing through the AV at a peak velocity of 1.35 ± 0.35 m s^{-1} (181). Valve closure occurs at the end of the deceleration phase of systole with minimal backflow

through the valve. This motion creates adverse axial pressure differences along in the developing boundary layer along the aortic wall, causing the inertial flow in this region to decelerate and then, reverse direction, creating vortices in the sinuses behind the AV leaflets. (209). The creation of these vortices facilitates the closing and coaptation of the AV leaflets. When coupled with the vortices that push the leaflet surfaces toward the closed position, this force leads to a very fast and efficient closure of the valve. *In vitro* studies have shown that the axial pressure difference alone is sufficient to close the valve during diastole (209). Although the AV remains functional in the absences of sinus vortices, its motion is not as efficient. This said, it is important to note that the AV must be considered a functional part of the left ventricular outflow track. Although the existence of aortic sinuses leads to important hemodynamic patterns that promote AV motion, particularly closure, they may have other functions as well. For example, the AV annulus expands and contracts during the cardiac cycle, altering AV leaflet function and possibly facilitating valve opening during systole. Characterizing the structural composition of the leaflet/sinus interface is key in understanding the importance of the geometry and structure of the AV. Histological data revealed a gradual transition from highly collagenous AV leaflets to the elastin-rich sinus wall (1), suggesting that the AV's highly specific microstructure and geometry play an important role by reducing the effects of flexural stresses at the leaflet/sinus interface. Although they are different in structure and can have multiple functions, we must keep in mind that the many valvular components interact in a complex yet ultimately, functional manner to ensure proper and efficient heart valve function. The velocity profile at the level of the AV annulus is relatively flat with a slight skew that is less than 10% of the centerline velocity toward the septal wall. The skew in velocity is caused by the orientation of the AV relative to the long axis of the left ventricle (121). Three-dimensional magnetic resonance phase velocity mappings have been used to analyze flow patterns just downstream of the AV, which are of particular interest due to their complexity and relevance to arterial disease. Highly skewed velocity profiles and helical flow patterns were observed (121).

The PV has a similar flow profile to the AV with lower velocity magnitudes. Two-dimensional and three-dimensional Doppler echocardiography was used to measure typical peak velocities at the valve outlets. In the healthy adult, the average peak velocity was found to be 0.75 ± 0.15 m s^{-1} (178). During acceleration, the peak velocity is observed inferiorly with this peak flow rotating counterclockwise throughout the remainder of the ejection phase (231). Although there is a region of reverse flow that occurs in late systole and that may represent flow separation, the mean spatial profile is relatively flat, with a slight skew to the profile. The peak velocity is generally within 20% of the spatial mean throughout the cardiac cycle. The pulmonary artery and its bifurcation can experience secondary flow patterns (i.e., minor flow patterns that are superimposed on the primary flow and that are significantly different in speed and direction from the flow that is predicted using analytical techniques). Several experiments that utilize *in vitro* laser Doppler anemometry have shown that the observed flow patterns are valve-specific and geometry dependent. These flow patterns are a good tool for the evaluation of the function and state of HVs (248–250).

Atrioventricular valve hemodynamics—We first examine the MV as the more studied AVV. Its functional demands: during isovolumic relaxation, the pressure difference between

the left atrium and the left ventricle causes the MV leaflets to open and allow blood to flow from the left atrium into the left ventricle during diastole. The active relaxation of the ventricle helps to maintain a positive transmitral pressure and enhances the initial filling of the ventricle. The flow reaches its peak during the early filling phase with normal peak velocities ranging from 50 to 80 cm s^{-1} (290). Soon after active ventricular relaxation, the fluid begins its deceleration and the MV partially closes. Late diastole is marked by atrial contraction during which the blood accelerates through the valve again to a secondary, lower velocity peak. In the PV, the major/minor velocity peak ratios range from 1.5 to 1.7 (290).

TV hemodynamics is similar to those of the MV, this said, TV flow profile velocities are significantly lower because of the larger tricuspid orifice area. Doppler echocardiography has been used to measure the peak early and late flow velocities across the TVT. These were found to be 051 and 0.35 m s^{-1}, respectively (198), which is very similar to the ratios in the MV. Due to the lower peak pressure in the right ventricle, the right ventricular pressure falls below the right atrial pressure faster than the corresponding time for the left side of the heart, leading to significantly different opening timing for the TV than the MV. Since the electrical stimulation of the left ventricle precedes that of the right ventricle, TV closure occurs after the MV (178).

Fluid dynamic studies of the MV that use magnetic resonance imaging (MRI) have demonstrated the presence of a large anterior vortex at the onset of partial valve closure and soon after atrial contraction (122). *In vitro* models have suggested that vortices generated by ventricular filling aid the partial closure of the MV following early diastole and are essential for the closing of the valve—without these vortices, the valve would not be able to close during ventricular contraction (18). More recent *in vitro* models have shown that although vortices aid in initial valve closure, the adverse pressure gradient dominates the closure effect of the MV (104). Other valve structures must be taken into account when studying valve closure. In this case, a more complete theory of valve closure should not only include flow deceleration and ventricular vortices, but also the contribution of chordal tension, which is a necessary condition for the other two (297).

Flow characteristics—Due to the limited access, it is difficult to quantify and characterize the hemodynamic environment of the HVs experimentally. Imaging modalities, such as ultrasound and MRI can oftentimes capture flow patterns produced in the vicinity of a fresh valve; this said, these techniques lack the spatial resolution that is needed to fully capture and quantify the flow profile at a small scale. For this reason, many research groups have turned to computational methods to investigate HV hemodynamics. These groups have developed unique computational tools that simulate blood flow in complex HV geometries. These computational fluid dynamic (CFD) techniques permit flow characterization at the microscale throughout the entire valve region, a capability that is not feasible through experimental flow methods. This said physiological conditions, which are represented by a peak systole Reynolds number of 6000, are not easy to simulate due to the complexity of the valve geometry and motion. The Reynolds number is a dimensionless quantity that gives a measure of the ratio of inertial forces to viscous forces for given flow conditions and describes whether the flow conditions lead to laminar (less than 2300) or turbulent flow (more than 4000). Using a lower Reynolds number to predict blood flow results in

successful simulations that capture characteristics that have already been quantified *in vitro*. These simulations provide important insights into the small-scale hemodynamics of valvular leaflets. Recent CFD modeling developments include the simulation of flow through a tricuspid semilunar HV-like geometry (Fig. 5). In this case, the kinematics of the valve was prescribed and the unsteady flow solution was computed for the case of a peak systole Reynolds number of 3000. The instability of the shear layers emanating from the leaflets dominates the accelerating flow phase and gives rise to complex vortex shedding. The flow predictions highlight the drastically different hemodynamic stresses experienced by the aortic and ventricular sides. To fully elucidate the effect of hemodynamic differences in the different sides of the leaflet, limiting streamlines (i.e., lines tangent to the shear stress vector field) and the shear stress magnitude at two instances in time were computed on both the aortic and ventricular sides of the leaflets (Fig. 6). Simulation results indicate that the ventricular stress field during the open phase has a smooth, straight, accelerating flow that is consistent with the favorable pressure gradient experienced by the flow as it is pushed by the contracting ventricle to pass through the leaflets. The rapid cross-sectional area expansion in the sinus region of the aortic side imposes an adverse streamwise pressure gradient that gives rise to a very complex and disorganized flow. The stress field changes drastically as soon as the leaflets begin to close. Though it is less orderly than during opening, the flow on the ventricular side during the closing phase remains fairly straight. In addition to the different flow patterns on the atrial and ventricular sides of the leaflet, the simulations also suggest the existence of significantly different magnitudes of the shear stress fields. The aortic side is generally characterized by lower magnitudes but more complex patterns in the shear stress vector field than the ventricular side.

Diseased valve hemodynamics—AV pathology can be caused by inflammation or degenerative valve disease, both of which can be caused by increasing longevity coupled with rheumatic and infective endocarditis (295). Although a significant amount of progress has been made in the development of heart valves, there is yet to be an “ideal” heart valve replacement available (225). A good understanding of the hemodynamics of the normal and diseased HVs will be invaluable in the treatment of HV disease. As such, many groups have focused on characterizing the fluid environment of diseased SLVs. AV stenosis, a condition that is characterized by substantial calcification of the leaflets and surrounding aortic tissue, induces a reduction in the effective orifice area as well as a significant increase in leaflet stiffness, leading to incomplete valve opening. Obtaining hemodynamic flow measurements on diseased valves is difficult, as a result, bioprosthetic heart valves were used to mimic different degrees of aortic stenosis *in vitro* (298). Flow visualization indicated that under physiological conditions (heart rate of 70 beats min^{-1}, systolic duration of 300 ms, and mean aortic pressure of 90–100 mmHg), the fluid exits from the stenotic valve as an asymmetric, angulated jet that has a diameter that decreases with the degree of stenosis. The flow field becomes more disturbed and chaotic as the degree of the stenosis increases. Additionally, laser Doppler anemometry data revealed that the stenotic valve is characterized by a jet-type flow field (maximum axial velocity of 7.0 m s^{-1}) with regions of separations located around the jet and highly turbulent shear layers (maximum r.m.s. axial velocity of 2.0 m s^{-1}). This is very different from the normal AV, which has an evenly distributed flow field at peak systole (maximum axial velocity of 1.2 m s^{-1}). These high levels of turbulence that exist

downstream of the stenotic valves can cause damage to blood components (red blood cells and platelets) as well as the endothelial cells lining the wall of the ascending aorta. The hemodynamics of the diseased AV *in vivo* are certainly more complex due to the calcification that occurs nonuniformly throughout the leaflets, leading to irregular shapes, particularly on the ventricular side, ultimately increasing the complexity of the flow patterns.

Doppler echocardiography was used to study the hemodynamic characteristics of reconstructed bicuspid AVs both at rest and during exercise (223). At rest, patients with reconstructed bicuspid AVs demonstrate maximum and mean pressure gradients across the AV (14 ± 5.5 and 7 ± 2.6 mmHg, respectively) higher than those observed in controls (7 ± 2.5 and 3.6 ± 2.1 mmHg, respectively). Yet, the valvular resistance of the reconstructed valves was comparable to that of normal valves (13.4 ± 4.8 vs. 13.6 ± 2.9 dyn s cm^{-5}, respectively). At exercise, the hemodynamic differences between repaired valves and normal valves are not as significant.

The hemodynamics of the Ross procedure, a surgery in which the diseased AV is replaced by a pulmonary autograft, have been extensively studied using echocardiography (294). Echo data have revealed that while the left ventricular diastolic volume decreases, the ejection fraction does not change significantly in young patient, but that it decreases significantly in older patients (more than 40 years old). On the other hand, pressure gradients across the valve were found to remain within a normal range after the procedure.

Pathologies of the MV can be characterized according to their hemodynamic properties and divided into two distinct groups: stenosis and regurgitation. Stenosis is the total or partial obstruction of the valve orifice and is oftentimes caused by rheumatic fever, endocarditis, ankylosing spondylitis, atrial myxoma, and Lutembacher syndrome. In severe, mitral stenosis, the mean pulmonary and transmitral pressures are raised significantly [greater than 60 mmHg and up to 17.8 ± 6.5 mmHg, respectively (275)]. Pressures of up to 25 mmHg in the left atrium are required to maintain a normal cardiac output.

MR, one of the most common functional abnormality of the MV, leads to the malcoaptation of the MV leaflets during valve closure, resulting in orifices in the coaptation line, and subsequent regurgitation jets with peak velocities on the order of 4 m s^{-1}. The velocity, volume, direction and duration of the regurgitation jets are highly variable and dependent on the patient and the nature of the pathology. MR is quantified by the ratio of the regurgitation volume to the stroke volume (regurgitation fraction). Regurgitation fractions of 20% are considered clinically significant and in severe cases of mitral regurgitation may be more than 60%. M-mode echocardiography has been used to measure mean regurgitant flow propagation velocities in mild, moderate, and severe MR, which were found to be equal to 26.4 ± 7, 43.3 ± 7, and 60.3 ± 7.3 cm s^{-1}, respectively (6).

Tissue-level biomechanics

Dynamic leaflet strains—A complete understanding of normal valve dynamics is required to not only accurately diagnose and treat valve disease, but also to develop improved surgical strategies and techniques. Although various groups have taken on the task of studying MV dynamics and left ventricular fluid dynamics

(17,103,167,179,180,209,227), it is still difficult to determine the functional role and importance of each individual component (10). Although computational models (125, 126, 128) present an exciting and efficient approach to elucidate the role of the many components of heart valves, they have not yet progressed to the point where fully dynamic function can be simulated and validated *in vivo* with available imaging technologies.

Different techniques have been used to quantify valvular dynamics and shed light on *in vivo* dynamic valve leaflet strains. To quantify dynamic valve function, Thubrikar et al. (258, 265, 266) used biplane fluoroscopy; in which lead radiopaque markers were sutured directly onto the valve leaflets and tracked optically. It was observed that the leaflet radial length did not change significantly during maximum flow but that instead the radial length increased during diastole (267). The mid-diastole reference configuration was used to obtain the displacement of the circumferentially and radially oriented markers throughout the cardiac cycle. Circumferential and radial *in vivo* strains of 10.1% and 30.8% were measured over a period of approximately 20 to 25 ms. The corresponding circumferential and radial strain rates were calculated and found to be 440 ± 80.0 and 1240 ± 160.0% s^{-1}, respectively. Subtle variations between species are expected to exist; this said, it is safe to assume that the strain rates are comparable. Since the measurements were based off of only two markers sutured at the basal and belly region of the leaflet, the *in vivo* measurements by Thubrikar et al. (258, 265, 266) did not follow the entire leaflet surface and underestimated actual changes in the leaflet. Even though the two markers were sutured directly to the leaflets and were spaced significantly apart, only straight distance measurements were possible. More recent work involves the use of high-resolution approaches, such as biplane X-ray imaging, which highlights the significant regional complexities that exist in valve motion (232). This said the number of markers used in these studies was small, leading to insufficient spatial resolution that did not allow detailed surface strain studies. Such detailed studies are considered critical considering the high degree of structural and mechanical heterogeneity in HV leaflets (22,217,235,277), which suggests an equally complex regional strain response over the cardiac cyclic.

To understand the complex and subtle deformations of HV leaflets, we used a combination of *in vitro* and *in vivo* techniques to quantify the in-surface strains of the MV anterior leaflet (MVAL) (105, 106, 214, 215). Using the *in vitro* technique, we focused on a 4 × 4 mm region of the center portion of the anterior leaflet and tracked the three-dimensional motion of 16 surface fiducial markers. We then used the resulting marker motion to compute the complete in-surface strain tensor along with the corresponding strain rates and related the principal strain directions to the underlying collagen fiber architecture. Key findings include the following:

- **i.** The anterior leaflet experienced large, anisotropic (i.e., directionally dependent) stretches during closure.
- **ii.** Once the valve is closed, further leaflet deformation ceases.
- **iii.** The closing deformation behavior is essentially symmetrically reversed during valve opening.

iv. The region of the anterior leaflet studied experienced relatively little shear throughout the cardiac cycle.

v. Peak stretch rates during the closing and opening phases were very high, reaching values of 500–1000% s^{-1}.

The *in vivo* approach involved the use of a sheep model and sonomicrometry array localization to compute, for the first time, the dynamic strains of the anterior leaflet over the cardiac cycle at varying afterloads (141). Anterior leaflets of Dorsett sheep were instrumented with nine 1 mm hemispherical piezoelectric transducers in a 15 mm square array (Fig. 7A) and the three-dimensional crystal spatial positions were recorded over several cardiac cycles and used to calculate the in-surface Eulerian strain tensor was computed from the crystal displacements.

Data of peak stretch versus time response demonstrated that overall, leaflet deformations were smooth and that the complete loading of the leaflet occurred in approximately 50 ms (Fig. 7B). Similar to the *in vitro* experiments (215), we observed large anisotropic strains. Mean peak circumferential strains ranged from 2.5 to 3.3% and mean peak radial strains ranged from 16% to 22%. We defined an areal strain measure to be the change in the area defined by the sonocrystals expressed as percent reference area to quantify the net change in leaflet dimensions. Corresponding areal strain ranged from 15% to 20% (Fig. 7B) and the mean peak strain rates were approximately 300% to 400% s^{-1} in the radial direction and 100% to 130% s^{-1} in the circumferential direction (Fig. 7C). Interestingly, the maximum pressure levels had little effect on either the peak stretches or the peak strain rates (Fig. 7C).

These leaflet deformation results were also qualitatively consistent with our previous *in vitro* work and key deformation patterns of the MV leaflet were very consistent between the two studies. In both studies, we observed large, very rapid strains to the point of full coaptation, followed by an absolute cessation of any deformation during systolic ejection. Deformations during the final valve opening phase are a mirror reversal of the loading phase, reflecting the overall behavior of the leaflet in which we observe an initial high-stiffness region that facilitates leaflet coaptation, followed by a rapidly stiffening region as soon as the valve coapts. Despite the qualitative similarities with our previous *in vitro* work, the magnitudes of peak stretches and stretch rates were found to be smaller *in vivo* than in our *in vitro* setup. These differences can be attributed to the different species (porcine, *in vitro*, vs. ovine, *in vivo*) as well as the strain measurement techniques that were used in each experiment. However, these differences also highlight the effect of the left ventricle on leaflet geometry and function, notably the deformation of the annulus and contraction of the papillary muscles. Although studies that involve fiducial markers, such as the ones used by our labs, can give unique information on valvular motion and function, the total number of markers needed to provide detailed regional information limits of this technique. As such, the fiducial marker approach should be viewed only as a first step to studying HV dynamic leaflet strains. Imaging heart valves with a high level of detail is beyond the forefront of what is possible with state-of-the-art imaging modalities for several reasons, including but not limited to the large anisotropic deformations, complex surface geometries, and highly dynamic motion. As progress is made in the imaging field, we anticipate progress in HV imaging as well, with the ability to image and quantify normal and diseased HVs in clinical

settings. This will not only result in major advancements in HV research, but will set the pace for improving patient care.

Functional tissue structure relevant to heart valve biomechanics—HVs have evolved into multilayered leaflet structures. These layers, which are composed of ECM components (collagen, elastin, proteoglycans, and glycosaminoglycans), are the ventricularis, spongiosa, and fibrosa (1, 224). The ventricularis layer faces the left ventricular chamber and is composed of a dense network of collagen and elastin fibers. The spongiosa layer contains a high concentration of proteoglycans and glycosaminoglycans and the fibrosa layer, thought to be the major stress-bearing layer, is composed predominantly of a dense network of collagen fibers (Figs. 2 and 3).

Although they have low torsional and flexural stiffness, collagen fibers can withstand high tensile forces. As a result, fiber orientation can be used to identify directions in which the tissue is able to withstand the greatest tensile stresses. In this technique, a laser light is passed through a tissue specimen and is then scattered. The spatial intensity distribution of the resulting scattered light represents the sum of all structural information within the light beam envelope. To quantify the changes that occur in AV leaflet structure with increasing transvalvular pressure (TVP), fresh porcine AVs were fixed at TVPs ranging from 0 to 90 mmHg and imaged using small angle light scattering (SALS). Overall, increasing TVP induced the greatest changes in fiber alignment between 0 and 1 mmHg, and past 4 mmHg, there was no detectable improvement in fiber alignment (Fig. 8B–D).

We have previously used the method of Hilbert et al. (109, 110) to quantify the amount of collagen fiber crimp in the native pulmonary and aortic HVs by identifying the cross-sectional regions that displayed observable crimp (119). We found that at 0 mmHg, approximately 60% of the AV transverse cross-sectional area was occupied by crimp structure (Fig. 8B). As the TVP increased, the percent crimp decreased rapidly until 20 mmHg, with minimal decreases in percent crimp thereafter. For the AV, much of the observed change in collagen structure is due to the finely tuned straightening of the collagen fibers, which must occur at the right strain level and at the right rate to facilitate coaptation without allowing excessive tissue deformations that could lead to regurgitation. The unique structure of the commissure region, which approximately corresponds to the coaptation region, highlights the adaptive structure of HVs. Instead of undergoing TVP differences, the coaptation region is loaded in a uniaxial-like manner due to tethering forces generated at the attachment of the commissures to the aortic root. Unlike the biaxially loaded belly regions of the valve, the uniaxial loading of the commissures makes them more highly aligned, similar to tendon. Fiber uncrimping with stress occurs very rapidly for this highly aligned fiber network, as demonstrated by the short transition region from low to high stiffness. The highly aligned nature of the commissure region at unloaded state and the more rapid realignment with TVP in the commissure regions are consistent with the pretransition strain level behavior of tendon-like materials.

Biomechanical behavior: Behaviors and models

Approaching heart valve biomechanics: To fully understand HV tissue-level biomechanics, it is useful to follow a two-way approach: first, focus on in-plane stretch and then, on flexural deformation modes. As the valve opens, it experiences not only flexure, but also surface shear stress from the local blood flow. When it closes, the valve experiences flexure and then tension during coaptation and full loading. Although these loading modes are common to all four valves, differing valve geometries, chordae tendineae tethering effects in the AVV suggest that the magnitudes and rates will vary from valve to valve and from patient to patient. Due to the higher prevalence of disease and surgical repair, most research on HV biomechanics has been carried out on the AV (3,21,22,43,165,217,277,279,280) and MV (91,92,215,235). Fortunately, several groups have also studied the PV in recent years (45, 54, 163, 246, 278). Overall, due to the extensive *in vivo* studies (255–257, 259, 261–264), we now have a good understanding of the full loading regimen required during both normal and pathological function. In the following, we present a summary of the three loading HV modes.

Planar biaxial tensile biomechanical behavior: The Mitral valve leaflet: Fundamental to the development of a deeper understanding of pathophysiological tissue remodeling for MV disease is the development of an accurate soft tissue constitutive model. We recently developed a novel mesoscale (i.e., at the level of the fiber, 10–100 μm in length scale) structural constitutive model for MV leaflet tissues, focusing on the contributions from the distinct collagen and elastin fiber networks within each tissue layer.

Details of this model have been recently presented (299). Briefly, as in previous structural approaches, we assume affine fiber kinematics. This assumption is supported by a recent study wherein we demonstrated that the MVAL collagen and elastin fibers all deformed in a manner consistent with affine deformation kinematics (135). We further assume each layer is structurally homogeneous (i.e., ignore intralayer structural variations). We derive the total individual layer response as a function of its collagen and elastin components by acquiring layer-specific information on (i) the structural composition (i.e., collagen and elastin mass fractions), (ii) the orientation distribution functions (ODFs) for collagen and elastin fibers, and (iii) the recruitment behaviors of the collagen fiber network. Using our current understanding of heart valve leaflets, we assume that all four layers of the MV are tightly bonded with no slippage (26) and no mechanical interactions between them, enabling them to deform with the bulk tissue. We also assume that the collagen fiber modulus is the same throughout the four layers and that fiber-fiber and fiber-matrix interactions are negligible.

Layer-specific mass fractions of the major ECM components were measured from Movat stained sections of the MV using color deconvolution techniques as described previously (299) (Fig. 9). Fiber ODFs for both collagen and elastin were quantified by SHG imaging using methods of Carruthers et al. (35) and Courtney et al. (50). Interestingly, we noted substantial layer-specific stress variations, with the fibrosa contributing most of the circumferential stress component and the atrialis layer contributing substantially to the radial stress component (Fig. 10). For the overall layer contributions, the mechanical response of the circumferential direction was mainly due to the elastin in the ventricularis at lower stress

and the collagen within the fibrosa, whereas the radial direction is a combination of collagen fibers in the fibrosa as they extend and rotate under physiological loading and collagen in the atrialis at higher strains (Fig. 10). The mechanical contribution from the spongiosa was, as anticipated, negligible for both leaflets. This modeling approach demonstrated excellent predictive ability over physiological and extra-physiological loading regimes not used in parameter estimation. Future utilization in computational models of the MV will aid in producing highly accurate simulations in nonphysiological loading states that can occur in repair situations, as well as guide the form of simplified models for real-time simulation tools for improving long-term durability of MV repairs.

Time-dependent behaviors: Our group, along with others (44, 158, 160) have conducted biomechanical tissue analyses at quasi-static (strain rates of 4%/s to 12%/s) experimental conditions and showed that heart valve leaflet deformations can reach strain rates as high as 300%/s (Fig. 7C), raising an important question on the link between HV quasi-static leaflet mechanical properties and HV physiology. Although strain-rate dependence has been extensively studied in soft-tissue biomechanics, the literature indicates a wide range of findings that are dependent on the specific tissue composition and structure as well as the specific testing methods utilized to characterize it. Thus, to be able to model physiological functions and understand the strain rate dependence of a particular tissue, one needs to property investigate it and quantify its mechanical properties under realistic physiological loading states. Using a custom-built high-speed biaxial testing device, we explored the effects of strain rate (from quasi-static to physiologic) on the planar biaxial mechanical properties of the MVAL (94, 95). Results indicated that the stress-strain responses of the MVAL specimens were remarkably independent of strain rate (Fig. 11A). Hysteresis was low (~12%) and did not vary with strain rate. These results were important and concluded that valve leaflets can be modeled as “quasi-elastic” biological materials. In a follow-up study, we performed biaxial stress-relaxation and creep experiments on porcine MVAL specimen to provide a more complete picture of the time-dependent mechanical properties of the MVAL. We found that while MVAL leaflets exhibited significant stress relaxation (Fig. 11B), they experienced negligible creep over the 3-h test (Fig. 11C), supporting our initial claim that the MVAL functions as an *anisotropic quasi-elastic material*, rather than a linear or nonlinear viscoelastic material. These results were unique in the soft tissue literature, highlighting heart valves’ unique ability to withstand a remarkable amount of loading without any time-dependent material effects.

The underlying structural basis for this unique *quasielastic* mechanical behavior is yet to be understood. Since collagen is the major structural component of the MVAL, we used small angle x-ray scattering to investigate the relationship between collagen fibril kinematics (rotation and stretch) and MVAL tissue-level mechanical properties under biaxial loading (141). To do so, we developed a novel biaxial stretching noel device that was utilized to perform simultaneous measurements of tissue level forces and strain under different planar biaxial loading states. Collagen fibril D-period strain (ε_D) and fibrillar angular distributions were also measured under equibiaxial tension, creep, and stress relaxation to a peak tension of 90 N/m. The results indicate that under equibi-axial tension, collagen fibril straining does not begin until the end of the nonlinear region of the tissue-level stress-strain curve. At

higher tissue tension levels, ε_D increased linearly with increasing tension. Changes in the angular distribution of the collagen fibrils mainly occurred in the toe region of the tissue. Using ε_D, the tangent modulus of collagen fibrils was estimated to be 95.5 ± 25.5 MPa, which was ~27 times higher than the tissue tensile tangent modulus of 3.58 ± 1.83 MPa. Creep tests were performed at 90 N/m equibiaxial tension for 60 min and the tissue strain and ε_D remained constant with no observable changes over the test length. On the other hand, the 90-min-long stress-relaxation tests that were performed indicated that ε_D rapidly decreases in the first 10 min and is then followed by a slower decay. Using a single exponential model, the time constant for the reduction in collagen fibril strain was 8.3 min. This is smaller than the tissue-level stress-relaxation time constants of 22.0 and 16.9 min in the circumferential and radial directions, respectively. No significant changes in fibril angular distribution were measured under creep and stress relaxation. These results reveal important information on the structure and function of HVs:

1. The collagen fibrils in HV leaflets do not intrinsically exhibit viscoelastic behaviors.
2. The removal of stress from the collagen fibrils causes valve leaflet tissue relaxation. This could be caused by a slipping mechanism modulated by noncollagenous ECM components, such as proteoglycans and glycosaminoglycans.
3. Valve leaflets exhibit a load-locking behavior under maintained loading conditions, as suggested by the lack of creep and occurrence of stress relaxation.

These unique mechanical characteristics are necessary for valve function. As such, further insights into these characteristics will lead to a better understanding of HV structure and function, and most importantly, will help guide and inform translational efforts, such as surgical repair and HV tissue engineered replacements.

Flexural response of native leaflets: Experimental measurements of the flexure of soft biological materials has two advantages over tensile mechanical testing: (i) the ability to discern very small changes in stiffness at low stress-strain and (ii) the ability to assess the contributions and interactions of individual layers of multilayered structures. Thus, multi-layered tissue, such as the AV leaflet is expected to reveal a distinct bending response in each direction of bending. As a result, flexural mechanical testing techniques provide a sensitive way to explore the effects of layer-specific contributions to the overall biomechanical function of the AV. We used circumferential strips of porcine AV leaflets to quantify the flexural properties of the belly region (Fig. 8A)—experimental details have been previously reported (69, 88, 162). It is important to note that in the unloaded state, the AV leaflet is curved both in the circumferential and radial directions; hence the frequently used term “cusp.” We use the change in curvature $\Delta\kappa$ (in units of mm^{-1}) from the initial unloaded reference state to account for the initial curvature of the test specimen. Applying bidirectional flexure can subject both the fibrosa and ventricularis layers to alternate states of tension and compression (Fig. 12A and B). These flexural directions are referred to as “with curvature” (WC) and “against curvature” (AC), both of which are with rest to the direction of the natural leaflet curvature. The effective stiffness measured in the WC direction is

dominated by the ventricular tension with little contribution form the fibrillar collagen in the fibrosa, which is not designed to support compressive loads. On the other hand, when the leaflet is bent in the AC direction, the fibrosa is in tension and the ventricularis is in compression. Data from this study show how the applied bending moment (M) changes with $\Delta\kappa$. The Euler-Bernoulli equation $M = EI\,\Delta\kappa$ (78), where E is the effective stiffness and I the second moment of inertia, can then be used to estimate the effective (i.e., total) bending stiffness.

Unlike the highly nonlinear in-plane tension tissue response (Fig. 9B), the moment (M)-change in curvature ($\Delta\kappa$) response of the AV leaflet was found to be linear (Fig. 12C and D). This is due to how tissue layers are loaded and can be explained by the micromechanical mechanisms underlying the flexural response, which are quite different from those that play a major role in in-plane tension. Additionally, flexure induces small strains and possible interlayer sliding that can lead to profoundly different results. Continued work, along with an improved knowledge of tissue micromechanics, are necessary to provide insights into these mechanisms and have a better understanding of native heart valve functional physiology.

Valve tissue adaptation to stress—Under altered *in vivo* loading conditions, heart valves adaptively remodel to compensate for the elevations in mechanical stress. Although it is harder to control the native environment, *in vivo* studies provide important information that leads to a better understanding of valve pathophysiology and can link organ-level deformations to cell-level response, an aspect that is not readily feasible in *in vitro* studies. Three-dimensional echocardiography and biplane videofluoroscopy are commonly used to quantify leaflet shape and regional geometry in different pathologies (38,208,241,243,270,272). Clinical studies by Chaput et al. showed that mitral leaflet area increased by >30% in response to chronic tethering in patients with inferior MI and dilated cardiomyopathy (39). Similarly, the MV undergoes adaptive changes in hearts with inferior wall motion abnormality and LV dilation caused by inferior MI that translate to an increase in area (38) and annular dilation (208, 270) over time, both indicate leaflet and annular remodeling of the MV. These results highlight the need to understand the mechanisms of heart valve compensatory responses and ultimately, link these organ- and tissue-level alterations that underlie leaflet adaptation to VIC mechanobiology.

In a recent study, Wells et al. determined the remodeling capacity of mature heart valve leaflets under nonpathological conditions by examining the response of the MV during the volume loading and cardiac expansion of pregnancy in a bovine model (191,288). The maternal cardiovascular system in humans and other species undergoes striking physiological changes during pregnancy that allow it to accommodate the developing placenta and deliver the necessary oxygen and nutrients to both mother and fetus. Consequently, the heart undergoes dramatic dimensional changes in early pregnancy to account for this volume overload, one of which is the rapid remodeling of the MVAL. Pregnancy caused a 33% increase in leaflet area, thickness, and chordae tendineae attachments. Hydrothermal isometric tension test results indicated an increase in collagen cross-linking and remodeling. Pierlot et al. related these changes to structural alterations in the collagenous leaflet matrix using SALS and hydroxyproline assay to assess both collagen

fiber alignment and content (191). Results indicated a decrease in fiber alignment, loss of collagen fiber crimp accompanied by a thickening of the fibrosa layer, and an increase in total collagen concentration, suggesting that collagen is being synthesized. These studies highlight the compensatory response of the MV to increasing loading conditions associated with pregnancy by adaptively remodeling and consequently, normalizing leaflet stress and maintaining coaptation. Pregnancy-induced changes and remodeling of the MV parallel changes observed in pathological heart valves and thus, linking these organ-level changes to ECM remodeling is important.

Many groups have investigated the effect of abnormal mechanical stress on MV collagen synthesis (47, 108, 199). Willems et al. used Wistar Kyoto rats to characterize structural alterations in heart valves during acute left ventricular pressure overload (291). Results indicated an increased DNA synthesis and mRNA amounts of both Type I and III collagen, suggesting that valves adapt to new mechanical environments by increasing DNA synthesis and collagen turnover. In a pilot study, Quick et al. showed that procollagen, a precursor to Type I collagen, was upregulated by a factor of 1.8 after MR and abnormal ventricular wall motion with a greater upregulation in the MVAL compared to the MVPL (199). Stephens et al. studied this response in detail using a chronic ovine model to test whether isolated MR alone can stimulate mitral leaflet remodeling (241). MR resulted in a reduced expression of Type I collagen, which is consistent with the measured increase in MMPs and an increased expression of prolyl 4-hydroxylase, decorin, a PG involved in collagen fibrillogenesis, and Type III collagen. Both the fibrosa and spongiosa layers had an increase in elastin content and upregulation of elastin-degrading MMP-9. These results demonstrate that MR causes an increase in matrix degradation and remodeling, particularly of collagen and elastin. In a similar *in vivo* study, tachycardia-induced cardiomyopathy (TIC) was found to cause significant remodeling in MV leaflets, including collagen and elastic fiber turnover, VIC activation, greater cell density, and less delineation between leaflet layers (243). The cellular response observed in this study is in agreement with the organ-level dimensional changes measured with three-dimensional echocardiography that highlight the mitral annulus dilation and flattening caused by TIC (271).

Similarly, the MV compensates for the ventricular remodeling that occurs after left ventricular infarction or dilation by increasing in size and becoming regurgitant. Dal-Bianco et al. used a large-animal model to investigate leaflet adaptation to tethering over time and gain insights on the compensatory mechanism of functional MR (53). Organ- and tissue-level alterations were linked to cellular response by quantifying leaflet area at different times using three-dimensional echocardiography and analyzing cell phenotype, more specifically, the expression of interstitial cell marker α-smooth muscle actin (α-SMA) by endothelial cells expressing CD31. At the organ- and tissue-level, pathological alterations to mechanical stress caused an increase in MV leaflet area and matrix thickness. At the cell level, results indicate cellular activation throughout the leaflet suggesting that the valve endothelium adapts to mechanical stress by adding interstitial cells through endothelial-mesenchymal differentiation and reactivation of embryonic developmental pathways (226). These results highlight the active adaptation of the MV to alterations in its local stress levels. Understanding how alterations in organ- and tissue-level mechanics lead to cell-mediated

remodeling of the ECM is important in developing new treatments and surgical repair techniques.

Cell-level mechanobiology

In biomechanics, the presence of normal tissue stresses is considered to be closely related to tissue homeostasis (46, 79, 131, 177, 251). Many studies have shown that pathophysiological alterations in mechanical loading lead to stress changes and tissue adaptation that affect tissue structure and composition (80,147). In heart valves, the ECM not only provides the tissue with its structural integrity, but it also influences cellular processes through three different mechanisms: (i) matricellular, in which the ECM signals through adhesion receptors, (ii) matricrine, which regulates growth factor and cytokine expression in cells, and (ii) mechanical, which can be characterized as either matrix elasticity or external forces (40). In mechanical signaling, the ECM can transmit external forces, such as stretch, shear stress, and pressure to the cells, but it can also regulate cellular function through its intrinsic composition and elasticity. The mechanical interaction of VICs with the surrounding ECM, particularly with the collagen fibrils, is fundamental to cellular response. The intrinsic ECM composition and its importance in modulating cellular response are apparent in ultrastructural studies by our group, which reveal the micromechanical environment of the cell and highlight the intimate contact between the collagen fibrils and the VIC. Collagen fibrils are circumferentially oriented and the VICs are aligned along the same direction. In heart valves, pathological factors, such as TIC (243), mitral regurgitation (MR) (241), and CAVD (242) have been shown to affect valve tissue structure and composition. The link between tissue-level deformations and ECM remodeling is essential in understanding cardiovascular and in particular, heart valve disease and pathologies. The reader is referred to previous reviews, particularly ones by Sacks and Yoganathan (218) and Sacks et al. (216) for a complete overview of valve biomechanics, Votta et al. (282) for patient-specific simulations of heart valves, and Sun et al. (247) for computational modeling of valve function.

Endothelial cells—Valve endothelial cells (VECs) play an important role in the establishment of valve structure during embryonic development and are essential for maintaining the valve's lifelong integrity and function. Endothelial cells line the surfaces of both blood vessels as well as heart valve leaflets. These cells are critical in the maintenance of a nonthrombogenic surface, nutrient transport, and mechanotransduction (31). This said, VECs have been shown to be morphologically different from aortic ECs (28, 31, 43). In healthy valves, VECs form a continuous endothelium and have an important role, which consists of regulating vascular tone, inflammation, thrombosis, and remodeling (132). This function, however, is different in malfunctioning and diseased valves in which VECs are disrupted. Heart valve failure has been traced to endothelial dysfunction and denudation (31), giving rise to valve leaflet thickening (sclerosis) and/or calcification and leading to an attenuation of responses to molecular and hemodynamic cues (29, 81). Within the proximal third of the leaflets, in which innervation occurs, a feedback mechanism between VECs and VICs exists, wherein the nerves transmit information on released substances from VECs (157). Release of cytokines has been shown to cause changes in interstitial cell structure and function (56, 60) and it was speculated that there exists some physical VEC/VIC

communication. This said, no direct junctions have been observed to date between the two cell populations (72).

Many groups have made important insights on endothelial function in different mechanical environments using different *in vitro* experimental setups. Endothelial cells reorganize their cytoskeletal filaments and focal adhesion complexes to align parallel to the direction of unidirectional flow while secreting vasoactive agents, such as nitric oxide and prostaglandin (52, 86, 234). Biomechanical stimuli exerted by blood flow, blood pressure, and cyclic strain cause endothelial cells to alter their morphology, growth rate, metabolism, and gene expression profile to ensure proper morphogenesis but also homeostasis. This is done through the activation of surface glycoproteins, cell adhesion molecules, secondary messengers, and phosphorylation of surface receptors (253). Several groups have investigated the disruption of the endothelial cell mechanotransduction and its effect on cell mechanobiology through the oscillation of fluid flow direction and signal pathway blockade (37,58,59,107,151,194). Data from these studies suggested that disruptions in these signaling events inhibit focal adhesion reorganization and consequently, cell alignment and agent release (31).

Although a significant amount of information is available on endothelial cells, little is known about valvular endothelial cells. The work by Nerem et al. has been instrumental in understanding VEC morphology, mechanobiology, and mechanotransduction. *In vitro*, VECs grow into cobblestone-like morphology and align perpendicular to fluid flow but parallel to the leaflet collagen fibers (63, 118), in contrast to vascular endothelial cells, which align parallel to fluid flow. The differing shear stress response of valve endothelial stress and vascular endothelial cells is due to observed differential molecular profiles and functional responses of these cell populations (30, 70). Recent work by Butcher et al. indicates that unlike vascular endothelial alignment, VEC alignment to fluid flow is mediated by the reorganization of focal adhesions within the cell and though it is calpain- and Rho-kinase-dependent like the vascular endothelial cells, it is independent of phosphatidylinositol 3-kinase (31).

Pathological changes in vascular endothelial cell-mediated responses have been associated with atherosclerosis, thrombosis, stroke, and hypertension (253). Valvular heart disease, a major cause of morbidity in the United States and around the world, is not only due to dysfunctional changes in VIC proliferation and ECM organization, but also VEC histopathological alterations. Some light has been recently shed on the events that initiate VEC dysfunction in diseased valves. Both genetic mutations associated with NOTCH1, Gata5, and endothelial-nitric oxide synthase (eNOS or NOS3) (130,136) as well as atherosclerosis-related environmental risk factors, such as diet (176, 287), smoking, ageing (252,287), hypertension, and diabetes, have been associated with valve pathogenesis (245). This said hemodynamic flow across the endothelium is the major player in the injury and subsequent dysfunction of both vascular as well as valvular endothelial cells. It is known that in the healthy heart, the left side of the heart is subject to greater stress due to the high-pressure difference that exists between the left atrium and the left ventricle. Thus, hemodynamic forces have a greater impact on the mitral and AVs than on the tricuspid and PVs (112, 165). Similarly, endothelia on opposing sides of the valves are subjected to very

different hemodynamics (57, 81, 173), which can be linked to the distinctly different patterns of focal calcification on the aortic side of the AV (184, 268, 269). Several *in vitro* studies have highlighted the link between hemodynamics and VEC molecular responses and linked it to valvular heart disease. Recent work by Simmons et al. and Butcher et al. indicates that VECs activate fibrocalcific responses to increases in hemodynamic forces (i.e., fluid shear stress, cyclic strain, and hydrostatic pressure) (32) and does so in a side-specific manner (i.e., VECs from the aortic side are protected from inflammatory processes compared to VECs isolated from the ventricular surface) (229).

VECs that line the surface of heart valve leaflets are unique in their ability to undergo endothelial-mesenchymal transformation (EMT) not only in valvulogenesis, as described above, but also as part of a regulatory mechanism that is necessary in pathological and stress overload scenarios such as ischemic cardiomyopathy and mitral regurgitation (12, 53, 139). More recently, Balachandran et al. have shown that valve tissue micromechanics plays an important role in EMT, whereby EMT induction in VECs occurs through different mechanisms when subjected to different strain levels: lower-strain induced EMT occurs via the TGF-β1 signaling pathway and higher-strain induced EMT via the wnt/β-catenin signaling pathway (12). These results suggest that VECs are sensitive to the micromechanical environment and initiate EMT differently in diseased and overstrained valve tissue than in healthy valves.

Interstitial cells—A heterogeneous population of interstitial cells, consisting of fibroblasts, smooth muscle cells, and myofibroblasts, resides within the different layers of heart valve leaflet tissue (72, 166, 171, 254). Studies of the interstitial cell population in both human and porcine subjects have revealed that this cell population is not localized to any one region or layer of the leaflet and is instead present throughout the leaflet tissue (11, 165). Interest in VIC mechanobiology has grown in recent years, as they are believed to be a major driving force behind valve pathophysiology. VICs play a critical role in valve tissue homeostasis and pathophysiology by maintaining the structural integrity of the leaflet tissue via protein synthesis and enzymatic degradation, thereby providing durability. VICs function mainly to synthesize and secrete cytokines, chemokines, growth factors, ECM components, MMPs, and their inhibitors (TIMPs) (254). Each valve layer is enriched in a specific ECM component and has a distinct function. The MV for example, consists of four layers: atrialis, spongiosa, fibrosa, and ventricularis. The fibrosa is the load-bearing layer and consists mainly of collagen. The ventricularis and atrialis are thin elastin-rich layers and the spongiosa consists mainly of PGs and GAG. Studies of VICs in both human and porcine valve tissues have revealed that the cell population is not localized to any particular region or layer of the valve leaflets, but is present throughout the tissues (11,55). VICs have a diverse and dynamic phenotype ranging from smooth muscle cells to fibroblasts and myofibroblasts. In normal healthy valves, VICs are quiescent and predominantly fibroblast-like (200). They become activated and contractile myofibroblasts during valve development, disease, and remodeling, and express excessive levels of catabolic enzymes that regulate matrix degradation and remodeling (201, 203), α-SMA stress fibers (190), and osteoblast-like cells identified by their expression of osteoblast transcription factors and bone matrix proteins (168,205). Thus, the VIC phenotypic state at any given time is related to the current

remodeling demands of the valvular tissue (201). While their dualistic nature is not fully understood, the multifunctionality of VICs involves cell-cell communication, tissue remodeling, wound healing, and contraction (171).

VIC contractile behavior: Aortic VIC (AVIC) contractility has been qualitatively studied with cultured cells on silicone substrates in the presence of multiple contractile chemical agents (72, 166). In both of these studies, contraction occurred for most agents within 3 minutes and reached a plateau within 10 min. The few cells that did not have an initial basal tonus did not respond to the administered vaso-constriction drugs. Isoproterenol was used to elicit relaxation from active cells, from which all cells recovered their previous basal tonus within 25 min. Although they do not provide any quantitative information, these findings were the first to demonstrate AVIC contractile response and shed light on VIC contractile behavior.

The flexural mechanical testing techniques described earlier are sensitive enough to explore the effects of cellular contraction on leaflet mechanical properties. These techniques were used by several groups, including our own, to investigate regional and directional receptor-mediated contractile response of AV leaflet tissue (41, 42). As described previously (162), circumferential strips of porcine AV leaflets were mechanically tested under flexure in both the WC and AC directions in a normal state, under contraction (induced by potassium chloride), and without contraction (i.e., contraction inhibited by thapsigargin). Results revealed a 48% increase in leaflet stiffness with AVIC contraction (from 703 kPa to 1040 kPa) when bent in the AC direction ($P = 0.004$) and only a 5% increase (from 491 kPa to 516.5 kPa) when bent in the WC direction (not significant) in the active state (Fig. 12B). The thapsigargin treated group (contraction-inhibition) experienced a 76% ($P = 0.001$) and a 54% ($P = 0.036$) decrease in leaflet stiffness, in the AC and WC directions, respectively, at 5 mmol/L KCl levels. As expected, contraction was completely inhibited with the addition of 90 mmol/L KCl as expected (Fig. 12C). We speculate that the observed layer-specific effects of AVIC contraction are primarily due to the varying ECM mechanical properties of the ventricularis and fibrosa layers. While these results demonstrate that AVIC contractile ability is a significant contributor to AV leaflet bending stiffness, its complete role in maintaining AV leaflet tissue homeostasis has yet to be elucidated.

VIC deformation under physiological loading: The extremely low forces generated by AVICs during contraction are unlikely to directly affect valvular function. This said, VICs are a dynamic source whose biosynthetic capabilities serve an important role in maintaining overall valve leaflet tissue homeostasis. *In vitro* studies of VICs indicate that these cells increase their collagen synthesis in the presence of vasoactive agents, suggesting that VICs use their contractile elements to mechanically communicate with the local microenvironment (102). The local stress-strain fields in the vicinity of a cell are dependent on a number of factor, including but not limited to, cell shape, orientation, and the relative mechanical properties of the cell and the surrounding ECM (97). Thus, it is not clear how the pressures imposed on different sides of the heart translate into local stress on the cells. To link valve leaflet tissue deformation to cell deformation (Figs. 1 and 2), our group performed a study on the effects of TVP on AVIC deformation (114). As described

previously (217), porcine AV leaflets were fixed under varying pressures and Movat stained histological sections were imaged and analyzed. We chose to use AVIC nuclear aspect ratio (NAR), defined as the ratio of the length divided as the width, as an index of overall cellular deformation. Since the AV leaflets consist of histologically distinct layers with different ECM structural components, we hypothesized that there may be a relationship between the valve tissue layer and the resulting deformation experienced by the cells that reside within that layer under varying applied TVP. Results, which were presented as AVIC NAR versus normalized thickness, indicated that AVIC nuclei underwent minimal deformation at low TVPs (0 and 4 mmHg) and in fact, maintained an almost constant level toward the ventricularis layer (Fig. 13A). While there were no detectable changes under 0 mmHg, fibrosa layer AVICs had a slightly higher NAR at 4 mmHg. As expected, high TVP (90 mmHg) resulted in much higher aspect ratios in AVIC nuclei than the zero- and low-pressure groups, with a clear demarcation in the fibrosa layer. It is important to note the magnitude of NAR ~5 at 90 mmHg, which highlights the profound region-specific cellular deformations that occur under physiological pressure levels. These deformations occur very rapidly, within ~75 ms, further emphasizing the ability to VICs to withstand stress in a dynamic environment (Fig. 7).

VICs are known to be in intimate contact with their surrounding microenvironment and collagenous ECM (Figs. 3 and 14). Quantifying TVP-induced deformations of the ECM provides insights into VIC mechanobiology and the role of the ECM in VIC mechanotransduction. To quantify the degree of fiber orientation, we used the SALS technique and measured the normalized orientation index (NOI). A highly oriented fiber network has an NOI value of 1, while a more randomly oriented network has an NOI value that is closer to 0. Figure 13 depicts the effect of increasing TVP on collagen fiber alignment and AVIC NAR for comparison. Gross visual comparison yields three distinct regions: (i) an asymptotic region between 0 and 1 mmHg: little change in AVIC NAR (+5%) with large increases in NOI (+25%), (ii) a transition region between 1 and 4 mmHg, and (iii) a steep region between 4 and 60 mmHg: large increase in AVIC NAR with little change in NOI. These observations suggest that at very low-pressure levels, though fiber network straightening occurs, it has little effect on nuclear geometry. On the other hand, at higher-pressure levels, an additional network effect induces large increases in AVIC NAR. Previous studies have also suggested that TVPs above ~5 mmHg lead to collagen fibers uncrimping and becoming more taut and ultimately result in ECM compaction (217). The ECM compaction that occurs with increasing pressure causes significant changes in AVIC NAR (114): at 90 mmHg, the AVIC nuclei aspect ratio increased from 2:1 (at 0 mmHg) to 4.8:1. These results highlight the fact that valvular tissue stresses are translated into large cellular and subcellular deformations.

During valve development, disease, and remodeling, VICs, which are known to be phenotypically plastic, transdifferentiate from a fibroblast phenotype to a myofibroblast phenotype (203). Under normal physiological conditions, the TVPs on the right and left side of the heart are vastly different due to the differing hemodynamic needs of each side of the heart. We hypothesized that the higher left side TVPs impose larger local tissue stresses on VICs in the AV and MV, thus, increasing their stiffness through cytoskeletal composition and ultimately affecting their biosynthetic capabilities, mainly collagen. To evaluate this

hypothesis, we need to decouple VIC response from ECM response and thus, quantify the mechanical properties of VICs isolated from their surrounding ECM (Fig. 1). We used a combination of experimental techniques [i.e., micropipette aspiration (MA), cytoskeletal composition, and collagen biosynthesis] to char-acterize intrinsic differences that exist between VICs from the four different heart valves. Results indicate that VICs from the AV and MV were significantly stiffer ($P < 0.001$) than PV and TV VICs (Fig. 15), and contained significantly more ($P < 0.001$) α-SMA and heat shock protein 47 (HSP47), a collagen binding chaperone. Mean VIC stiffness correlated well ($r = 0.973$) with TVP; α-SMA and HSP47 also correlated well ($r = 0.996$) with one another. Moreover, assays were repeated for VICs *in situ*, and as with the in vitro results, the left side VIC protein levels were significantly greater ($P < 0.05$).

These findings indicate that VICs respond to local tissue stress by altering cellular stiffness, as suggested in this study, through α-SMA content and collagen biosynthesis. VICs are thus responsive to their local micromechanical environment and are able to maintain proper tissue homeostasis through their biosynthetic activity. Specifically, the increased α-SMA in left side VIC populations suggests that these cells have adapted to withstand the stresses imposed on them, while the increased HSP47 highlights the collagen synthesis that is needed to maintain HV structural integrity. α-SMA and HSP47 quantified from *in situ* VICs showed a similar correlation, indicating that the isolation of VICs hindered their normal function but was proportional among all populations. This functional VIC stress-dependent biosynthetic relationship may be crucial to maintaining valvular tissue homeostasis and also prove useful in understanding valvular pathologies.

VIC mechanosensitivity and response to local tissue stress: VICs sense and transduce extracellular mechanical stimuli into intracellular biomechanical signals directly and indirectly through mechanisms that involve receptors, ion channels, caveolin, G proteins, cell cytoskeleton, kinases, and transcriptional factors (140). Integrins, which are transmembrane signal receptors that physically link the cell surface to the surrounding ECM, sort and process these signals, and play a key role in transducing them to the cell interior, leading to a network of intracellular signaling pathways that result in the cell response. In the MV, for example, the integrin $\alpha_2\beta_1$, which shows higher affinity for type I collagen, is the main collagen binding integrin (15,236). Mechanical stimuli activate the mitogen-activated-protein kinase pathway, which controls gene expression (222). Cellular mechanotransduction pathways are beyond the scope of this review; however, the reader is referred to work by Juliano and Haskill (120) and others (24, 137, 213, 219) for a complete overview of signal transduction from the ECM. A normal mechanical environment results in constant tissue renewal in the valve leaflet to maintain tissue integrity whereas altered loading conditions may lead to valve dysfunction and disease (123,199). Several groups have characterized VIC response to alterations in the hemodynamic/mechanical environment *in vitro* and *ex vivo* to understand the link between tissue level deformations and cell response and help elucidate mechanisms of disease development and progression.

Collagen is the main load-bearing ECM component in heart valves. VICs respond and adapt to alterations in local tissue stress by increasing collagen biosynthesis to maintain valvular tissue homeostasis. Our group investigated this functional stress-dependent biosynthetic

response by using MA to link cellular stiffness to cytoskeletal composition and collagen biosynthesis, which were quantified using HSP47 and α-SMA, respectively. Left-side isolated VICs were stiffer and contained significantly more HSP47 and α-SMA than right-side VICs (165): this is explained by the higher left-side TVPs which impose larger local tissue stresses on VICs. These differences were also observed between aortic and pulmonary VICs using atomic force microscopy (AFM) (163). These result demonstrate VIC mechanical adaptability and ability to sense and respond to tissue-level mechanical stimuli. In a similar study, Wyss et al. found that VIC elastic modulus measured using MA increased with pathological differentiation (fibroblast, osteoblast, and myofibroblast) in proportion to α-SMA content (293). Stephens et al. studied age- and valve-region specific response of VICs to substrate stiffness by seeding 6-week, 6-month, and 6-year old porcine VICs from the MVAL and posterior leaflet (MVPL) into poly(ethylene) glycol hydrogels of different stiffness and analyzing VIC activation and phenotypic markers α-SMA, HSP47 and prolyl 4-hydroxylase (240). Results highlight the link between VIC phenotype and matrix-driven material properties in both age-and valve-region-specific cell responses. In the context of valve physiology, these age-related responses could explain the occurrence of certain valve diseases at particular ages (237, 238), whereas the valve-region-related responses could be due to the different loading patterns that these regions experience (158). Collectively, these studies suggest that the *in vivo* mechanical environment plays a fundamental role on the mechanobiology and responsiveness of VICs to external mechanical stimuli caused by aging, disease, or surgical repair.

Cyclic stretch alters ECM remodeling activity of AVICs: Mechanical forces modulate cell physiology and affect the biosynthetic activity of cells in tissue matrices. The AV is exposed to many hemodynamic forces during the cardiac cycle, one of which is cyclic stretch, which allows the valve leaflets to extend and form a coaptive seal with each other during diastole (257,260). Under normal physiological conditions, the AV experiences ~10% stretch during diastole (149) with a 5% increase for every 40 mmHg increase in pressure (14). To fully elucidate the role of cyclic stretch on ECM remodeling and VIC phenotype, Balachandran et al. quantified collagen, sulfated GAG (sGAG), and elastin contents of AV leaflets subjected to cyclic circumferential stretch in a sterile *ex vivo* bioreactor (15% strain for 48h) and examined cell phenotype (13). Circumferential cyclic stretch causes an increase in α-SMA expression, which enhances the contractile and fibrotic phenotype of VICs and alters ECM remodeling activity as seen by the increase in collagen content. Similarly, Ku et al. examined the ability of VICs to synthesize collagen in response to stretch by measuring the incorporation of [^{3}H]-proline and assessing gene expression of different collagen types by RT-PCR. Ku et al. found that collagen synthesis by VICs depends on the degree and duration of stretch (124). Recent work by our group linked cellular deformation to biosynthetic response in the AV. We quantified VIC micromechanical environment in response to increasing strain by measuring the NAR and collagen orientation (216). AVIC response to increasing strain was found to be linear, along with the collagen fiber alignment. These results highlight the tight binding of the AVICs with their microenvironment.

In AV disease (i.e., AS), there is an overexpression of proteolytic enzymes such as MMPs, TIMPs, and cathepsins, which are involved in key cellular processes such as apoptosis, proliferation, and cell differentiation and play an important role in valve disease progression pathways (74). To further elucidate the link between altered stretch and AV disease, Balachandran et al. used a tensile stretch bioreactor to investigate the acute effects of cyclic stretch on expression and activity of MMP-1, MMP-2, MMP-9, tissue inhibitor of MMP-1, and cathepsin L, S, and K at 10%, 15%, and 20% stretch (14). Normal cyclic stretch (10%) maintains the native levels of matrix remodeling activity whereas elevated levels of cyclic stretch cause activated cell phenotype that leads to altered cell turnover and MMP and cathepsin expression. These changes lead to a cascade of events including cellular proliferation and apoptosis that set the stage for valve degeneration.

AVIC plasticity as a hallmark of pathological progression in CAVD: The AV is a highly specialized structure composed of distinctive cellular population (mostly VICs) and complex ECM structures (23, 165, 171). VICs reside within the AV leaflets, where they synthesize and maintain the ECM that forms the tissue architecture. From the cellular and molecular points of view, the process of calcification follows a highly programmed sequence of events resulting in VICs adopting an osteogenic-like phenotype and subsequently, the formation of calcified nodules (171, 211, 292). In healthy adult valves, 95% of VICs have a fibroblast-like phenotype and the remaining 5% is divided in myofibroblast-like and smooth muscle cells (SMC). VIC phenotype is believed to be plastic and reversible, with fibroblasts in healthy valves representing the majority of the cells. Fibroblasts are a quiescent population (qVIC) that, in response to injury or disease, could acquire a secretory myofibroblast-like phenotype (aVIC), where the principal indicator for aVICs is α-SMA. This process allows the secretion and turnover of ECM proteins, which repair the tissue micro-damage and enable the long-term durability of leaflet structure. During the pathogenesis of CAVD, the activation of VICs results in the expression of specific markers such as osteopontin (OPN), osteonectin (ON), runt-related transcription factor 2 (RUNX2), *a*-SMA, osteocalcin (OCN) and alkaline phosphatase (ALP). Notably, most of these markers are overexpressed in the subclinical presentation of the disease (i.e., ASCs), in the absence of noticeable calcium accumulation. Furthermore, activated VICs express and actively remodel fibronectin (FN), which is a major component of the insoluble ECM. Bone morphogenic protein 2 (BMP2) and 4 (BMP4) are known to be potent osteogenic morphogens and to be present in ossified valves and directly affects osteogenic marker expression.

Impact of mechanotransduction on AVIC activation and calcification: Recent studies, including ours, have shown that altered AV loading forces, characteristic of a dysfunctional valve, induce biomechanical changes associated with tissue remodeling of the cusps. When applied to human subclinical specimens, uniaxial biomechanical stimulation promotes VIC activation *ex vivo* (192,193). The local environment (paracrine endothelium derived signals), inflammatory cytokines (TGF-β1 and BMPs), biochemical and biomechanical properties of the ECM, and mechanical stimuli induced by hemodynamic forces (normal or pathological stretching of the valve tissue) regulate VIC phenotype and function (27, 164, 192, 193). A combination of uniaxial mechanical stimulation and cytokines can induce the expression of markers that characterize end-stage disease in surgically resected AV leaflets from

asymptomatic AVSc patients (193). In addition, the fibrosa layer in non-calcified AVSc was found to be more susceptible to biomineralization similar to pathological accumulation in end-stage disease. The deposition of calcium on the aortic side of aortic sclerosis tissue is likely due to the presence of nucleation centers, which provide the starting point for calcium nodule formation. Similar results were obtained using a tissue-engineering approach based on ovine decellularized scaffolds repopulated with aortic sclerosis-derived VICs (193). Similarly, human isolated VICs could be seeded on a 3D scaffold and induced by biomechanical stimuli to transdifferentiate into osteogenic VICs.

GAG/PG upregulation in the MV in response to mechanical strain: In many valve pathologies (i.e., myxomatous valve disease, MR, CAVD), significantly altered profiles of ECM components accompany alterations in the mechanical strains within the tissue (93, 98, 199, 238): these measured differences initiated numerous *in vitro* studies to fully characterize and link tissue-level deformation to cellular response. Static and cyclic tissue strains can profoundly influence the biosynthetic responses of VICs *in vitro* and modulate cell function through the synthesis of new ECM molecules and the degradation of matrix by MMPs and other proteases. Gupta et al. used an *in vitro* 3-dimensional tissue-engineering collagen model to investigate the effects of various static strain conditions (i.e., uniaxial and biaxial) on the production of specific GAG profiles by VICs isolated from MV leaflets and chordae separately (99). To fully elucidate the role of the *in vivo* environment on GAG/PG synthesis, Gupta et al. used a similar 3D culture model and a cyclic stretching device to analyze the strain response of these cells to cyclic stretch (100). Cyclic stretch induces upregulation of total GAGs and of individual GAG classes secreted into the culture medium. Chordal cells respond to cyclic strains more rapidly than cells from the MV leaflets, which is in line with the physiology of myxomatous valve disease in which chordal regions undergo the most change. The results from this study are important in understanding the role of GAG/PGs in valve remodeling.

MVIC plasticity in Myxomatous MV disease: The prolapse of the MV leaflet is a hallmark of several disorders affecting this heart valve, such as myxomatous mitral valve disease (MMVD) or the pseudo-prolapse in chronic ischemic mitral regurgitation (MR) among others, and is only treated surgically (75,101). MMVD is expected to occur in approximately 7.2 million individuals in the US, and over 144 million worldwide and is therefore an important clinical and social problem (101, 220). Myxomatous degeneration is defined by the accumulation of mucopolysaccharides responsible for the thickening and “proliferative” aspect of valve tissue. Increasing evidence suggests that MVICs play a critical role in the pathological remodeling of MV leaflets. Histological analysis and cellular characterization of human MV explants suggest that during myxomatous MVP development, healthy quiescent MVICs undergo a phenotypic activation via the upregulation of the BMP4-mediated pathway (20,48,220). Recent studies have suggested developmentally regulated expression of BMPs and Sox9 during the AVV formation (20). BMPs belong to TGF-β super family of cytokines and have been implicated in numerous developmental processes including proper septation and valvulogenesis. BMP2 and BMP4 are known to be potent osteogenic morphogens and are shown to be present in ossified valves (168). BMP4 is also a potent inducer of collagen, proteoglycan synthesis, and matrix mineralization and acts

as a signal from the myocardium directly mediating atrioventricular septation. Defects in this process are shown to cause one of the most common human congenital heart abnormalities, atrioventricular canal defect. A possible association of BMP signaling pathways is suggested in a MMP-2 transgenic mouse model of MVP (153). Histological analysis of human explants reveal that the structure of the MV leaflet is well preserved in the control tissues, while the prolapsed segment show an increase in PG, collagen degradation, and increased cellularity, predominantly in the spongiosa suggesting accumulation of VICs in myxomatous, but not in normal valves. Phenotypically MVICs are characterized by a chondro-osteogenic-like pathway, with elevated levels of α-SMA, Fibronectin and SM22α transcripts when compared to controls.

Multi-scale computational approaches

In the past two decades, many groups have conducted intensive research on predictive heart valve computational models. Advances in numerical modeling and experimental biomechanics have enabled these newly developed models to become increasingly comprehensive and accurate. For the MV for example, studies have included development of constitutive models (159, 196, 197, 230, 285), image-based patient-specific computational models (155, 244, 281, 284), fluid-structure interaction modeling (67,127), inverse models that enable the assessment of the *in vivo* biomechanical properties (133, 207), and coupled modeling of the left ventricle and MV for investigating ischemic MR (289). For example, Einstein et al. modeled the transient vibrations of the MV by constructing a dynamic nonlinear fluid-coupled finite element model of the valve leaflets and chordae tendineae (67, 68). The application of physiological pressure loads results in valvular movement and small-scale acoustic vibrations of the valvular structures. Material changes that preserved leaflet anisotropy were found to preserve overall valve function. On the other hand, material changes that altered leaflet anisotropy had a profound effect on valvular function. These changes were manifest in the acoustic signatures of the valve closure sounds. Abnormally, stiffened valves closed more slowly and were accompanied by lower peak frequencies. Driessen et al. (65, 66) developed a finite-element (FE) model that relates changes in collagen fiber content and orientation to the mechanical loading condition within engineered heart valve constructs, hypothesizing that collagen fibers aligned with principal strain directions and that collagen content increased with fiber stretch. Results from this study indicate that the computed preferred fiber directions are very similar to experimental data from native aortic heart valves. Although these models are a step toward the development of more physiologically relevant models of heart valve structure and function, there is a still a need for true dynamic models that couple tissue (solid) and blood (fluid) and include cell-level interactions. This said, investigators face theoretical, computational, and experimental challenges that makes this a difficult feat.

A good understanding of myocardial biomechanics is necessary for modeling the heart and heart valves. The MV has a particularly complex structure that includes the left ventricular (LV) wall as a structural element. This said the majority of FE efforts have generated isolated MV models but assume that the papillary muscles fixed in space (125). These models have been useful in answering important questions on valve deformation with artificial chordae and the effects of annuloplasty ring shape (154, 195, 283), yet still lack the

important connection to the LV. More recently however, Wenk et al. used MRI to develop an LV FE model that not only includes myocardial contractility, but also the MV leaflets and associated chordae tendineae apparatus (289). The model was then used to answer specific questions on the effect of infarct stiffness on ischemic mitral regurgitation, mainly the degree of MR and the distribution of leaflet stress, whereby a decrease in infarct stiffness causes ventricular wall distension and a 30% increase in the gap area between the leaflets (289). Such work demonstrates the utility and power of computational techniques in answering important questions non-invasively.

Previous FE models of the MV have assumed that the papillary muscles are fixed in space.

Heart valves function at multiple length-scales, as a result, mechanical stimuli have a significant biological impact at the organ, tissue, and cellular levels. As in many physiological systems with responses at various length scales, multiscale-modeling (MSM) methodologies can be used to understand and characterize the dynamics of healthy and diseased heart valves and ultimately, predict VIC mechanobiological response. The ideal MSM will capture the overall behavior of heart valves by enabling communication between simulations at three different length scales: cell, tissue, and organ. Although there are many experimental tools that allow us to investigate the mechanical behavior and response of heart valves at individual scales, fewer techniques are available that span all three levels. For this reason, computational tools that link different scales together become a necessity. Weinberg et al. used a linked framework to create a set of multiscale simulations that examine the behavior of the human AV at all three scales (285, 286). This framework allowed them to compute organ-scale motion, from which they extracted tissue-scale deformations, which were then translated to cell-scale deformations (286). The organ-scale model predicts the motion of the blood, leaflets, and aortic root throughout the full cycle of closing and opening using a dynamic fluid-structure interaction approach. The tissue-scale model simulates AV leaflet response including the layer-specific undulated geometries. Finally, the cell-scale model predicts cellular deformation in the leaflets of the AV by integrating information from the increasing length-scales of the whole organ and tissue. Weinberg et al.'s model enables the analysis of the transient, three-dimensional behavior of the AV at the organ-, tissue-, and cell-scales and provides promising applications to further understand healthy and diseased AV function. The reader is referred to the review by Weinberg et al. (286) for a more detailed overview of multiscale modeling of heart valve biomechanics.

Integrated computational-experimental approaches—As in all areas of scientific inquiry, experimental data are necessary and must be used to acquire data on heart valve response to different stress levels in all size scales. When tightly integrated with computational models, it can give unique insights into the function and physiology of heart valves and provide a powerful platform that can generate confirmable predictions of heart valve physiological behavior and ultimately, link organ-level and tissue-level deformations to cellular response. Computational models that are linked to experimental data are formed during three distinct phases in the model development process: observation, fitting, and validation (174). We show two examples of this approach.

Layer specific MVIC-ECM coupling: More recently, several groups have linked tissue-level induced stress and the resulting MV interstitial cell (MVIC) deformation to abnormal biosynthetic activity that can lead to reduced tissue-level maintenance and subsequent organ-level failure. To link tissue-level loading and cellular response and thus, gain more insights into MVIC mechanobiology, we developed an integrated experimental-computational approach that informs us on MVIC biophysical state. First, we quantified the *in situ* layer-specific MVIC deformation for all four layers of the MV under controlled biaxial tension using a biaxial stretching device that is coupled to a multi-photon microscope (35) (Fig. 16). We then used a macro-micro finite element computational model to explore the relationship between layer-specific mechanical and structure properties and MVIC stiffness and deformation. The experimental results indicate a significantly larger deformation in both the ventricularis and fibrosa layers of the MV compared to the spongiosa and atrialis layers, with a NAR as high as 3.3 at the maximum physiological tension of 150 N/m. The simulated MVIC moduli however were found to be relatively similar and within a narrow range of 4.71–5.35 kPa (Figs. 16 and 17). This is an important finding that suggests that MVIC deformation is controlled by the structure and composition of the microenvironment rather than the intrinsic cellular stiffness. From this finding, it can be concluded that while MVICs may phenotypically similar throughout the layers of the leaflet, they experience different mechanical stimuli from the layer-specific microenvironment in which they reside.

Isolated VIC behavior: We recently developed a novel solid-mixture model for VIC biomechanical behavior that captures the modulating mechanical responses of VICs resulting from different activation sates and loading conditions (221). One major driver for this study was the 100-fold disparity between the micropipette and AFM VIC moduli observed, where the micropipette estimated a ~0.5 kPa modulus (Fig. 15) while the AFM exhibited a ~50 kPa modulus (Figs. 18 and 21). While differences in experimental loading configurations may account for some of the observed differences, the major discrepancies in activation states (MA – inactivated, AFM – highly activated) are likely the major underlying cause.

To explore this hypothesis, we developed the following model, which incorporated: (1) the underlying cytoskeletal network, (2) the α-SMA stress fibers, and (3) a finite deformable elastic nucleus. To handle the material and geometric nonlinearity, we implemented the model in a 3D finite element simulation and calibrated the model parameters using combined mechanical responses of VICs in both MA and AFM experiments (163, 165) (Fig. 18). We then used the resulting model to examine the mechanical responses of both aortic and pulmonary VICs (AVICs and PVICs, respectively) in both their inactivated states (during MA experiments) and activated states (during AFM experiments) (Figs. 19 and 20).

The resulting simulation indicated that AVICs exhibit 9 to 16 times stronger intrinsic contractile responses to PVICs, highlighting the model's ability to predict the cellular stiffening that is caused by the underlying α-SMA fiber contraction (Fig. 21). We used the same model to calculate traction forces exerted by the VICs on the substrate and found good agreement with previously reported traction force microscopy results. The estimated nuclear stiffness for both AVIC and PVIC were similar and comparable to the literature, and were unaffected by VIC activation level. Results from this study highlight that in inactivated

states, the α-SMA fiber stiffness is the main contributor of the underlying cytoskeletal stiffness, suggesting that any increases that are seen in VIC stiffness when it changes from inactive to active state are due to the contraction of the α-SMA fibers. Although we chose to follow a continuum approach, such a model can be easily incorporated into a multiscale model of the heart valve, wherein the multiscale model is used to answer important questions on the mechanics and mechanobiology of heart valve disease and surgical repair.

Conclusions

Physiological function and stimuli occur on multiple length scales. Similar to other biological systems, heart valve functional physiology can be explored using a multiscale organ/tissue/cell approach. Biomechanics is thus ideal for the study of heart valve functional physiology as it takes a more “integrated” approach that is more common in the biological sciences. While the literature on heart valve biomechanics and mechanobiology is extensive, there are still many gaps that need to be filled. Key aspects can be concluded, following our organ → tissue → cell level approach (Figs. 1 and 2):

At the organ level:

1. Heart valves ensure the unidirectional blood flow in the heart. While this physiological function may seem basic and simple, it requires extremely sophisticated valvular “apparatus” that permits blood to flow both efficiently and rapidly with minimal fluid loss.
2. Though they consist of a number of different components (i.e., leaflets, chordae tendineae, and annulus), heart valves function as fully integrated units whose motion encompasses all of its different components.
3. Valve motion is rapid and involves complex hemodynamic and mechanical interactions with the surrounding blood, inducing large, spatial- and time-varying flow patterns as well as fluid-induced shear forces on valve surfaces.

At the tissue level:

1. Tissue level function is dominated by the following functional needs:
    a. High tensile strength to resist the high TVPs.
    b. Low flexural rigidity to allow passive interaction with the surrounding blood.
    c. Ability to undergo large, rapid, directionally dependent strain during closing.
2. Tissue functional requirements are met through a uniquely designed structure that:
    a. Consists of type I collagen fibers, which have high tensile strength.
    b. Uses *synchronized* collagen crimp waveform to allow modest strains in the circumferential direction followed by rapid stiffening.

c. Utilizes the rotation of collagen fibers to facilitate the very large radial strains—this is an important design feature since collagen fibers typically fail at 8% to 10% strain once fully straightened.

d. Takes on a multilayered structure to facilitate low flexural rigidity and provide additional support during valve closure and coaptation.

e. Consist of elastic fibers in the ventricularis (and atrialis in AVV), which help facilitate rapid retraction of the valve in the radial direction during opening.

3. The high level of durability that is required is accomplished by a largely redundant design—heart valves are "overbuilt" and have an estimated failure stress that is ~20 times larger than functional stress levels.

At the cell level:

1. Heart valves consist of VECs and VICs. Although physical communication between the two cell populations may exist, there have been no observable direction junctions to date.

2. VICs reside within the different layers of the valve leaflets and consist of a heterogeneous population of smooth muscle cells, fibroblasts, and myofibroblasts that are phenotypically reversible, transdifferentiating into myofibroblasts during valve development, disease, and remodeling.

3. Higher TVPs on the left side of the heart impose larger local tissue stresses on VICs. As such, AVICs and MVICs have a higher intracellular stiffness and biosynthetic capability.

The focus of this review has been on heart valve functional physiology, more specifically the biomechanical behavior and the underlying VIC mechanobiology. We are now entering a level of bioengineering knowledge of valvular function wherein integrated computational-experimental approaches can be more realistically applied. As such, this review has offered a balance of experimental and computational techniques, which have been crucial in furthering our knowledge of heart valves. The ideal heart valve model would be able to simulate VIC behavior in response to mechanical inputs, such as tissue and cellular strains. Such a model will prove to be a useful tool that can predict VIC mechanobiological response to altered valvular tissue stresses in different disease states and surgical repair scenarios. Predicted outputs should not only include VIC three-dimensional geometry and deformation, but also phenotypic and biosynthetic cellular response will include cytokine and chemokine levels, the expression of MMPs, collagen (i.e., HSP47 and prolyl 4-hydroxylase), GAGs/PGs, and phenotypic markers, such as α-SMA. Although significant computational and experimental work in this area still remains, the development of innovative and physiologically realistic models that connect VIC mechanobiological response to organ- and tissue-level deformations will improve our understanding of the underlying functional physiology of heart valves. Such models will enable us to quantitatively establish the relations and mechanisms that lead to recovered tissue homeostasis after variations in valve tissue stress at various length scales. These approaches will pave the way for powerful and

exciting platforms that will improve our understanding of valve disease and lay the basis for more successful treatments and novel surgical repair techniques.

Acknowledgments

This work is funded by the National Institutes for Health (NIH) grants R01 HL119297, HL63954, HL103723, HL73021, and HL131872, the American Heart Association (AHA) GRNT24810002 (G. Ferrari), and The Valley Hospital Foundation “Marjorie G. Bunnell Charitable Fund” (G. Ferrari).

References

1. Abrams J. The aortic valve by Mano Thubrikar Crc Press, Inc., Boca Raton (1990) 221 pages, illustrated, $97.50 ISBN: 0–8493–4771–8. Clin Cardiol. 1991; 14:364a–365.
2. Accola KD, Scott ML, Thompson PA, Palmer GJ III, Sand ME, Ebra G. Midterm outcomes using the physio ring in mitral valve reconstruction: Experience in 492 patients. Ann Thorac Surg. 2005; 79:1276–1283. discussion 1276–1283. [PubMed: 15797062]
3. Adamczyk MM, Vesely I. Characteristics of compressive strains in porcine aortic valves cusps. J Heart Valve Dis. 2002; 11:75–83. [PubMed: 11843509]
4. Aikawa E, Otto CM. Look more closely at the valve: Imaging calcific aortic valve disease. Circulation. 2012; 125:9–11. [PubMed: 22090164]
5. Aikawa E, Whittaker P, Farber M, Mendelson K, Padera RF, Aikawa M, Schoen FJ. Human semilunar cardiac valve remodeling by activated cells from fetus to adult: Implications for postnatal adaptation, pathology, and tissue engineering. Circulation. 2006; 113:1344–1352. [PubMed: 16534030]
6. Akdemir R, Ozhan H, Bulur S, Unlu H, Gunduz H, Arinc H, Yildiz A, Uyan C. Color M-mode regurgitant flow propagation velocity: A new echocardiographic method for grading of mitral regurgitation. Echocardiography (Mount Kisco, NY. 2005; 22:713–722.
7. Alfieri CM, Cheek J, Chakraborty S, Yutzey KE. Wnt signaling in heart valve development and osteogenic gene induction. Dev Biol. 2010; 338:127–135. [PubMed: 19961844]
8. Anderson RH, Ho SY, Becker AE. Anatomy of the human atrioventricular junctions revisited. Anat Rec. 2000; 260:81–91. [PubMed: 10967539]
9. Armstrong EJ, Bischoff J. Heart valve development: Endothelial cell signaling and differentiation. Circ Res. 2004; 95:459–470. [PubMed: 15345668]
10. Arts T, Meerbaum S, Reneman R, Corday E. Stresses in the closed mitral valve: A model study. J Biomech. 1983; 16:539–547. [PubMed: 6619171]
11. Bairati A, DeBiasi S. Presence of a smooth muscle system in aortic valve leaflets. Anat Embryol (Berl). 1981; 161:329–340. [PubMed: 7187826]
12. Balachandran K, Alford PW, Wylie-Sears J, Goss JA, Grosberg A, Bischoff J, Aikawa E, Levine RA, Parker KK. Cyclic strain induces dual-mode endothelial-mesenchymal transformation of the cardiac valve. Proc Natl Acad Sci U S A. 2011; 108:19943–19948. [PubMed: 22123981]
13. Balachandran K, Konduri S, Sucosky P, Jo H, Yoganathan A. An ex vivo study of the biological properties of porcine aortic valves in response to circumferential cyclic stretch. Ann Biomed Eng. 2006; 34:1655–1665.
14. Balachandran K, Sucosky P, Jo H, Yoganathan AP. Elevated cyclic stretch alters matrix remodeling in aortic valve cusps: Implications for degenerative aortic valve disease. Am J Physiol Heart Circ Physiol. 2009; 296:H756–H764. [PubMed: 19151254]
15. Barczyk M, Carracedo S, Gullberg D. Integrins. Cell Tissue Res. 2010; 339:269–280. [PubMed: 19693543]
16. Beckmann E, Grau JB, Sainger R, Poggio P, Ferrari G. Insights into the use of biomarkers in calcific aortic valve disease. J Heart Valve Dis. 2010; 19:441–452. [PubMed: 20845891]
17. Bellhouse BJ, Bellhouse FH. Fluid mechanics of the mitral valve. Nature. 1969; 224:615–618. [PubMed: 5346605]
18. Bellhouse BJ, Reid KG. Fluid mechanics of the aortic valve. Br Heart J. 1969; 31:391.

19. Benton JA, Kern HB, Leinwand LA, Mariner PD, Anseth KS. Statins block calcific nodule formation of valvular interstitial cells by inhibiting alpha-smooth muscle actin expression. Arterioscler Thromb Vasc Biol. 2009; 29:1950–1957. [PubMed: 19679827]
20. Beppu H, Malhotra R, Beppu Y, Lepore JJ, Parmacek MS, Bloch KD. BMP type II receptor regulates positioning of outflow tract and remodeling of atrioventricular cushion during cardiogenesis. Dev Biol. 2009; 331:167–175. [PubMed: 19409885]
21. Billiar KL, Sacks MS. Biaxial mechanical properties of the native and glutaraldehyde-treated aortic valve cusp: Part II–A structural constitutive model. J Biomech Eng. 2000b; 122:327–335. [PubMed: 11036555]
22. Billiar KL, Sacks MS. Biaxial mechanical properties of the natural and glutaraldehyde treated aortic valve cusp–Part I: Experimental results. J Biomech Eng. 2000a; 122:23–30. [PubMed: 10790826]
23. Blevins TL, Carroll JL, Raza AM, Grande-Allen KJ. Phenotypic characterization of isolated valvular interstitial cell subpopulations. J Heart Valve Dis. 2006; 15:815–822. [PubMed: 17152790]
24. Booz GW, Baker KM. Molecular signalling mechanisms controlling growth and function of cardiac fibroblasts. Cardiovasc Res. 1995; 30:537–543. [PubMed: 8575002]
25. Bouma W, Lai EK, Levack MM, Shang EK, Pouch AM, Eperjesi TJ, Plappert TJ, Yushkevich PA, Mariani MA, Khabbaz KR, Gleason TG, Mahmood F, Acker MA, Woo YJ, Cheung AT, Jackson BM, Gorman JH III, Gorman RC. Preoperative three-dimensional valve analysis predicts recurrent ischemic mitral regurgitation after mitral annuloplasty. Ann Thorac Surg. 2016; 101:567–575. [PubMed: 26688087]
26. Buchanan RM, Sacks MS. Interlayer micromechanics of the aortic heart valve leaflet. Biomech Model Mechanobiol. 2013; 13:813–826. [PubMed: 24292631]
27. Butcher JT, Mahler GJ, Hockaday LA. Aortic valve disease and treatment: The need for naturally engineered solutions. Adv Drug Deliv Rev. 2011; 63:242–268. [PubMed: 21281685]
28. Butcher JT, Nerem RM. Porcine aortic valve interstitial cells in three-dimensional culture: Comparison of phenotype with aortic smooth muscle cells. J Heart Valve Dis. 2004; 13:478–485. discussion 485–476. [PubMed: 15222296]
29. Butcher JT, Nerem RM. Valvular endothelial cells and the mechanoregulation of valvular pathology. Philos Trans R Soc Lond B Biol Sci. 2007; 362:1445–1457. [PubMed: 17569641]
30. Butcher JT, Nerem RM. Valvular endothelial cells regulate the phenotype of interstitial cells in co-culture: Effects of steady shear stress. Tissue Eng. 2006; 12:905–915. [PubMed: 16674302]
31. Butcher JT, Penrod AM, Garcia AJ, Nerem RM. Unique morphology and focal adhesion development of valvular endothelial cells in static and fluid flow environments. Arterioscler Thromb Vasc Biol. 2004; 24:1429–1434. [PubMed: 15117733]
32. Butcher JT, Tressel S, Johnson T, Turner D, Sorescu G, Jo H, Nerem RM. Transcriptional profiles of valvular and vascular endothelial cells reveal phenotypic differences: Influence of shear stress. Arterioscler Thromb Vasc Biol. 2006; 26:69–77. [PubMed: 16293796]
33. Carpentier A. Cardiac valve surgery–the “French correction”. J Thorac Cardiovasc Surg. 1983; 86:323–337. [PubMed: 6887954]
34. Carpentier A, Chauvaud S, Fabiani JN, Deloche A, Relland J, Lessana A, D’Allaines C, Blondeau P, Piwnica A, Dubost C. Reconstructive surgery of mitral valve incompetence: Ten-year appraisal. J Thorac Cardiovasc Surg. 1980; 79:338–348. [PubMed: 7354634]
35. Carruthers, CA., Good, B., D’Amore, A., Liao, J., Amini, R., Watkins, SC., Sacks, MS. ASME 2012 Summer Bioengineering Conference. Fajardo, Puerto Rico: American Society of Mechanical Engineers; 2012. Alterations in the microstructure of the anterior mitral valve leaflet under physiological stress; p. 227-228.
36. Chakraborty S, Cheek J, Sakthivel B, Aronow BJ, Yutzey KE. Shared gene expression profiles in developing heart valves and osteoblast progenitor cells. Physiol Genomics. 2008; 35:75–85. [PubMed: 18612084]
37. Chappell DC, Varner SE, Nerem RM, Medford RM, Alexander RW. Oscillatory shear stress stimulates adhesion molecule expression in cultured human endothelium. Circ Res. 1998; 82:532–539. [PubMed: 9529157]

38. Chaput M, Handschumacher MD, Guerrero JL, Holmvang G, Dal-Bianco JP, Sullivan S, Vlahakes GJ, Hung J, Levine RA. Mitral leaflet adaptation to ventricular remodeling: Prospective changes in a model of ischemic mitral regurgitation. Circulation. 2009; 120:S99–S103. [PubMed: 19752393]
39. Chaput M, Handschumacher MD, Tournoux F, Hua L, Guerrero JL, Vlahakes GJ, Levine RA. Mitral leaflet adaptation to ventricular remodeling: Occurrence and adequacy in patients with functional mitral regurgitation. Circulation. 2008; 118:845–852. [PubMed: 18678770]
40. Chen JH, Simmons CA. Cell-matrix interactions in the pathobiology of calcific aortic valve disease: Critical roles for matricellular, matricrine, and matrix mechanics cues. Circ Res. 2011; 108:1510–1524. [PubMed: 21659654]
41. Chester, AH., Kershaw, JDB., Misfeld, M., Sievers, H-H., Yacoub, MH. Second Biennial Meeting of the Society for Heart Valve Disease. Paris: 2003. Specific regional and direcrtional contractile response of aortic cusp tissue-Relevance to valve function; p. 67
42. Chester AH, Misfeld M, Yacoub MH. Receptor-mediated contraction of aortic valve leaflets. J Heart Valve Dis. 2000; 9:250–254. discussion 254–255. [PubMed: 10772043]
43. Christie GW, Barratt-Boyes BG. Age-dependent changes in the radial stretch of human aortic valve leaflets determined by biaxial stretching. Ann Thorac Surg. 1995; 60:S156–S159. [PubMed: 7646149]
44. Christie GW, Barratt-Boyes BG. Biaxial mechanical properties of explanted aortic allograft leaflets. Ann Thorac Surg. 1995; 60:S160–S164. [PubMed: 7646150]
45. Christie GW, Barratt-Boyes BG. Mechanical properties of porcine pulmonary valve leaflets: How do they differ from aortic leaflets? Ann Thorac Surg. 1995; 60:S195–S199. [PubMed: 7646158]
46. Chuong CJ, Fung YC. On residual stress in arteries. J Biomech Eng. 1986; 108:189–192. [PubMed: 3079517]
47. Cole WG, Chan D, Hickey AJ, Wilcken DE. Collagen composition of normal and myxomatous human mitral heart valves. Biochem J. 1984; 219:451–460. [PubMed: 6430269]
48. Combs MD, Yutzey KE. Heart valve development: Regulatory networks in development and disease. Circ Res. 2009; 105:408–421. [PubMed: 19713546]
49. Combs MD, Yutzey KE. VEGF and RANKL regulation of NFATc1 in heart valve development. Circ Res. 2009; 105:565–574. [PubMed: 19661463]
50. Courtney T, Sacks MS, Stankus J, Guan J, Wagner WR. Design and analysis of tissue engineering scaffolds that mimic soft tissue mechanical anisotropy. Biomaterials. 2006; 27:3631–3638. [PubMed: 16545867]
51. Cowell SJ, Newby DE, Prescott RJ, Bloomfield P, Reid J, Northridge DB, Boon NA. A randomized trial of intensive lipid-lowering therapy in calcific aortic stenosis. N Engl J Med. 2005; 352:2389–2397. [PubMed: 15944423]
52. Cucina A, Sterpetti AV, Pupelis G, Fragale A, Lepidi S, Cavallaro A, Giustiniani Q, Santoro D'Angelo L. Shear stress induces changes in the morphology and cytoskeleton organisation of arterial endothelial cells. Eur J Vasc Endovasc Surg. 1995; 9:86–92. [PubMed: 7664019]
53. Dal-Bianco JP, Aikawa E, Bischoff J, Guerrero JL, Handschumacher MD, Sullivan S, Johnson B, Titus JS, Iwamoto Y, Wylie-Sears J, Levine RA, Carpentier A. Active adaptation of the tethered mitral valve: Insights into a compensatory mechanism for functional mitral regurgitation. Circulation. 2009; 120:334–342. [PubMed: 19597052]
54. David H, Boughner DR, Vesely I, Gerosa G. The pulmonary valve. Is it mechanically suitable for use as an aortic valve replacement? Asaio J. 1994; 40:206–212. [PubMed: 8003760]
55. David Merryman W, Shadow Huang HY, Schoen FJ, Sacks MS. The effects of cellular contraction on aortic valve leaflet flexural stiffness. J Biomech. 2006; 39:88–96. [PubMed: 16271591]
56. Davies PF. Mechanisms involved in endothelial responses to hemodynamic forces. Atherosclerosis. 1997; 131(Suppl):S15–17. [PubMed: 9253470]
57. Davies PF, Passerini AG, Simmons CA. Aortic valve: Turning over a new leaf(let) in endothelial phenotypic heterogeneity. Arterioscler Thromb Vasc Biol. 2004; 24:1331–1333. [PubMed: 15297285]
58. Davies PF, Remuzzi A, Gordon EJ, Dewey CF Jr, Gimbrone MA Jr. Turbulent fluid shear stress induces vascular endothelial cell turnover in vitro. Proc Natl Acad Sci U S A. 1986; 83:2114–2117. [PubMed: 3457378]

59. Davies PF, Shi C, Depaola N, Helmke BP, Polacek DC. Hemodynamics and the focal origin of atherosclerosis: A spatial approach to endothelial structure, gene expression, and function. Ann N Y Acad Sci. 2001; 947:7–16. discussion 16–17. [PubMed: 11795312]
60. Davies PF, Tripathi SC. Mechanical stress mechanisms and the cell. An endothelial paradigm. Circ Res. 1993; 72:239–245. [PubMed: 8418981]
61. de la Pompa JL, Timmerman LA, Takimoto H, Yoshida H, Elia AJ, Samper E, Potter J, Wakeham A, Marengere L, Langille BL, Crabtree GR, Mak TW. Role of the NF-ATc transcription factor in morphogenesis of cardiac valves and septum. Nature. 1998; 392:182–186. [PubMed: 9515963]
62. de Lange FJ, Moorman AF, Anderson RH, Manner J, Soufan AT, de Gier-de Vries C, Schneider MD, Webb S, van den Hoff MJ, Christoffels VM. Lineage and morphogenetic analysis of the cardiac valves. Circ Res. 2004; 95:645–654. [PubMed: 15297379]
63. Deck JD. Endothelial cell orientation on aortic valve leaflets. Cardiovasc Res. 1986; 20:760–767. [PubMed: 3791342]
64. Dreger SA, Taylor PM, Allen SP, Yacoub MH. Profile and localization of matrix metalloproteinases (MMPs) and their tissue inhibitors (TIMPs) in human heart valves. J Heart Valve Dis. 2002; 11:875–880. discussion 880. [PubMed: 12479292]
65. Driessen NJ, Boerboom RA, Huyghe JM, Bouten CV, Baaijens FP. Computational analyses of mechanically induced collagen fiber remodeling in the aortic heart valve. J Biomech Eng. 2003; 125:549–557. [PubMed: 12968580]
66. Driessen NJ, Bouten CV, Baaijens FP. Improved prediction of the collagen fiber architecture in the aortic heart valve. J Biomech Eng. 2005; 127:329–336. [PubMed: 15971711]
67. Einstein DR, Kunzelman KS, Reinhall PG, Cochran RP, Nicosia MA. Haemodynamic determinants of the mitral valve closure sound: A finite element study. Med Biol Eng Comput. 2004; 42:832–846. [PubMed: 15587476]
68. Einstein DR, Kunzelman KS, Reinhall PG, Nicosia MA, Cochran RP. The relationship of normal and abnormal microstructural proliferation to the mitral valve closure sound. J Biomech Eng. 2005; 127:134–147. [PubMed: 15868796]
69. Engelmayr GC Jr, Hildebrand DK, Sutherland FW, Mayer JE Jr, Sacks MS. A novel bioreactor for the dynamic flexural stimulation of tissue engineered heart valve biomaterials. Biomaterials. 2003; 24:2523–2532. [PubMed: 12695079]
70. Farivar RS, Cohn LH, Soltesz EG, Mihaljevic T, Rawn JD, Byrne JG. Transcriptional profiling and growth kinetics of endothelium reveals differences between cells derived from porcine aorta versus aortic valve. Eur J Cardiothorac Surg. 2003; 24:527–534. [PubMed: 14500070]
71. Fasol R, Meinhart J, Deutsch M, Binder T. Mitral valve repair with the Colvin-Galloway Future Band. Ann Thorac Surg. 2004; 77:1985–1988. discussion 1988. [PubMed: 15172250]
72. Filip DA, Radu A, Simionescu M. Interstitial cells of the heart valve possess characteristics similar to smooth muscle cells. Circ Res. 1986; 59:310–320. [PubMed: 3769149]
73. Flameng W, Herijgers P, Bogaerts K. Recurrence of mitral valve regurgitation after mitral valve repair in degenerative valve disease. Circulation. 2003; 107:1609–1613. [PubMed: 12668494]
74. Fondard O, Detaint D, Iung B, Choqueux C, Adle-Biassette H, Jarraya M, Hvass U, Couetil JP, Henin D, Michel JB, Vahanian A, Jacob MP. Extracellular matrix remodelling in human aortic valve disease: The role of matrix metalloproteinases and their tissue inhibitors. Eur Heart J. 2005; 26:1333–1341. [PubMed: 15827062]
75. Freed LA, Benjamin EJ, Levy D, Larson MG, Evans JC, Fuller DL, Lehman B, Levine RA. Mitral valve prolapse in the general population: The benign nature of echocardiographic features in the Framingham Heart Study. J Am Coll Cardiol. 2002; 40:1298–1304. [PubMed: 12383578]
76. Freeman RV, Otto CM. Management of asymptomatic valvular aortic stenosis. Indian Heart J. 2002; 54:31–38. [PubMed: 11999085]
77. Freeman RV, Otto CM. Spectrum of calcific aortic valve disease: Pathogenesis, disease progression, and treatment strategies. Circulation. 2005; 111:3316–3326. [PubMed: 15967862]
78. Frisch-Fay, R. Flexible Bars. Washington, DC: Butterworths; 1962.
79. Fung YC. What are the residual stresses doing in our blood vessels? Ann Biomed Eng. 1991; 19:237–249. [PubMed: 1928868]

80. Fung YC, Liu SQ. Changes of zero-stress state of rat pulmonary arteries in hypoxic hypertension. J Appl Physiol. 1991; 70:2455–2470. [PubMed: 1885439]
81. Ge L, Sotiropoulos F. Direction and magnitude of blood flow shear stresses on the leaflets of aortic valves: Is there a link with valve calcification? J Biomech Eng. 2010; 132:014505. [PubMed: 20524753]
82. Gharacholou SM, Karon BL, Shub C, Pellikka PA. Aortic valve sclerosis and clinical outcomes: Moving toward a definition. Am J Med. 2011; 124:103–110. [PubMed: 21295189]
83. Gillinov AM, Blackstone EH, White J, Howard M, Ahkrass R, Marullo A, Cosgrove DM. Durability of combined aortic and mitral valve repair. Ann Thorac Surg. 2001; 72:20–27. [PubMed: 11465179]
84. Gillinov AM, Cosgrove DM III, Shiota T, Qin J, Tsujino H, Stewart WJ, Thomas JD, Porqueddu M, White JA, Blackstone EH. Cosgrove-Edwards Annuloplasty System: Midterm results. Ann Thorac Surg. 2000; 69:717–721. [PubMed: 10750749]
85. Gillinov AM, Cosgrove DM, Blackstone EH, Diaz R, Arnold JH, Lytle BW, Smedira NG, Sabik JF, McCarthy PM, Loop FD. Durability of mitral valve repair for degenerative disease. J Thorac Cardiovasc Surg. 1998; 116:734–743. [PubMed: 9806380]
86. Girard PR, Nerem RM. Shear stress modulates endothelial cell morphology and F-actin organization through the regulation of focal adhesion-associated proteins. J Cell Physiol. 1995; 163:179–193. [PubMed: 7534769]
87. Gittenberger-de Groot AC, Vrancken Peeters MP, Mentink MM, Gour-die RG, Poelmann RE. Epicardium-derived cells contribute a novel population to the myocardial wall and the atrioventricular cushions. Circ Res. 1998; 82:1043–1052. [PubMed: 9622157]
88. Gloeckner DC, Billiar KL, Sacks MS. Effects of mechanical fatigue on the bending properties of the porcine bioprosthetic heart valve. Asaio J. 1999; 45:59–63. [PubMed: 9952009]
89. Go AS, Mozaffarian D, Roger VL, Benjamin EJ, Berry JD, Blaha MJ, Dai S, Ford ES, Fox CS, Franco S, Fullerton HJ, Gillespie C, Hailpern SM, Heit JA, Howard VJ, Huffman MD, Judd SE, Kissela BM, Kittner SJ, Lackland DT, Lichtman JH, Lisabeth LD, Mackey RH, Magid DJ, Marcus GM, Marelli A, Matchar DB, McGuire DK, Mohler ER III, Moy CS, Mussolino ME, Neumar RW, Nichol G, Pandey DK, Paynter NP, Reeves MJ, Sorlie PD, Stein J, Towfighi A, Turan TN, Virani SS, Wong ND, Woo D, Turner MB. Heart disease and stroke statistics–2014 update: A report from the American Heart Association. Circulation. 2014; 129:e28–e292. [PubMed: 24352519]
90. Goldstein D, Moskowitz AJ, Gelijns AC, Ailawadi G, Parides MK, Perrault LP, Hung JW, Voisine P, Dagenais F, Gillinov AM, Thourani V, Argenziano M, Gammie JS, Mack M, Demers P, Atluri P, Rose EA, O'Sullivan K, Williams DL, Bagiella E, Michler RE, Weisel RD, Miller MA, Geller NL, Taddei-Peters WC, Smith PK, Moquete E, Overbey JR, Kron IL, O'Gara PT, Acker MA. Two-year outcomes of surgical treatment of severe ischemic mitral regurgitation. N Engl J Med. 2016; 374:344–353. [PubMed: 26550689]
91. Gorman JH III, Gupta KB, Streicher JT, Gorman RC, Jackson BM, Ratcliffe MB, Bogen DK, Edmunds LH Jr. Dynamic three-dimensional imaging of the mitral valve and left ventricle by rapid sonomicrometry array localization. J Thorac Cardiovasc Surg. 1996; 112:712–726. [PubMed: 8800160]
92. Gorman JH III, Jackson BM, Enomoto Y, Gorman RC. The effect of regional ischemia on mitral valve annular saddle shape. Ann Thorac Surg. 2004; 77:544–548. [PubMed: 14759435]
93. Grande-Allen KJ, Griffin BP, Ratliff NB, Cosgrove DM, Vesely I. Glycosaminoglycan profiles of myxomatous mitral leaflets and chordae parallel the severity of mechanical alterations. J Am Coll Cardiol. 2003; 42:271–277. [PubMed: 12875763]
94. Grashow JS, Sacks MS, Liao J, Yoganathan AP. Planar biaxial creep and stress relaxation of the mitral valve anterior leaflet. Ann Biomed Eng. 2006a; 34:1509–1518. [PubMed: 17016761]
95. Grashow JS, Yoganathan AP, Sacks MS. Biaxial stress-stretch behavior of the mitral valve anterior leaflet at physiologic strain rates. Ann Biomed Eng. 2006b; 34:315–325. [PubMed: 16450193]
96. Grau JB, Poggio P, Sainger R, Vernick WJ, Seefried WF, Branchetti E, Field BC, Bavaria JE, Acker MA, Ferrari G. Analysis of osteopontin levels for the identification of asymptomatic patients with calcific aortic valve disease. Ann Thorac Surg. 2012; 93:79–86. [PubMed: 22093695]

97. Guilak F, Mow VC. The mechanical environment of the chondrocyte: A biphasic finite element model of cell-matrix interactions in articular cartilage. J Biomech. 2000; 33:1663–1673. [PubMed: 11006391]

98. Gupta V, Grande-Allen KJ. Effects of static and cyclic loading in regulating extracellular matrix synthesis by cardiovascular cells. Cardiovasc Res. 2006; 72:375–383. [PubMed: 17010955]

99. Gupta V, Werdenberg JA, Blevins TL, Grande-Allen KJ. Synthesis of glycosaminoglycans in differently loaded regions of collagen gels seeded with valvular interstitial cells. Tissue Eng. 2007; 13:41–49. [PubMed: 17518580]

100. Gupta V, Werdenberg JA, Lawrence BD, Mendez JS, Stephens EH, Grande-Allen KJ. Reversible secretion of glycosaminoglycans and proteoglycans by cyclically stretched valvular cells in 3D culture. Ann Biomed Eng. 2008; 36:1092–1103. [PubMed: 18425579]

101. Guy TS, Hill AC. Mitral valve prolapse. Annu Rev Med. 2012; 63:277–292. [PubMed: 22248324]

102. Hafizi S, Taylor PM, Chester AH, Allen SP, Yacoub MH. Mitogenic and secretory responses of human valve interstitial cells to vasoactive agents. J Heart Valve Dis. 2000; 9:454–458. [PubMed: 10888105]

103. Hartiala JJ, Mostbeck GH, Foster E, Fujita N, Dulce MC, Chazouilleres AF, Higgins CB. Velocity-encoded cine MRI in the evaluation of left ventricular diastolic function: Measurement of mitral valve and pulmonary vein flow velocities and flow volume across the mitral valve. Am Heart J. 1993; 125:1054–1066. [PubMed: 8465728]

104. Haussinger G, Pfennigs H, Chelapurath A, Reul H, Essers U. Influence of platelet aggregation inhibitors on platelet damage at prosthetic heart valves in-vitro (author's transl). Biomed Tech (Berlin). 1981; 26:99–102. [PubMed: 6788103]

105. He Z, Ritchie J, Grashow JS, Sacks MS, Yoganathan AP. In vitro dynamic strain behavior of the mitral valve posterior leaflet. J Biomech Eng. 2005; 127:504–511. [PubMed: 16060357]

106. He Z, Sacks MS, Baijens L, Wanant S, Shah P, Yoganathan AP. Effects of papillary muscle position on in-vitro dynamic strain on the porcine mitral valve. J Heart Valve Dis. 2003; 12:488–494. [PubMed: 12918852]

107. Helmlinger G, Geiger RV, Fau-Schreck S, Schreck S, Fau-Nerem RM, Nerem RM. Effects of pulsatile flow on cultured vascular endothelial cell morphology. J Biomech Eng. 1991; 113:123–131. [PubMed: 1875686]

108. Henney AM, Parker DJ, Davies MJ. Collagen biosynthesis in normal and abnormal human heart valves. Cardiovasc Res. 1982; 16:624–630. [PubMed: 7168838]

109. Hilbert SL, Barrick MK, Ferrans VJ. Porcine aortic valve bioprostheses: A morphologic comparison of the effects of fixation pressure. J Biomed Mater Res. 1990; 24:773–787. [PubMed: 2113925]

110. Hilbert SL, Ferrans VJ, Swanson WM. Optical methods for the nondestructive evaluation of collagen morphology in bioprosthetic heart valves. J Biomed Mater Res. 1986; 20:1411–1421. [PubMed: 3782189]

111. Hinton RB Jr, Lincoln J, Deutsch GH, Osinska H, Manning PB, Benson DW, Yutzey KE. Extracellular matrix remodeling and organization in developing and diseased aortic valves. Circ Res. 2006; 98:1431–1438. [PubMed: 16645142]

112. Hinton RB, Yutzey KE. Heart valve structure and function in development and disease. Annu Rev Physiol. 2011; 73:29–46. [PubMed: 20809794]

113. Hoffman JI, Kaplan S. The incidence of congenital heart disease. J Am Coll Cardiol. 2002; 39:1890–1900. [PubMed: 12084585]

114. Huang HY, Liao J, Sacks MS. In-situ deformation of the aortic valve interstitial cell nucleus under diastolic loading. J Biomech Eng. 2007; 129:880–889. [PubMed: 18067392]

115. Hurle JM, Kitten GT, Sakai LY, Volpin D, Solursh M. Elastic extracellular matrix of the embryonic chick heart: An immunohistological study using laser confocal microscopy. Dev Dyn. 1994; 200:321–332. [PubMed: 7994079]

116. Hurlstone AF, Haramis AP, Wienholds E, Begthel H, Korving J, Van Eeden F, Cuppen E, Zivkovic D, Plasterk RH, Clevers H. The Wnt/beta-catenin pathway regulates cardiac valve formation. Nature. 2003; 425:633–637. [PubMed: 14534590]

117. Jiang X, Rowitch DH, Soriano P, McMahon AP, Sucov HM. Fate of the mammalian cardiac neural crest. Development. 2000; 127:1607–1616. [PubMed: 10725237]
118. Johnson CM, Fass DN. Porcine cardiac valvular endothelial cells in culture. A relative deficiency of fibronectin synthesis in vitro. Lab Invest. 1983; 49:589–598. [PubMed: 6314039]
119. Joyce EM, Liao J, Schoen FJ, Mayer JE Jr, Sacks MS. Functional collagen fiber architecture of the pulmonary heart valve cusp. Ann Thorac Surg. 2009; 87:1240–1249. [PubMed: 19324159]
120. Juliano RL, Haskill S. Signal transduction from the extracellular matrix. J Cell Biol. 1993; 120:577–585. [PubMed: 8381117]
121. Kilner PJ, Yang GZ, Mohiaddin RH, Firmin DN, Longmore DB. Helical and retrograde secondary flow patterns in the aortic arch studied by three-directional magnetic resonance velocity mapping. Circulation. 1993; 88:2235–2247. [PubMed: 8222118]
122. Kim WY, Walker PG, Pedersen EM, Poulsen JK, Oyre S, Houlind K, Yoganathan AP. Left ventricular blood flow patterns in normal subjects: A quantitative analysis by three-dimensional magnetic resonance velocity mapping. J Am Coll Cardiol. 1995; 26:224–238. [PubMed: 7797756]
123. Konduri S, Xing Y, Warnock JN, He Z, Yoganathan AP. Normal physiological conditions maintain the biological characteristics of porcine aortic heart valves: An ex vivo organ culture study. Ann Biomed Eng. 2005; 33:1158–1166. [PubMed: 16133923]
124. Ku CH, Johnson PH, Batten P, Sarathchandra P, Chambers RC, Taylor PM, Yacoub MH, Chester AH. Collagen synthesis by mesenchymal stem cells and aortic valve interstitial cells in response to mechanical stretch. Cardiovasc Res. 2006; 71:548–556. [PubMed: 16740254]
125. Kunzelman KS, Cochran RP, Chuong C, Ring WS, Verrier ED, Eberhart RD. Finite element analysis of the mitral valve. J Heart Valve Dis. 1993; 2:326–340. [PubMed: 8269128]
126. Kunzelman KS, Cochran RP, Verrier ED, Eberhart RC. Anatomic basis for mitral valve modelling. J Heart Valve Dis. 1994; 3:491–496. [PubMed: 8000582]
127. Kunzelman KS, Einstein DR, Cochran RP. Fluid-structure interaction models of the mitral valve: Function in normal and pathological states. Philos Trans R Soc Lond B Biol Sci. 2007; 362:1393–1406. [PubMed: 17581809]
128. Kunzelman KS, Quick DW, Cochran RP. Altered collagen concentration in mitral valve leaflets: Biochemical and finite element analysis. Ann Thorac Surg. 1998; 66:S198–S205. [PubMed: 9930448]
129. Kurtz CE, Otto CM. Aortic stenosis: Clinical aspects of diagnosis and management, with 10 illustrative case reports from a 25-year experience. Medicine. 2010; 89:349–379. [PubMed: 21057260]
130. Laforest B, Andelfinger G, Nemer M. Loss of Gata5 in mice leads to bicuspid aortic valve. J Clin Invest. 2011; 121:2876–2887. [PubMed: 21633169]
131. Lanir Y. Mechanisms of residual stress in soft tissues. J Biomech Eng. 2009; 131:044506. [PubMed: 19275448]
132. Leask RL, Jain N, Butany J. Endothelium and valvular diseases of the heart. Microsc Res Tech. 2003; 60:129–137. [PubMed: 12539167]
133. Lee CH, Amini R, Gorman RC, Gorman JH III, Sacks MS. An inverse modeling approach for stress estimation in mitral valve anterior leaflet valvuloplasty for in-vivo valvular biomaterial assessment. J Biomech. 2014; 47:2055–2063. [PubMed: 24275434]
134. Lee CH, Carruthers CA, Ayoub S, Gorman RC, Gorman JH III, Sacks MS. Quantification and simulation of layer-specific mitral valve interstitial cells deformation under physiological loading. J Theor Biol. 2015; 373:26–39. [PubMed: 25791285]
135. Lee CH, Zhang W, Liao J, Carruthers CA, Sacks JI, Sacks MS. On the presence of affine fibril and fiber kinematics in the mitral valve anterior leaflet. Biophys J. 2015; 108:2074–2087. [PubMed: 25902446]
136. Lee TC, Zhao YD, Courtman DW, Stewart DJ. Abnormal aortic valve development in mice lacking endothelial nitric oxide synthase. Circulation. 2000; 101:2345–2348. [PubMed: 10821808]
137. Lehoux S, Tedgui A. Cellular mechanics and gene expression in blood vessels. J Biomech. 2003; 36:631–643. [PubMed: 12694993]

138. Levay AK, Peacock JD, Lu Y, Koch M, Hinton RB Jr, Kadler KE, Lincoln J. Scleraxis is required for cell lineage differentiation and extracellular matrix remodeling during murine heart valve formation in vivo. Circ Res. 2008; 103:948–956. [PubMed: 18802027]
139. Levine RA, Hagege AA, Judge DP, Padala M, Dal-Bianco JP, Aikawa E, Beaudoin J, Bischoff J, Bouatia-Naji N, Bruneval P, Butcher JT, Carpentier A, Chaput M, Chester AH, Clusel C, Delling FN, Dietz HC, Dina C, Durst R, Fernandez-Friera L, Handschumacher MD, Jensen MO, Jeunemaitre XP, Marec HL, Tourneau TL, Markwald RR, Merot J, Messas E, Milan DP, Neri T, Norris RA, Peal D, Perrocheau M, Probst V, Puceat M, Rosenthal N, Solis J, Schott JJ, Schwammenthal E, Slaugenhaupt SA, Song JK, Yacoub MH. Mitral valve disease-morphology and mechanisms. Nat Rev Cardiol. 2015; 12:689–710. [PubMed: 26483167]
140. Li C, Xu Q. Mechanical stress-initiated signal transductions in vascular smooth muscle cells. Cell Signal. 2000; 12:435–445. [PubMed: 10989277]
141. Liao J, Yang L, Grashow J, Sacks MS. The relation between collagen fibril kinematics and mechanical properties in the mitral valve anterior leaflet. J Biomech Eng. 2007; 129:78–87. [PubMed: 17227101]
142. Liebner S, Cattelino A, Gallini R, Rudini N, Iurlaro M, Piccolo S, Dejana E. Beta-catenin is required for endothelial-mesenchymal transformation during heart cushion development in the mouse. J Cell Biol. 2004; 166:359–367. [PubMed: 15289495]
143. Lincoln J, Alfieri CM, Yutzey KE. BMP and FGF regulatory pathways control cell lineage diversification of heart valve precursor cells. Dev Biol. 2006; 292:292–302. [PubMed: 16680829]
144. Lincoln J, Alfieri CM, Yutzey KE. Development of heart valve leaflets and supporting apparatus in chicken and mouse embryos. Dev Dyn. 2004; 230:239–250. [PubMed: 15162503]
145. Lincoln J, Kist R, Scherer G, Yutzey KE. Sox9 is required for precursor cell expansion and extracellular matrix organization during mouse heart valve development. Dev Biol. 2007; 305:120–132. [PubMed: 17350610]
146. Lincoln J, Lange AW, Yutzey KE. Hearts and bones: Shared regulatory mechanisms in heart valve, cartilage, tendon, and bone development. Dev Biol. 2006; 294:292–302. [PubMed: 16643886]
147. Liu SQ, Fung YC. Relationship between hypertension, hypertrophy, and opening angle of zero-stress state of arteries following aortic constriction. J Biomech Eng. 1989; 111:325–335. [PubMed: 2486372]
148. Lloyd-Jones D, Adams RJ, Brown TM, Carnethon M, Dai S, De Simone G, Ferguson TB, Ford E, Furie K, Gillespie C, Go A, Greenlund K, Haase N, Hailpern S, Ho PM, Howard V, Kissela B, Kittner S, Lackland D, Lisabeth L, Marelli A, McDermott MM, Meigs J, Mozaffarian D, Mussolino M, Nichol G, Roger VL, Rosamond W, Sacco R, Sorlie P, Stafford R, Thom T, Wasserthiel-Smoller S, Wong ND, Wylie-Rosett J. Executive summary: Heart disease and stroke statistics–2010 update: A report from the American Heart Association. Circulation. 2010; 121:948–954. [PubMed: 20177011]
149. Lo D, Vesely I. Biaxial strain analysis of the porcine aortic valve. Ann Thorac Surg. 1995; 60:S374–S378. [PubMed: 7646191]
150. Loukas M, Bilinsky E, Bilinsky S, Blaak C, Tubbs RS, Anderson RH. The anatomy of the aortic root. Clin Anat. 2014; 27:748–756. [PubMed: 24000000]
151. Luscinskas FW, Lawler J. Integrins as dynamic regulators of vascular function. FASEB J. 1994; 8:929–938. [PubMed: 7522194]
152. Ma L, Lu M-F, Schwartz RJ, Martin JF. Bmp2 is essential for cardiac cushion epithelial-mesenchymal transition and myocardial patterning. Development. 2005; 132:5601–5611. [PubMed: 16314491]
153. Mahimkar R, Nguyen A, Mann M, Yeh CC, Zhu BQ, Karliner JS, Lovett DH. Cardiac transgenic matrix metalloproteinase-2 expression induces myxomatous valve degeneration: A potential model of mitral valve prolapse disease. Cardiovasc Pathol. 2009; 18:253–261. [PubMed: 18835790]
154. Maisano F, Redaelli A, Soncini M, Votta E, Arcobasso L, Alfieri O. An annular prosthesis for the treatment of functional mitral regurgitation: Finite element model analysis of a dog bone-shaped ring prosthesis. Ann Thorac Surg. 2005; 79:1268–1275. [PubMed: 15797061]

155. Mansi T, Voigt I, Georgescu B, Zheng X, Mengue EA, Hackl M, Ionasec RI, Noack T, Seeburger J, Comaniciu D. An integrated framework for finite-element modeling of mitral valve biomechanics from medical images: Application to MitralClip intervention planning. Med Image Anal. 2012; 16:1330–1346. [PubMed: 22766456]
156. Markwald RR, Norris RA, Moreno-Rodriguez R, Levine RA. Developmental basis of adult cardiovascular diseases: Valvular heart diseases. Ann N Y Acad Sci. 2010; 1188:177–183. [PubMed: 20201901]
157. Marron K, Yacoub MH, Polak JM, Sheppard MN, Fagan D, Whitehead BF, de Leval MR, Anderson RH, Wharton J. Innervation of human atrioventricular and arterial valves. Circulation. 1996; 94:368–375. [PubMed: 8759078]
158. May-Newman K, Yin FC. Biaxial mechanical behavior of excised porcine mitral valve leaflets. Am J Physiol. 1995; 269:H1319–H1327. [PubMed: 7485564]
159. May-Newman K, Yin FC. A constitutive law for mitral valve tissue. J Biomech Eng. 1998; 120:38–47. [PubMed: 9675679]
160. Mayne AS, Christie GW, Smaill BH, Hunter PJ, Barratt-Boyes BG. An assessment of the mechanical properties of leaflets from four second-generation porcine bioprostheses with biaxial testing techniques. J Thorac Cardiovasc Surg. 1989; 98:170–180. [PubMed: 2755150]
161. McGee EC, Gillinov AM, Blackstone EH, Rajeswaran J, Cohen G, Najam F, Shiota T, Sabik JF, Lytle BW, McCarthy PM, Cosgrove DM. Recurrent mitral regurgitation after annuloplasty for functional ischemic mitral regurgitation. J Thorac Cardiovasc Surg. 2004; 128:916–924. [PubMed: 15573077]
162. Merryman WD, Huang H-YS, Schoen FJ, Sacks MS. The effects of cellular contraction on aortic valve leaflet flexural stiffness. J Biomech. 2006; 39:88–96. [PubMed: 16271591]
163. Merryman WD, Liao J, Parekh A, Candiello JE, Lin H, Sacks MS. Differences in tissue-remodeling potential of aortic and pulmonary heart valve interstitial cells. Tissue Eng. 2007; 13:2281–2289. [PubMed: 17596117]
164. Merryman WD, Lukoff HD, Long RA, Engelmayr GC Jr, Hopkins RA, Sacks MS. Synergistic effects of cyclic tension and transforming growth factor-beta1 on the aortic valve myofibroblast. Cardiovasc Pathol. 2007; 16:268–276. [PubMed: 17868877]
165. Merryman WD, Youn I, Lukoff HD, Krueger PM, Guilak F, Hopkins RA, Sacks MS. Correlation between heart valve interstitial cell stiffness and transvalvular pressure: Implications for collagen biosynthesis. Am J Physiol Heart Circ Physiol. 2006; 290:H224–H231. [PubMed: 16126816]
166. Messier RH Jr, Bass BL, Aly HM, Jones JL, Domkowski PW, Wallace RB, Hopkins RA. Dual structural and functional phenotypes of the porcine aortic valve interstitial population: Characteristics of the leaflet myofibroblast. J Surg Res. 1994; 57:1–21. [PubMed: 8041124]
167. Ming L, Zhen HK. Study of the closing mechanism of natural heart valves. Appl Math Mec. 1986; 7:955–964.
168. Mohler ER III, Gannon F, Reynolds C, Zimmerman R, Keane MG, Kaplan FS. Bone formation and inflammation in cardiac valves. Circulation. 2001; 103:1522–1528. [PubMed: 11257079]
169. Montero JA, Giron B, Arrechedera H, Cheng YC, Scotting P, Chimal-Monroy J, Garcia-Porrero JA, Hurle JM. Expression of Sox8, Sox9 and Sox10 in the developing valves and autonomic nerves of the embryonic heart. Mech Dev. 2002; 118:199–202. [PubMed: 12351187]
170. Moura LM, Ramos SF, Zamorano JL, Barros IM, Azevedo LF, Rocha-Goncalves F, Rajamannan NM. Rosuvastatin affecting aortic valve endothelium to slow the progression of aortic stenosis. J Am Coll Cardiol. 2007; 49:554–561. [PubMed: 17276178]
171. Mulholland DL, Gotlieb AI. Cell biology of valvular interstitial cells. Can J Cardiol. 1996; 12:231–236. [PubMed: 8624972]
172. Nakamura T, Colbert MC, Robbins J. Neural crest cells retain multi-potential characteristics in the developing valves and label the cardiac conduction system. Circ Res. 2006; 98:1547–1554. [PubMed: 16709902]
173. Nicosia MA, Cochran RP, Einstein DR, Rutland CJ, Kunzelman KS. A coupled fluid-structure finite element model of the aortic valve and root. J Heart Valve Dis. 2003; 12:781–789. [PubMed: 14658821]

174. Niederer SA, Smith NP. At the heart of computational modelling. J Physiol. 2012; 590:1331–1338. [PubMed: 22271869]
175. Nkomo VT, Gardin JM, Skelton TN, Gottdiener JS, Scott CG, Enriquez-Sarano M. Burden of valvular heart diseases: A population-based study. Lancet. 2006; 368:1005–1011. [PubMed: 16980116]
176. Nus M, MacGrogan D, Martinez-Poveda B, Benito Y, Casanova JC, Fernandez-Aviles F, Bermejo J, de la Pompa JL. Diet-induced aortic valve disease in mice haploinsufficient for the Notch pathway effector RBPJK/CSL. Arterioscler Thromb Vasc Biol. 2011; 31:1580–1588. [PubMed: 21493891]
177. Ogden, R. Nonlinear elasticity, anisotropy, material stability, and residual stresses in soft tissue. In: Ogden, RW., editor. Biomechanics of Soft Tissue in Cardiovascular System. New York: Springer; 2003.
178. Oh JK, Appleton CP, Hatle LK, Nishimura RA, Seward JB, Tajik AJ. The noninvasive assessment of left ventricular diastolic function with two-dimensional and Doppler echocardiography. J Am Soc Echocardiogr. 1997; 10:246–270. [PubMed: 9109691]
179. Ormiston JA, Shah PM, Tei C, Wong M. Size and motion of the mitral valve annulus in man. I. A two-dimensional echocardiographic method and findings in normal subjects. Circulation. 1981; 64:113–120. [PubMed: 7237707]
180. Otsuji Y, Handschumacher MD, Schwammenthal E, Jiang L, Song JK, Guerrero JL, Vlahakes GJ, Levine RA. Insights from three-dimensional echocardiography into the mechanism of functional mitral regurgitation: Direct in vivo demonstration of altered leaflet tethering geometry. Circulation. 1997; 96:1999–2008. [PubMed: 9323092]
181. Otto CM. Clinical practice. Evaluation and management of chronic mitral regurgitation. N Engl J Med. 2001; 345:740–746. [PubMed: 11547744]
182. Otto CM. Calcific aortic valve disease: Outflow obstruction is the end stage of a systemic disease process. Eur Heart J. 2009; 30:1940–1942. [PubMed: 19608595]
183. Otto CM. Calcific aortic valve disease: New concepts. Semin Thorac Cardiovasc Surg. 2010; 22:276–284. [PubMed: 21549267]
184. Otto CM, Kuusisto J, Reichenbach DD, Gown AM, O'Brien KD. Characterization of the early lesion of 'degenerative' valvular aortic stenosis. Histological and immunohistochemical studies. Circulation. 1994; 90:844–853. [PubMed: 7519131]
185. Owens DS, Otto CM. Is it time for a new paradigm in calcific aortic valve disease? JACC Cardiovasc Imaging. 2009; 2:928–930. [PubMed: 19679279]
186. Parolari A, Tremoli E, Cavallotti L, Trezzi M, Kassem S, Loardi C, Veglia F, Ferrari G, Pacini D, Alamanni F. Do statins improve outcomes and delay the progression of non-rheumatic calcific aortic stenosis? Heart (British Cardiac Society). 2011; 97:523–529. [PubMed: 21270077]
187. Perez-Pomares JM, Gonzalez-Rosa JM, Munoz-Chapuli R. Building the vertebrate heart - an evolutionary approach to cardiac development. Int J Dev Biol. 2009; 53:1427–1443. [PubMed: 19247975]
188. Person AD, Klewer SE, Runyan RB. Cell biology of cardiac cushion development. Int Rev Cytol. 2005; 243:287–335. [PubMed: 15797462]
189. Pflederer T, Achenbach S. Aortic valve stenosis: CT contributions to diagnosis and therapy. J Cardiovasc Comput Tomogr. 2010; 4:355–364. [PubMed: 21051310]
190. Pho M, Lee W, Watt DR, Laschinger C, Simmons CA, McCulloch CA. Cofilin is a marker of myofibroblast differentiation in cells from porcine aortic cardiac valves. Am J Physiol Heart Circ Physiol. 2008; 294:H1767–H1778. [PubMed: 18263709]
191. Pierlot CM, Lee JM, Amini R, Sacks MS, Wells SM. Pregnancy-induced remodeling of collagen architecture and content in the mitral valve. Ann Biomed Eng. 2014; 42:2058–2071. [PubMed: 25103603]
192. Poggio P, Branchetti E, Grau JB, Lai EK, Gorman RC, Gorman JH III, Sacks MS, Bavaria JE, Ferrari G. Osteopontin-CD44v6 interaction mediates calcium deposition via phospho-Akt in valve interstitial cells from patients with noncalcified aortic valve sclerosis. Arterioscler Thromb Vasc Biol. 2014; 34:2086–2094. [PubMed: 25060796]

193. Poggio P, Sainger R, Branchetti E, Grau JB, Lai EK, Gorman RC, Sacks MS, Parolari A, Bavaria JE, Ferrari G. Noggin attenuates the osteogenic activation of human valve interstitial cells in aortic valve sclerosis. Cardiovasc Res. 2013; 98:402–410. [PubMed: 23483047]

194. Prasad AR, Logan SA, Nerem RM, Schwartz CJ, Sprague EA. Flow-related responses of intracellular inositol phosphate levels in cultured aortic endothelial cells. Circ Res. 1993; 72:827–836. [PubMed: 8443870]

195. Prot V, Haaverstad R, Skallerud B. Finite element analysis of the mitral apparatus: Annulus shape effect and chordal force distribution. Biomech Model Mechanobiol. 2009; 8:43–55. [PubMed: 18193309]

196. Prot V, Skallerud B. Nonlinear solid finite element analysis of mitral valves with heterogeneous leaflet layers. Comput Mech. 2009; 43:353–368.

197. Prot V, Skallerud B, Holzapfel G. Transversely isotropic membrane shells with application to mitral valve mechanics. Constitutive modelling and finite element implementation. Int J Numer Methods Eng. 2007; 71:987–1008.

198. Pye MP, Pringle SD, Cobbe SM. Reference values and reproducibility of Doppler echocardiography in the assessment of the tricuspid valve and right ventricular diastolic function in normal subjects. Am J Cardiol. 1991; 67:269–273. [PubMed: 1990791]

199. Quick DW, Kunzelman KS, Kneebone JM, Cochran RP. Collagen synthesis is upregulated in mitral valves subjected to altered stress. Asaio J. 1997; 43:181–186. [PubMed: 9152488]

200. Rabkin E, Aikawa M, Stone JR, Fukumoto Y, Libby P, Schoen FJ. Activated interstitial myofibroblasts express catabolic enzymes and mediate matrix remodeling in myxomatous heart valves. Circulation. 2001; 104:2525–2532. [PubMed: 11714645]

201. Rabkin E, Hoerstrup SP, Aikawa M, Mayer JE Jr, Schoen FJ. Evolution of cell phenotype and extracellular matrix in tissue-engineered heart valves during in-vitro maturation and in-vivo remodeling. J Heart Valve Dis. 2002; 11:308–314. discussion 314. [PubMed: 12056720]

202. Rabkin-Aikawa E, Aikawa M, Farber M, Kratz JR, Garcia-Cardena G, Kouchoukos NT, Mitchell MB, Jonas RA, Schoen FJ. Clinical pulmonary autograft valves: Pathologic evidence of adaptive remodeling in the aortic site. J Thorac Cardiovasc Surg. 2004; 128:552–561. [PubMed: 15457156]

203. Rabkin-Aikawa E, Farber M, Aikawa M, Schoen FJ. Dynamic and reversible changes of interstitial cell phenotype during remodeling of cardiac valves. J Heart Valve Dis. 2004; 13:841–847. [PubMed: 15473488]

204. Rajamannan NM, Evans FJ, Aikawa E, Grande-Allen KJ, Demer LL, Heistad DD, Simmons CA, Masters KS, Mathieu P, O'Brien KD, Schoen FJ, Towler DA, Yoganathan AP, Otto CM. Calcific aortic valve disease: Not simply a degenerative process: A review and agenda for research from the National Heart and Lung and Blood Institute Aortic Stenosis Working Group. Executive summary: Calcific aortic valve disease-2011 update. Circulation. 2011; 124:1783–1791. [PubMed: 22007101]

205. Rajamannan NM, Subramaniam M, Rickard D, Stock SR, Donovan J, Springett M, Orszulak T, Fullerton DA, Tajik AJ, Bonow RO, Spelsberg T. Human aortic valve calcification is associated with an osteoblast phenotype. Circulation. 2003; 107:2181–2184. [PubMed: 12719282]

206. Ranger AM, Grusby MJ, Hodge MR, Gravallese EM, de la Brousse FC, Hoey T, Mickanin C, Baldwin HS, Glimcher LH. The transcription factor NF-ATc is essential for cardiac valve formation. Nature. 1998; 392:186–190. [PubMed: 9515964]

207. Rausch MK, Famaey N, Shultz TO, Bothe W, Miller DC, Kuhl E. Mechanics of the mitral valve: A critical review, an in vivo parameter identification, and the effect of prestrain. Biomech Model Mechanobiol. 2012; 12:1053–1071. [PubMed: 23263365]

208. Rausch MK, Tibayan FA, Miller DC, Kuhl E. Evidence of adaptive mitral leaflet growth. J Mech Behav Biomed Mater. 2012; 15:208–217. [PubMed: 23159489]

209. Reul, H., Talukder, N. The Heart. 7th. McGraw Hill; 1989. Heart valve mechanics.

210. Roberts WC, Ko JM. Frequency by decades of unicuspid, bicuspid, and tricuspid aortic valves in adults having isolated aortic valve replacement for aortic stenosis, with or without associated aortic regurgitation. Circulation. 2005; 111:920–925. [PubMed: 15710758]

211. Rodriguez KJ, Piechura LM, Masters KS. Regulation of valvular interstitial cell phenotype and function by hyaluronic acid in 2-D and 3-D culture environments. Matrix Biol. 2011; 30:70–82. [PubMed: 20884350]
212. Rossebo AB, Pedersen TR, Boman K, Brudi P, Chambers JB, Egstrup K, Gerdts E, Gohlke-Barwolf C, Holme I, Kesaniemi YA, Malbecq W, Nienaber CA, Ray S, Skjaerpe T, Wachtell K, Willenheimer R. Intensive lipid lowering with simvastatin and ezetimibe in aortic stenosis. N Engl J Med. 2008; 359:1343–1356. [PubMed: 18765433]
213. Ruwhof C, van der Laarse A. Mechanical stress-induced cardiac hypertrophy: Mechanisms and signal transduction pathways. Cardiovasc Res. 2000; 47:23–37. [PubMed: 10869527]
214. Sacks MS, Enomoto Y, Graybill JR, Merryman WD, Zeeshan A, Yoganathan AP, Levy RJ, Gorman RC, Gorman JH III. In-vivo dynamic deformation of the mitral valve anterior leaflet. Ann Thorac Surg. 2006; 82:1369–1377. [PubMed: 16996935]
215. Sacks MS, He Z, Baijens L, Wanant S, Shah P, Sugimoto H, Yoganathan AP. Surface strains in the anterior leaflet of the functioning mitral valve. Ann Biomed Eng. 2002; 30:1281–1290. [PubMed: 12540204]
216. Sacks MS, Merryman WD, Schmidt DE. On the biomechanics of heart valve function. J Biomech. 2009; 42:1804–1824. [PubMed: 19540499]
217. Sacks MS, Smith DB, Hiester ED. The aortic valve microstructure: Effects of transvalvular pressure. J Biomed Mater Res. 1998; 41:131–141. [PubMed: 9641633]
218. Sacks MS, Yoganathan AP. Heart valve function: A biomechanical perspective. Philos Trans R Soc Lond B Biol Sci. 2008; 363:2481.
219. Sadoshima J, Izumo S. The cellular and molecular response of cardiac myocytes to mechanical stress. Annu Rev Physiol. 1997; 59:551–571. [PubMed: 9074777]
220. Sainger R, Grau JB, Branchetti E, Poggio P, Seefried WF, Field BC, Acker MA, Gorman RC, Gorman JH III, Hargrove CW III, Bavaria JE, Ferrari G. Human myxomatous mitral valve prolapse: Role of bone morphogenetic protein 4 in valvular interstitial cell activation. J Cell Physiol. 2012; 227:2595–2604. [PubMed: 22105615]
221. Sakamoto Y, Buchanan RM, Sacks MS. On intrinsic stress fiber contractile forces in semilunar heart valve interstitial cells using a continuum mixture model. J Mech Behav Biomed Mater. 2016; 54:244–258. [PubMed: 26476967]
222. Schmidt C, Pommerenke H, Durr F, Nebe B, Rychly J. Mechanical stressing of integrin receptors induces enhanced tyrosine phosphorylation of cytoskeletally anchored proteins. J Biol Chem. 1998; 273:5081–5085. [PubMed: 9478959]
223. Schmidtke C, Poppe D, Dahmen G, Sievers HH. Echocardiographic and hemodynamic characteristics of reconstructed bicuspid aortic valves at rest and exercise. Z Kardiol. 2005; 94:437–444. [PubMed: 15997344]
224. Schoen F. Aortic valve structure-function correlations: Role of elastic fibers no longer a stretch of the imagination. J Heart Valve Dis. 1997; 6:1–6. [PubMed: 9044068]
225. Schoen FJ. Cardiac valves and valvular pathology: Update on function, disease, repair, and replacement. Cardiovasc Pathol. 2005; 14:189–194. [PubMed: 16009317]
226. Schoen FJ. Evolving concepts of cardiac valve dynamics: The continuum of development, functional structure, pathobiology, and tissue engineering. Circulation. 2008; 118:1864–1880. [PubMed: 18955677]
227. Schwammenthal E, Chen C, Benning F, Block M, Breithardt G, Levine RA. Dynamics of mitral regurgitant flow and orifice area. Physiologic application of the proximal flow convergence method: Clinical data and experimental testing. Circulation. 1994; 90:307–322. [PubMed: 8026013]
228. Shelton EL, Yutzey KE. Twist1 function in endocardial cushion cell proliferation, migration, and differentiation during heart valve development. Dev Biol. 2008; 317:282–295. [PubMed: 18353304]
229. Simmons CA, Grant GR, Manduchi E, Davies PF. Spatial heterogeneity of endothelial phenotypes correlates with side-specific vulnerability to calcification in normal porcine aortic valves. Circ Res. 2005; 96:792–799. [PubMed: 15761200]

230. Skallerud B, Prot V, Nordrum IS. Modeling active muscle contraction in mitral valve leaflets during systole: A first approach. Biomech Model Mechanobiol. 2011; 10:11–26. [PubMed: 20419330]

231. Sloth E, Houlind KC, Oyre S, Kim WY, Pedersen EM, Jorgensen HS, Hasenkam JM. Three-dimensional visualization of velocity profiles in the human main pulmonary artery with magnetic resonance phase-velocity mapping. Am Heart J. 1994; 128:1130–1138. [PubMed: 7985593]

232. Smith DB, Sacks MS, Vorp DA, Thornton M. Surface geometric analysis of anatomic structures using biquintic finite element interpolation. Ann Biomed Eng. 2000; 28:598–611. [PubMed: 10983706]

233. Snarr BS, Kern CB, Wessels A. Origin and fate of cardiac mesenchyme. Dev Dyn. 2008; 237:2804–2819. [PubMed: 18816864]

234. Stamatas GN, McIntire LV. Rapid flow-induced responses in endothelial cells. Biotechnol Prog. 2001; 17:383–402. [PubMed: 11386856]

235. Stella JA, Sacks MS. On the biaxial mechanical properties of the layers of the aortic valve leaflet. J Biomech Eng. 2007; 129:757–766. [PubMed: 17887902]

236. Stephens E, Durst C, Swanson J, Grande-Allen KJ, Ingels N Jr, Miller DC. Functional coupling of valvular interstitial cells and collagen via α2β1 integrins in the mitral leaflet. Cel Mol Bioeng. 2010; 3:428–437.

237. Stephens E, Grande-Allen K. Age-related changes in collagen synthesis and turnover in porcine heart valves. J Heart Valve Dis. 2007; 16:672–682. [PubMed: 18095519]

238. Stephens EH, Chu CK, Grande-Allen KJ. Valve proteoglycan content and glycosaminoglycan fine structure are unique to microstructure, mechanical loads, and age: Relevance to an age-specific tissue engineered heart valve. Acta Biomaterial. 2008; 4:1148–1160.

239. Stephens EH, de Jonge N, McNeill MP, Durst CA, Grande-Allen KJ. Age-related changes in material behavior of porcine mitral and aortic valves and correlation to matrix composition. Tissue Eng Part A. 2010; 16:867–878. [PubMed: 19814589]

240. Stephens EH, Durst CA, West JL, Grande-Allen KJ. Mitral valvular interstitial cell responses to substrate stiffness depend on age and anatomic region. Acta Biomater. 2011; 7:75–82. [PubMed: 20624493]

241. Stephens EH, Nguyen TC, Itoh A, Ingels NB Jr, Miller DC, Grande-Allen KJ. The effects of mitral regurgitation alone are sufficient for leaflet remodeling. Circulation. 2008; 118:S243–S249. [PubMed: 18824762]

242. Stephens EH, Saltarrelli JG, Baggett LS, Nandi I, Kuo JJ, Davis AR, Olmsted-Davis EA, Reardon MJ, Morrisett JD, Grande-Allen KJ. Differential proteoglycan and hyaluronan distribution in calcified aortic valves. Cardiovasc Pathol. 2011; 20:334–342. [PubMed: 21185747]

243. Stephens EH, Timek TA, Daughters GT, Kuo JJ, Patton AM, Baggett LS, Ingels NB, Miller DC, Grande-Allen KJ. Significant changes in mitral valve leaflet matrix composition and turnover with tachycardia-induced cardiomyopathy. Circulation. 2009; 120:S112–S119. [PubMed: 19752355]

244. Stevanella M, Maffessanti F, Conti CA, Votta E, Arnoldi A, Lombardi M, Parodi O, Caiani EG, Redaelli A. Mitral valve patient-specific finite element modeling from cardiac MRI: Application to an annuloplasty procedure. Cardiovas Eng Tech. 2011; 2:66–76.

245. Stewart BF, Siscovick D, Lind BK, Gardin JM, Gottdiener JS, Smith VE, Kitzman DW, Otto CM. Clinical factors associated with calcific aortic valve disease. Cardiovascular Health Study. J Am Coll Cardiol. 1997; 29:630–634. [PubMed: 9060903]

246. Stradins P, Lacis R, Ozolanta I, Purina B, Ose V, Feldmane L, Kasyanov V. Comparison of biomechanical and structural properties between human aortic and pulmonary valve. Eur J Cardiothorac Surg. 2004; 26:634–639. [PubMed: 15302062]

247. Sun W, Martin C, Pham T. Computational modeling of cardiac valve function and intervention. Annu Rev Biomed Eng. 2014; 16:53–76. [PubMed: 24819475]

248. Sung HW, Philpot EF, Nanda NC, Yoganathan AP. Axial flow velocity patterns in a pulmonary artery model with varying degrees of valvular pulmonic stenosis: Pulsatile in vitro studies. J Biomech. 1990; 23:563–578. [PubMed: 2187876]

249. Sung HW, Yoganathan AP. Axial flow velocity patterns in a normal human pulmonary artery model: Pulsatile in vitro studies. J Biomech. 1990; 23:201–214. [PubMed: 2324117]
250. Sung HW, Yoganathan AP. Secondary flow velocity patterns in a pulmonary artery model with varying degrees of valvular pulmonic stenosis: Pulsatile in vitro studies. J Biomech Eng. 1990; 112:88–92. [PubMed: 2308309]
251. Taber LA, Humphrey JD. Stress-modulated growth, residual stress, and vascular heterogeneity. J Biomech Eng. 2001; 123:528–535. [PubMed: 11783722]
252. Tanaka K, Sata M, Fukuda D, Suematsu Y, Motomura N, Takamoto S, Hirata Y, Nagai R. Age-associated aortic stenosis in apolipoprotein E-deficient mice. J Am Coll Cardiol. 2005; 46:134–141. [PubMed: 15992647]
253. Tao G, Kotick JD, Lincoln J. Heart valve development, maintenance, and disease: The role of endothelial cells. Curr Top Dev Biol. 2012; 100:203–232. [PubMed: 22449845]
254. Taylor PM, Batten P, Brand NJ, Thomas PS, Yacoub MH. The cardiac valve interstitial cell. Int J Biochem Cell Biol. 2003; 35:113–118. [PubMed: 12479860]
255. Thubrikar M, Aouad J, Nolan SP. Comparison of the in-vivo and in-vitro mechanical properties of aortic valve leafelts. J Thorac Cardiovasc Surg. 1986; 92
256. Thubrikar M, Bosher LP, Harry RR, Nolan SP. Mechanism of opening of the natural aortic valve in relation to the design of trileaflet prostheses. Surg Forum. 1977; 28:264–266. [PubMed: 617439]
257. Thubrikar M, Bosher LP, Nolan SP. The mechanism of opening of the aortic valve. J Thorac Cardiovasc Surg. 1979; 77:863–870. [PubMed: 439922]
258. Thubrikar M, Carabello BA, Aouad J, Nolan SP. Interpretation of aortic root angiography in dogs and in humans. Cardiovasc Res. 1982; 16:16–21. [PubMed: 7060057]
259. Thubrikar M, Harry R, Nolan SP. Normal aortic valve function in dogs. Am J Cardiol. 1977; 40:563–568. [PubMed: 910719]
260. Thubrikar M, Nolan SP, Bosher LP, Deck JD. The cyclic changes and structure of the base of the aortic valve. Am Heart J. 1980; 99:217–224. [PubMed: 7352404]
261. Thubrikar M, Piepgrass W, Bosher L, Nolan S. The elastic modulus of canine aortic valve leaflets in vivo and in vitro. Circ Res. 1980; 47:792–800. [PubMed: 7418136]
262. Thubrikar M, Piepgrass W, Deck J, Nolan S. Stresses of natural versus prosthetic aortic valve leaflets in vivo. Ann Thorac Surg. 1980; 30:230–239. [PubMed: 7425702]
263. Thubrikar M, Piepgrass WC, Shaner TW, Nolan SP. Design and dynamic variations of aortic valve leaflets in vivo. Surg Forum. 1979; 30:241–243. [PubMed: 538608]
264. Thubrikar M, Piepgrass WC, Shaner TW, Nolan SP. The design of the normal aortic valve. Am J Physiol. 1981; 241:H795–H801. [PubMed: 7325246]
265. Thubrikar M, Skinner J, Eppink R, Nolan S. Stress analysis of porcine bioprosthetic heart valves in vivo. J Biomed Mater Res. 1982; 16:811. [PubMed: 7174710]
266. Thubrikar M, Skinner JR, Aouad J, Finkelmeier BA, Nolan SP. Analysis of the design and dynamics of aortic bioprostheses in vivo. J Thorac Cardiovasc Surg. 1982; 84:282–290. [PubMed: 7098513]
267. Thubrikar MJ, Aouad J, Nolan SP. Comparison of the in vivo and in vitro mechanical properties of aortic valve leaflets. J Thorac Cardiovasc Surg. 1986; 92:29–36. [PubMed: 3724225]
268. Thubrikar MJ, Aouad J, Nolan SP. Patterns of calcific deposits in operatively excised stenotic or purely regurgitant aortic valves and their relation to mechanical stress. Am J Cardiol. 1986; 58:304–308. [PubMed: 3739919]
269. Thubrikar MJ, Nolan SP, Aouad J, Deck JD. Stress sharing between the sinus and leaflets of canine aortic valve. Ann Thorac Surg. 1986; 42:434–440. [PubMed: 3767514]
270. Tibayan FA, Rodriguez F, Langer F, Zasio MK, Bailey L, Liang D, Daughters GT, Ingels NB Jr, Miller DC. Annular remodeling in chronic ischemic mitral regurgitation: Ring selection implications. Ann Thorac Surg. 2003; 76:1549–1554. discussion 1554–1545. [PubMed: 14602284]

271. Timek TA, Dagum P, Lai DT, Liang D, Daughters GT, Tibayan F, Ingels NB Jr, Miller DC. Tachycardia-induced cardiomyopathy in the ovine heart: Mitral annular dynamic three-dimensional geometry. J Thorac Cardiovasc Surg. 2003; 125:315–324. [PubMed: 12579100]

272. Timek TA, Lai DT, Dagum P, Liang D, Daughters GT, Ingels NB Jr, Miller DC. Mitral leaflet remodeling in dilated cardiomyopathy. Circulation. 2006; 114:I518–I523. [PubMed: 16820630]

273. Timmerman LA, Grego-Bessa J, Raya A, Bertran E, Perez-Pomares JM, Diez J, Aranda S, Palomo S, McCormick F, Izpisua-Belmonte JC, de la Pompa JL. Notch promotes epithelial-mesenchymal transition during cardiac development and oncogenic transformation. Genes Dev. 2004; 18:99–115. [PubMed: 14701881]

274. Towler DA. Molecular and cellular aspects of calcific aortic valve disease. Circ Res. 2013; 113:198–208. [PubMed: 23833294]

275. Umesan CV, Kapoor A, Sinha N, Kumar AS, Goel PK. Effect of Inoue balloon mitral valvotomy on severe pulmonary arterial hypertension in 315 patients with rheumatic mitral stenosis: Immediate and long-term results. J Heart Valve Dis. 2000; 9:609–615. [PubMed: 11041172]

276. Verzi MP, McCulley DJ, De Val S, Dodou E, Black BL. The right ventricle, outflow tract, and ventricular septum comprise a restricted expression domain within the secondary/anterior heart field. Dev Biol. 2005; 287:134–145. [PubMed: 16188249]

277. Vesely I. The role of elastin in aortic valve mechanics. J Biomech. 1998; 31:115–123. [PubMed: 9593204]

278. Vesely I, Casarotto DC, Gerosa G. Mechanics of cryopreserved aortic and pulmonary homografts. J Heart Valve Dis. 2000; 9:27–37. [PubMed: 10678373]

279. Vesely I, Mako WJ. Comparison of the compressive buckling of porcine aortic valve cusps and bovine pericardium. J Heart Valve Dis. 1998; 7:34–39. [PubMed: 9502137]

280. Vesely I, Noseworthy R. Micromechanics of the fibrosa and the ventricularis in aortic valve leaflets. J Biomech. 1992; 25:101–113. [PubMed: 1733978]

281. Votta E, Caiani E, Veronesi F, Soncini M, Montevecchi FM, Redaelli A. Mitral valve finite-element modelling from ultrasound data: A pilot study for a new approach to understand mitral function and clinical scenarios. Philos Trans A Math Phys Eng Sci. 2008; 366:3411–3434. [PubMed: 18603525]

282. Votta E, Le TB, Stevanella M, Fusini L, Caiani EG, Redaelli A, Sotiropoulos F. Toward patient-specific simulations of cardiac valves: State-of-the-art and future directions. J Biomech. 2013; 46:217–228. [PubMed: 23174421]

283. Votta E, Maisano F, Bolling SF, Alfieri O, Montevecchi FM, Redaelli A. The Geoform disease-specific annuloplasty system: A finite element study. Ann Thorac Surg. 2007; 84:92–101. [PubMed: 17588392]

284. Wang Q, Sun W. Finite element modeling of mitral valve dynamic deformation using patient-specific multi-slices computed tomography scans. Ann Biomed Eng. 2013; 41:142–153. [PubMed: 22805982]

285. Weinberg EJ, Mofrad MRK. Transient, three-dimensional, multiscale simulations of the human aortic valve. Cardiovasc Eng. 2007; 7:140–155. [PubMed: 18026835]

286. Weinberg EJ, Shahmirzadi D, Mofrad MRK. On the multiscale modeling of heart valve biomechanics in health and disease. Biomech Model Mechanobiol. 2010; 9:373–387. [PubMed: 20066464]

287. Weiss RM, Ohashi M, Miller JD, Young SG, Heistad DD. Calcific aortic valve stenosis in old hypercholesterolemic mice. Circulation. 2006; 114:2065–2069. [PubMed: 17075015]

288. Wells SM, Pierlot CM, Moeller AD. Physiological remodeling of the mitral valve during pregnancy. Am J Physiol Heart Circ Physiol. 2012; 303:H878–H892. [PubMed: 22886410]

289. Wenk JF, Zhang Z, Cheng G, Malhotra D, Acevedo-Bolton G, Burger M, Suzuki T, Saloner DA, Wallace AW, Guccione JM, Ratcliffe MB. First finite element model of the left ventricle with mitral valve: Insights into ischemic mitral regurgitation. Ann Thorac Surg. 2010; 89:1546–1553. [PubMed: 20417775]

290. Weyman, AE. Principles and Practices of Echocardiography. Philadelphia, PA: Lea & Febiger; 1994.

291. Willems IE, Havenith MG, Smits JF, Daemen MJ. Structural alterations in heart valves during left ventricular pressure overload in the rat. Lab Invest. 1994; 71:127–133. [PubMed: 8041112]

292. Wirrig EE, Hinton RB, Yutzey KE. Differential expression of cartilage and bone-related proteins in pediatric and adult diseased aortic valves. J Mol Cell Cardiol. 2011; 50:561–569. [PubMed: 21163264]

293. Wyss K, Yip CY, Mirzaei Z, Jin X, Chen J-H, Simmons CA. The elastic properties of valve interstitial cells undergoing pathological differentiation. J Biomech. 2012; 45:882–887. [PubMed: 22189247]

294. Xie GY, Bhakta D, Smith MD. Echocardiographic follow-up study of the Ross procedure in older versus younger patients. Am Heart J. 2001; 142:331–335. [PubMed: 11479474]

295. Yacoub MH, Cohn LH. Novel approaches to cardiac valve repair: From structure to function: Part II. Circulation. 2004; 109:1064–1072. [PubMed: 15007015]

296. Yang J, Weinberg RA. Epithelial-mesenchymal transition: At the crossroads of development and tumor metastasis. Dev Cell. 2008; 14:818–829. [PubMed: 18539112]

297. Yellin EL, Peskin C, Yoran C, Koenigsberg M, Matsumoto M, Laniado S, McQueen D, Shore D, Frater RW. Mechanisms of mitral valve motion during diastole. Am J Physiol. 1981; 241:H389–H400. [PubMed: 7282948]

298. Yoganathan AP. Fluid mechanics of aortic stenosis. Eur Heart J. 1988; 9(Suppl E):13–17.

299. Zhang W, Ayoub S, Liao J, Sacks MS. A meso-scale layer-specific structural constitutive model of the mitral heart valve leaflets. Acta Biomater. 2015

300. Zhao B, Etter L, Hinton RB Jr, Benson DW. BMP and FGF regulatory pathways in semilunar valve precursor cells. Dev Dyn. 2007; 236:971–980. [PubMed: 17326134]

301. Zhou B, von Gise A, Ma Q, Hu YW, Pu WT. Genetic fate mapping demonstrates contribution of epicardium-derived cells to the annulus fibrosis of the mammalian heart. Dev Biol. 2010; 338:251–261. [PubMed: 20025864]

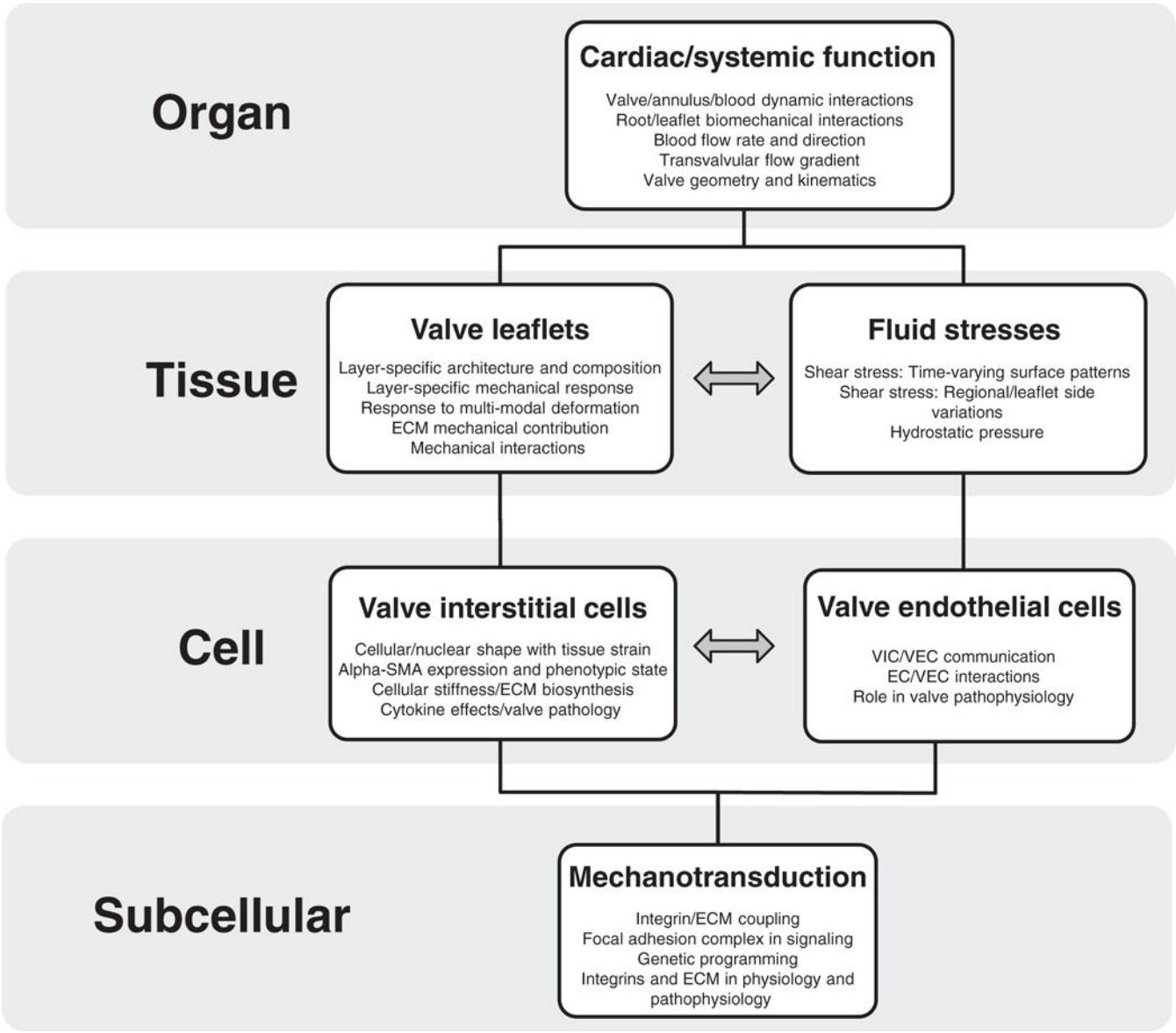

Figure 1.

A schematic approach to the biomechanics and mechanobiology of heart valve function. Heart valve function can be divided into multiple length scales: organ, tissue, cell, and subcell levels.

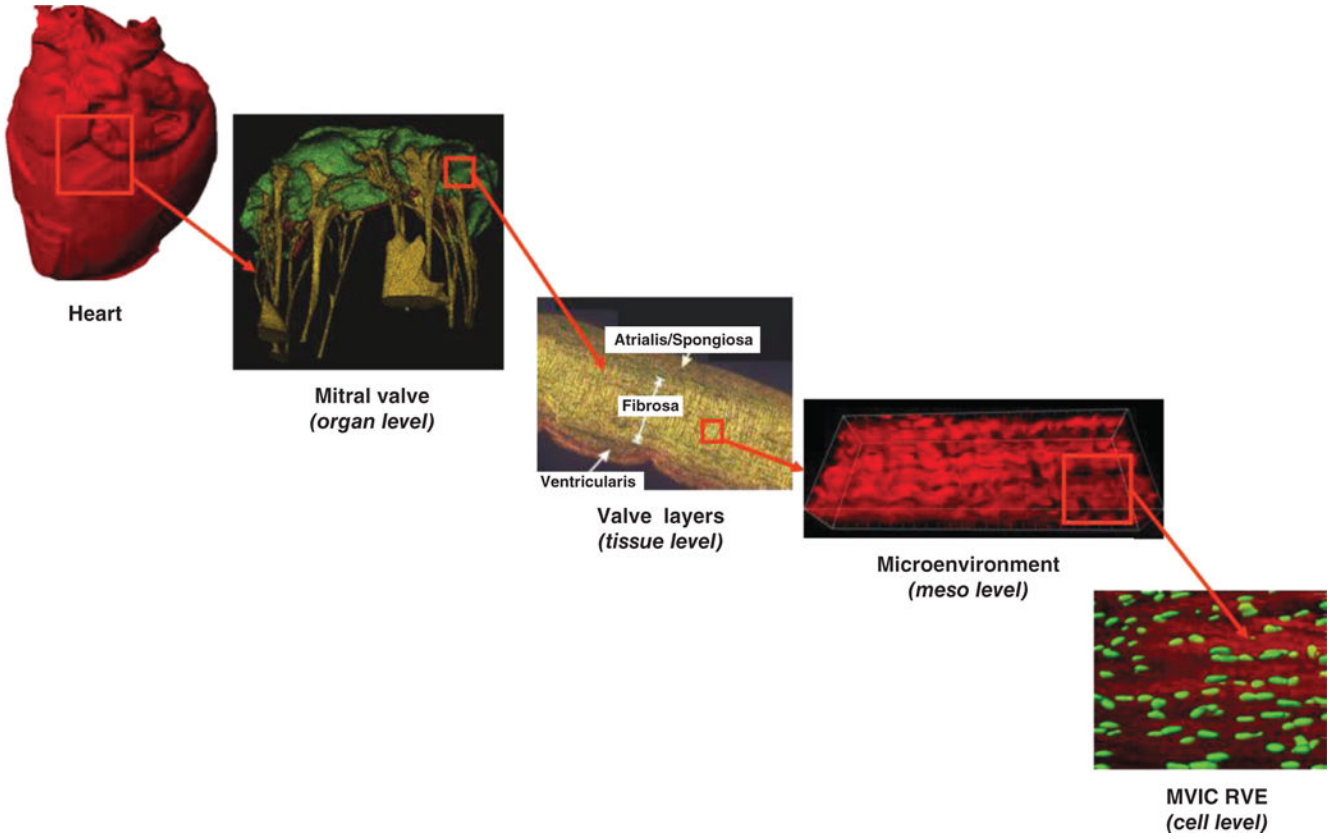

Figure 2.

The multiscale nature of heart valve biomechanics: a representation of the MV at the organ, tissue, and cell levels. At the tissue level: a circumferentially oriented cross section of the MV anterior leaflet stained with Movat pentachrome, which colors collagen yellow, elastic fibers black, and hydrated PGs and GAGs blue. At the cell-level: a transmission electron micrograph of a mitral VIC from the fibrosa layer.

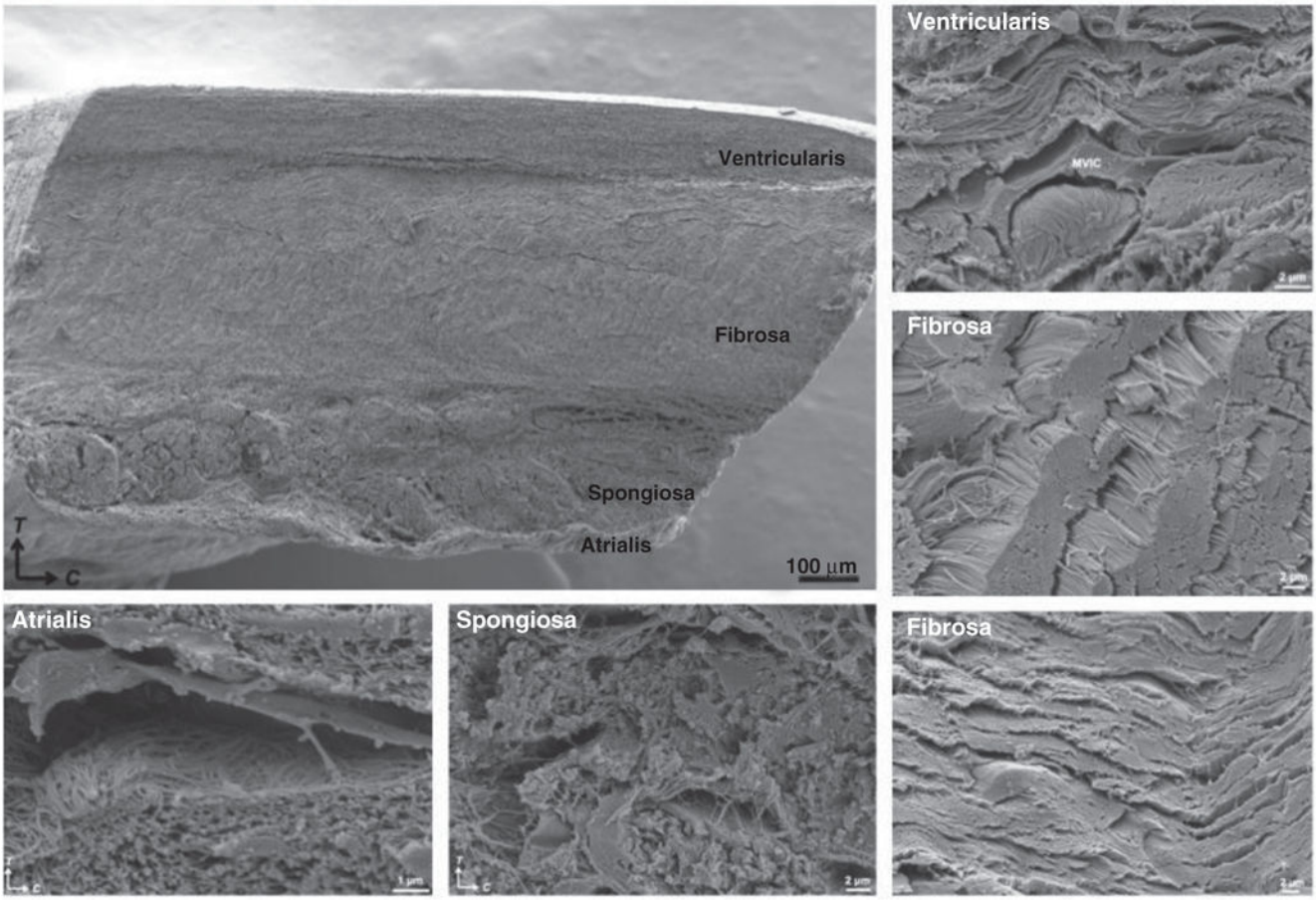

Figure 3.

Scanning electron micrograph of the multilayered microenvironment of the MVAL. Individual micrographs of each layer are also presented: elastin-rich ventricularis and atrialis, highly collagenous fibrosa, and proteoglycan-rich spongiosa. The collagen fibrils and elastic fibers closely surround the interstitial cells and highlight the long cellular extensions. In the fibrosa, collagen fibrils are aligned in the circumferential direction of the leaflet, which is responsible for the observed anisotropy in leaflet mechanical behavior. (T: transmural, C: circumferential.)

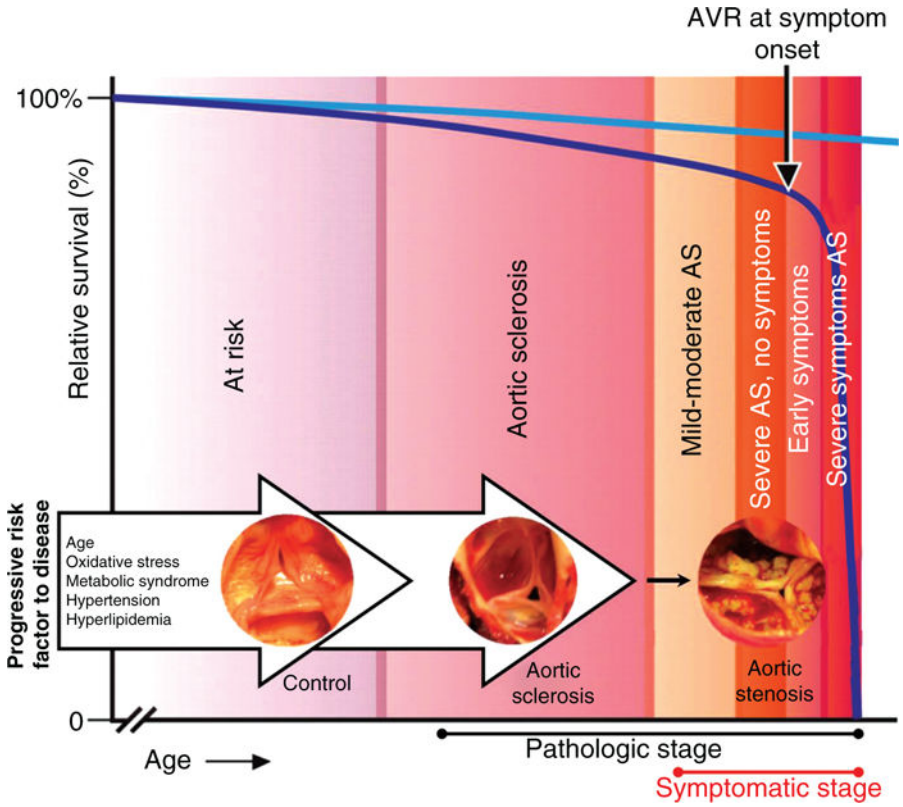

Figure 4.

A conceptual framework of the natural history of CAVD. The spectrum of disease ranges from the “at risk” patient to the patient with end-stage severe symptomatic aortic stenosis. The light blue line represents the expected event-free survival and the purple line represents the survival curve at the onset of aortic sclerosis, which deviates from the expected survival line. Atherosclerotic risk factors involved in the development of AV disease from aortic sclerosis to calcified AV disease are included. Adapted from Otto et al. (182) with permission and Rajamannan et al. (203).

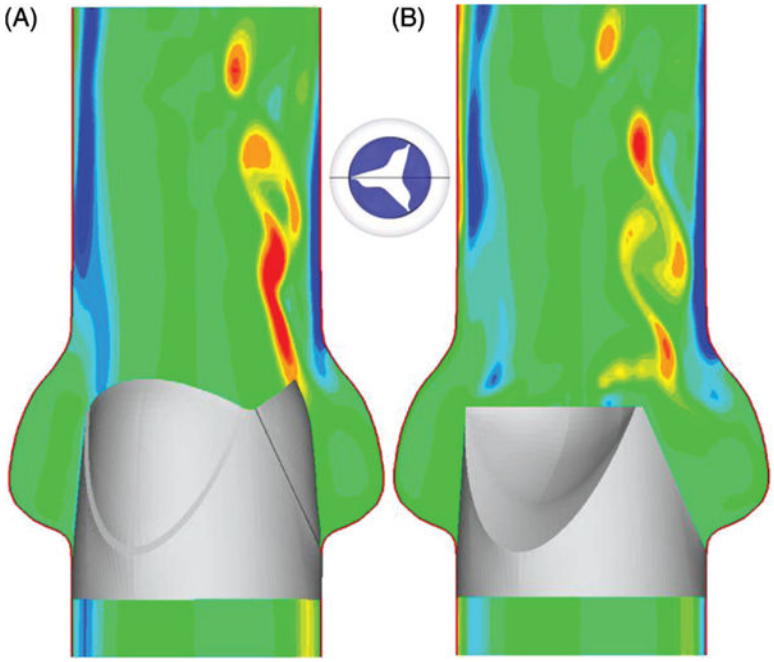

Figure 5.
Numerical simulation of the unsteady, pulsatile flow in a tricuspid prosthetic HV. Contours of the out-of-plane vorticity are shown at two phases during the cardiac cycle: (A) fully open phase and (B) closing phase.

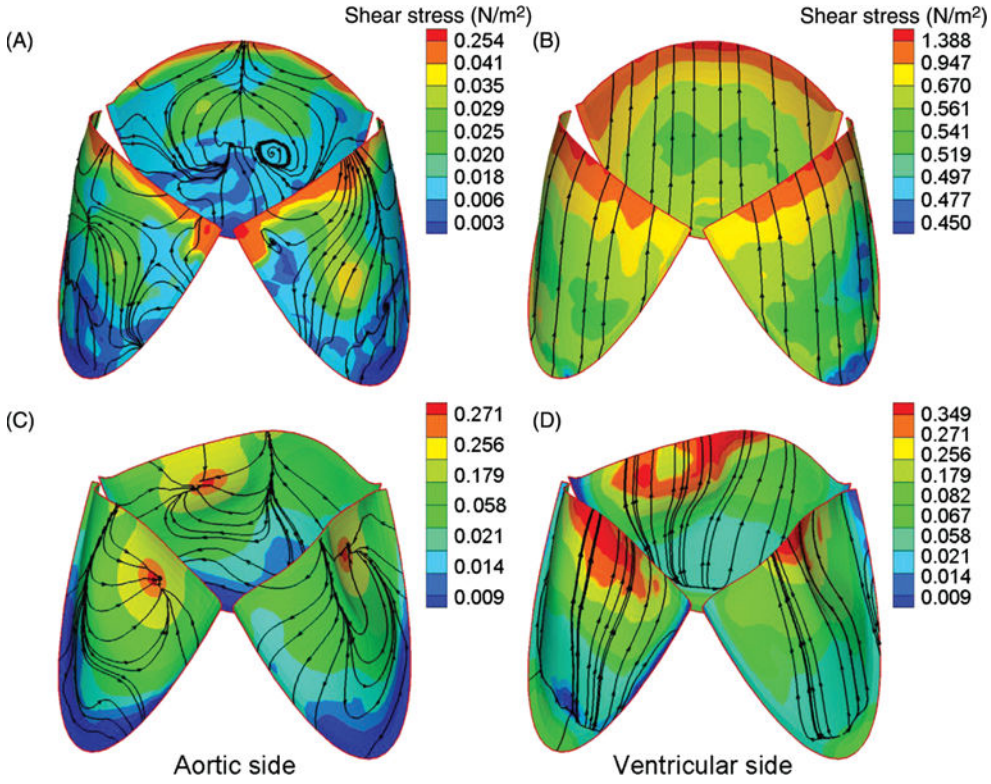

Figure 6.

Instantaneous friction streamline and shear stress magnitude plots on the aortic (A and C) and ventricular (B and D) sides of the leaflets during the fully open (A and B) and early closing (C and D) phases of the cardiac cycle.

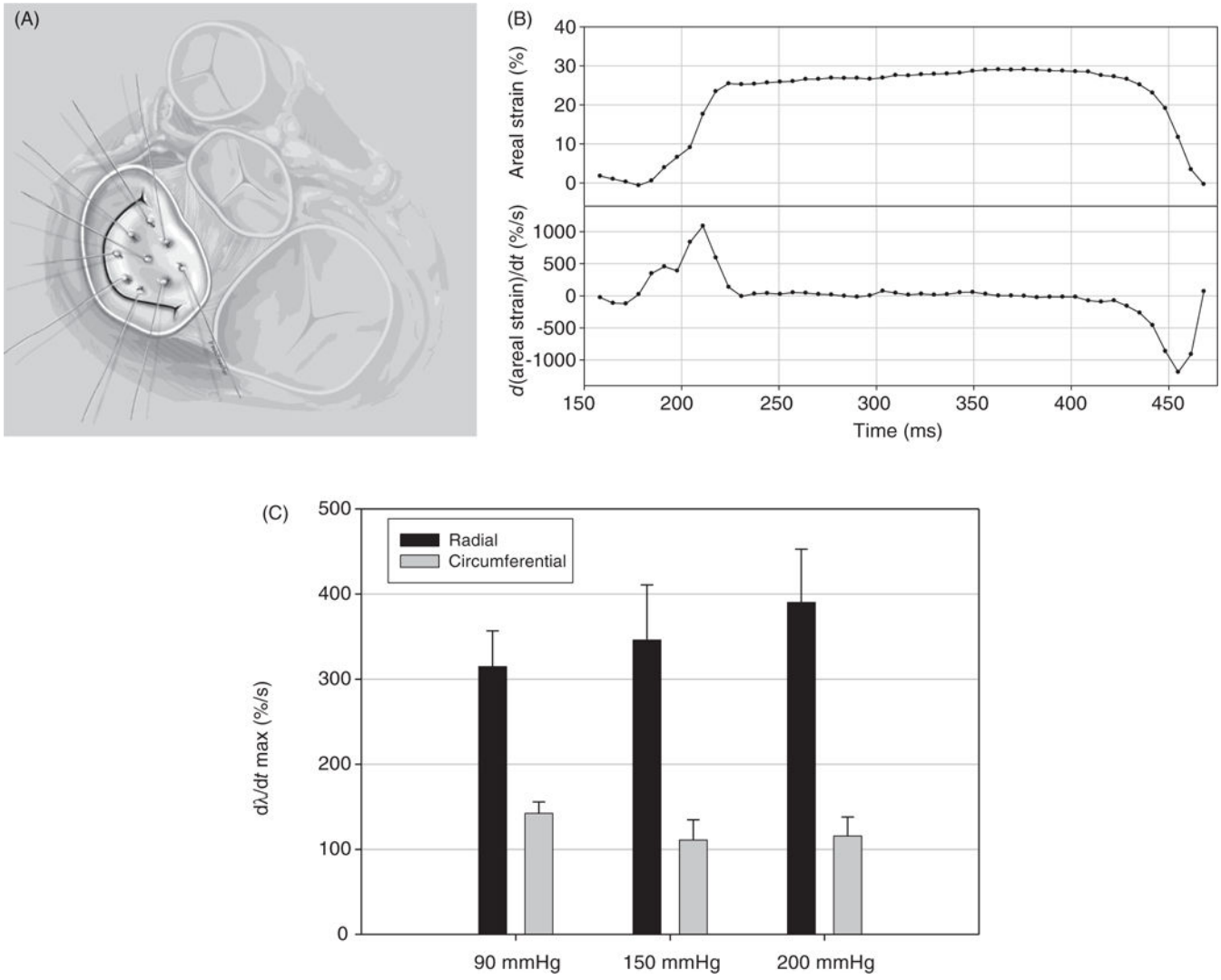

Figure 7.

(A) Schematic of the MVAL with the nine transducers used for sonomicrometry array localization. (B) Representative areal strain traces and corresponding areal strain rate data. The high strain rates (on the order of 1000% s^{-1}) underscore the highly dynamic nature of the MV. Once the valve coapts fully, no further deformations occurred. (C) Mean principal strains for three pressure levels: 90, 150, and 200 mmHg. Other than the differences between the circumferential and radial peak strains, there were no significant differences in strain with increasing LV pressure. Adapted, with permission, from Sacks et al. (214).

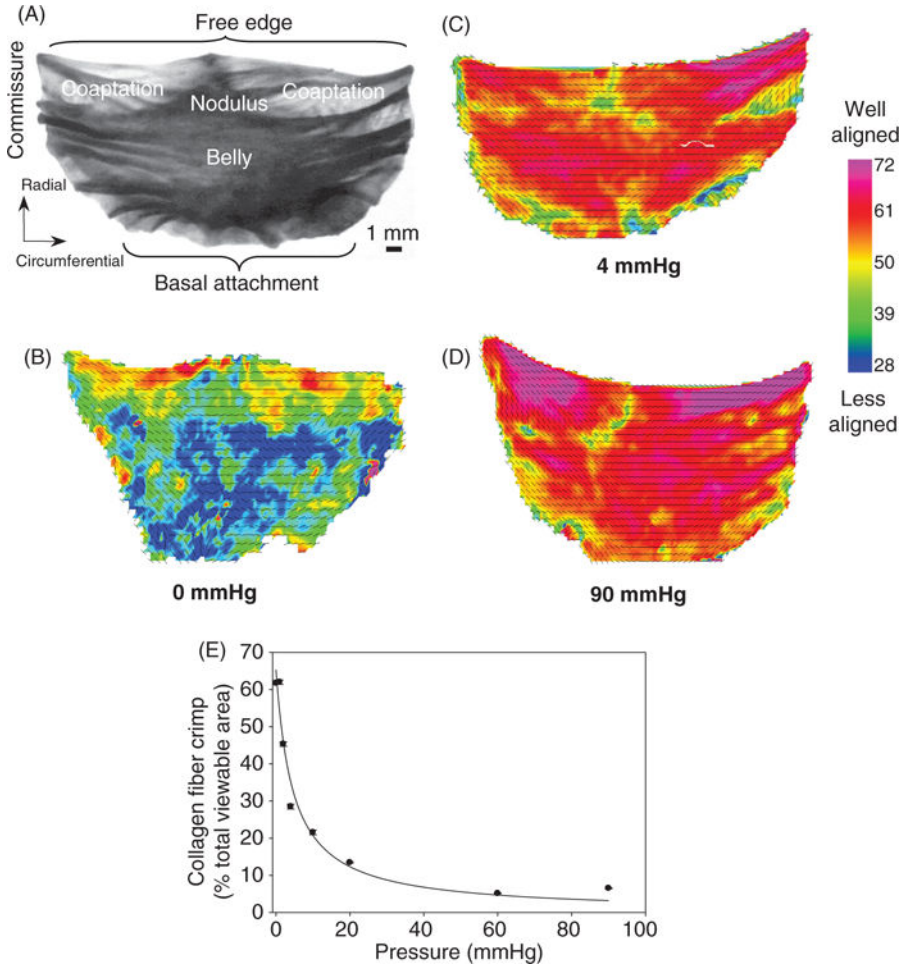

Figure 8.

(A) Diagram of the AV cusp highlighting the belly, commissures, nodulus, and regions of coaptation. SALS results with the orientation index at (B) 0mmHg, (C) 4 mmHg, and (D) 90 mmHg TVP. No further changes in fiber alignment were observed past 4 mmHg. These results are consistent with histological-based data that quantifies the percent area of tissue displaying collagen fiber crimp (E). Adapted, with permission, from Sacks et al. (217).

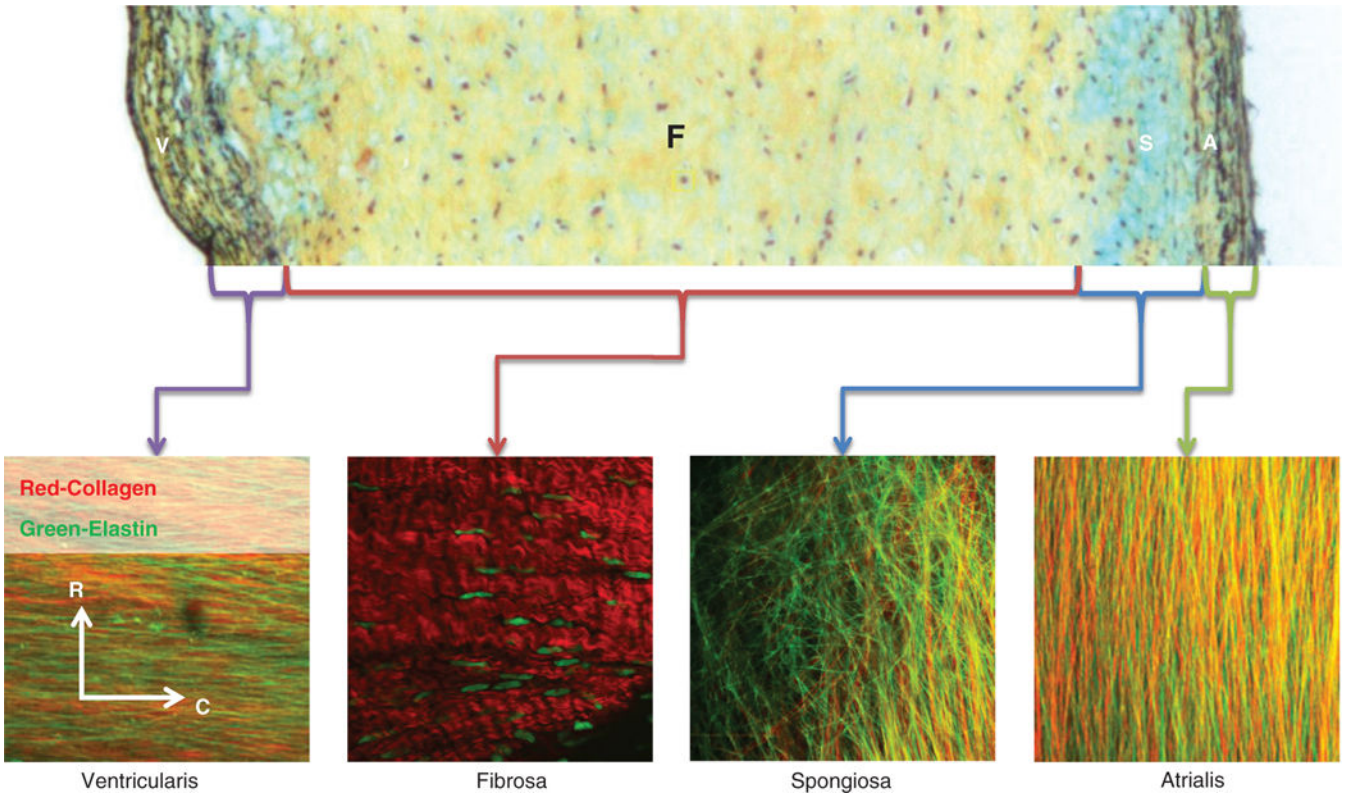

Figure 9.

Movat pentachrome stain of the transverse-radial section of the center region of the MVAL, and multiphoton microscopy of the ventricularis, fibrosa, spongiosa, and atrialis layer of the anterior leaflet is also shown. Adapted, with permission, from Zhang et al. (299).

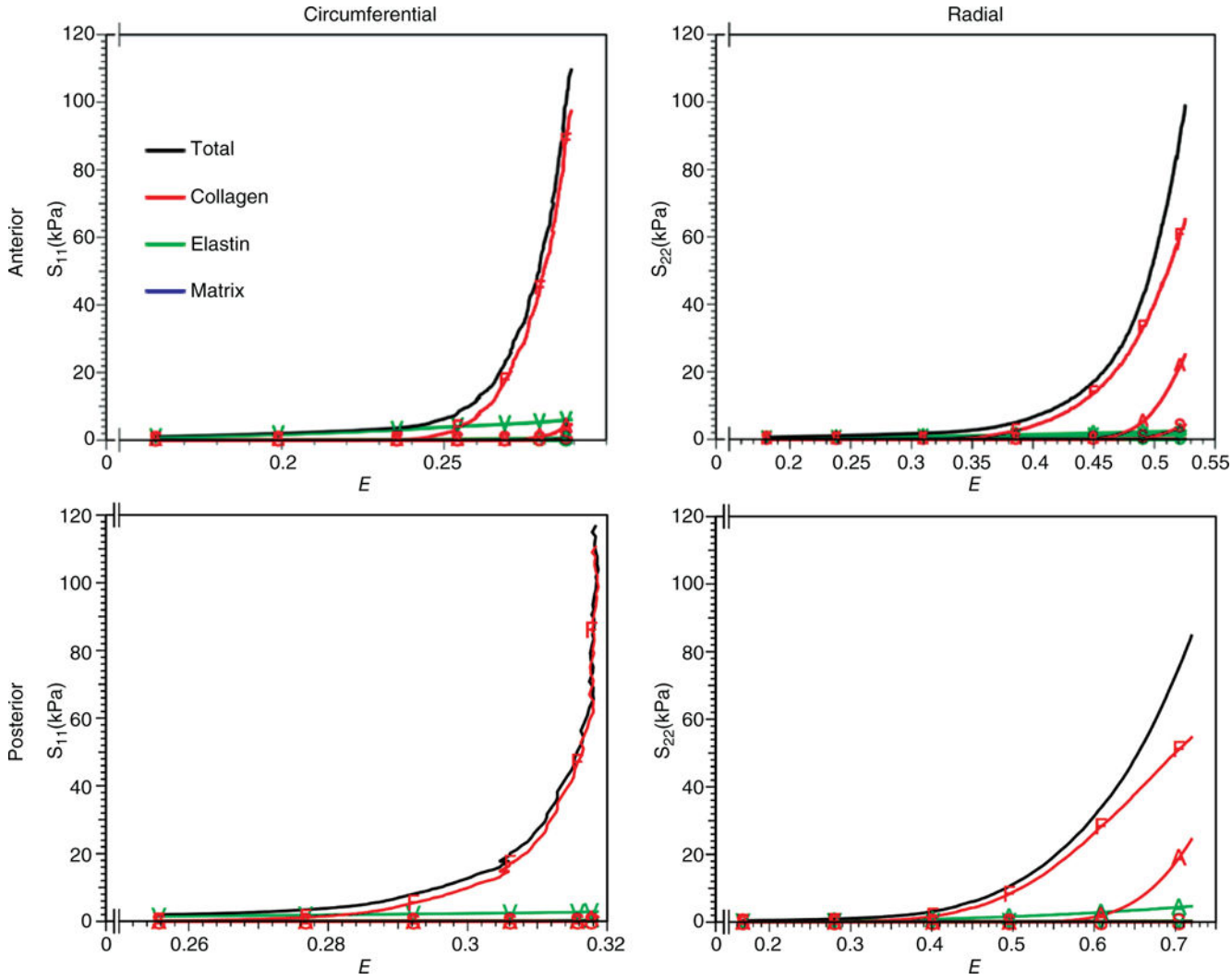

Figure 10.

The net stress contribution from each ECM component from each layer for the equibiaxial stress protocol is shown for the circumferential and radial direction of the anterior and posterior leaflets. Here, the contributions from the layers are ventricularis (V), fibrosa (F), spongiosa (S), and atrialis (A). Interestingly, while the fibrosa layer is dominant circumferential directions in both leaflets, the atrialis also contributes substantially in the radial direction. Adapted, with permission, from Zhang et al. (299).

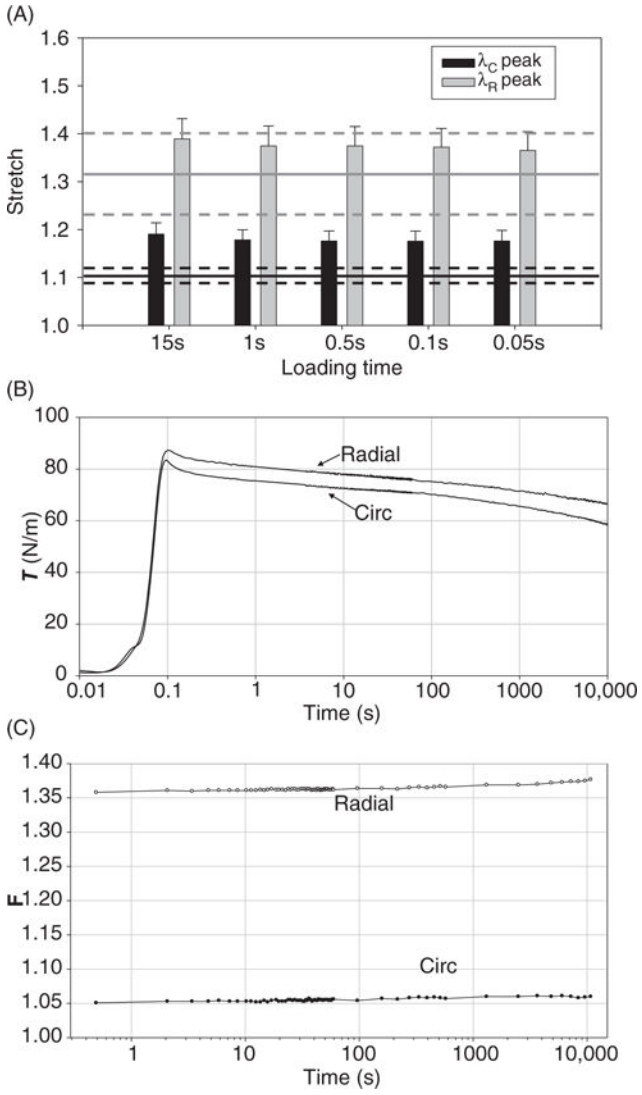

Figure 11.

(A) The circumferential and radial stretches of the MV leaflet at the 90 N/m equitension state, λ_C^{peak} and λ_R^{peak}, revealed no significant differences among the prescribed set of loading time protocols in both the circumferential ($P = 0.987$) and radial ($P = 0.996$) directions. Stretches observed previously in mock flow loop (solid horizontal lines) ±SEM (dotted lines) are plotted for the circumferential (black) and radial (gray) specimen axes. λ_C^{peak} and λ_R^{peak} exceeded those observed *in vitro*; however, the ratio of λ_C^{peak} to λ_R^{peak} (0.86 ± 0.02) was very close to the ratio of peak circumferential and radial stretches observed *in vitro* (0.83). (B) Representative biaxial stress-relaxation data, demonstrating continued relaxation throughout the 3-h time frame. (C) Representative stretch versus time curves for a typical biaxial creep experiment. Adapted, with permission, from Zhang et al. (299).

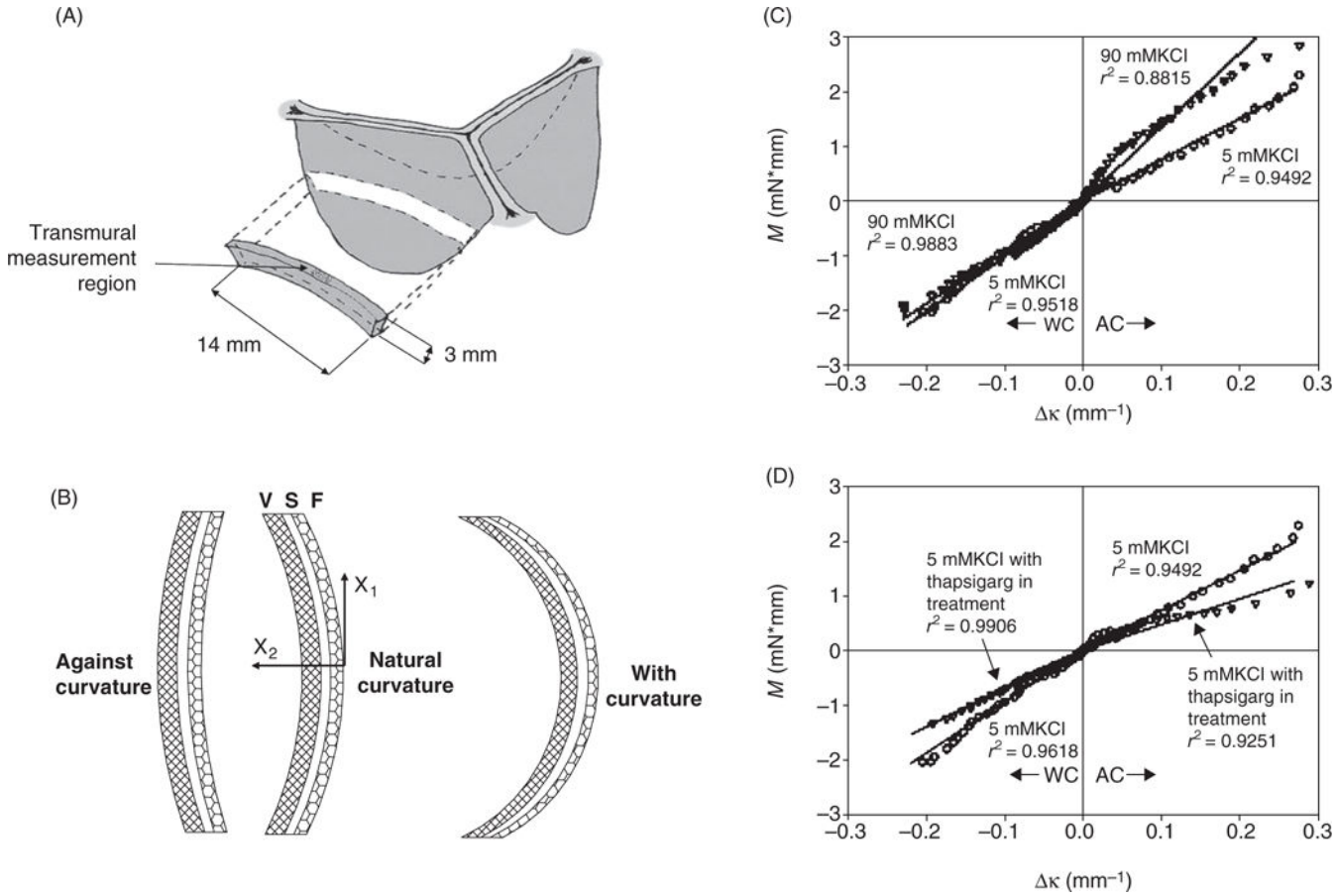

Figure 12.

(A) Schematic showing the region of tissue used for bending tests in the AV. (B) Schematic showing directions of bending for the AV with respective layers (V: ventricularis, S: spongiosa, and F: fibrosa). M versus Dk relations in both the AC and WC directions for (C) specimens tested in 5 and 90 mmol/L KCl, and (D) specimens flexed in 5 mmol/L KCl and samples treated in 10 mmol/L thapsigargin overnight and then flexed in 5 mmol/L KCl. While the application of 90 mmol/L KCL induced an increase in stiffness in the AC direction only, both bending directions experienced a loss of stiffness with the addition of thapsigargin to the bathing medium.

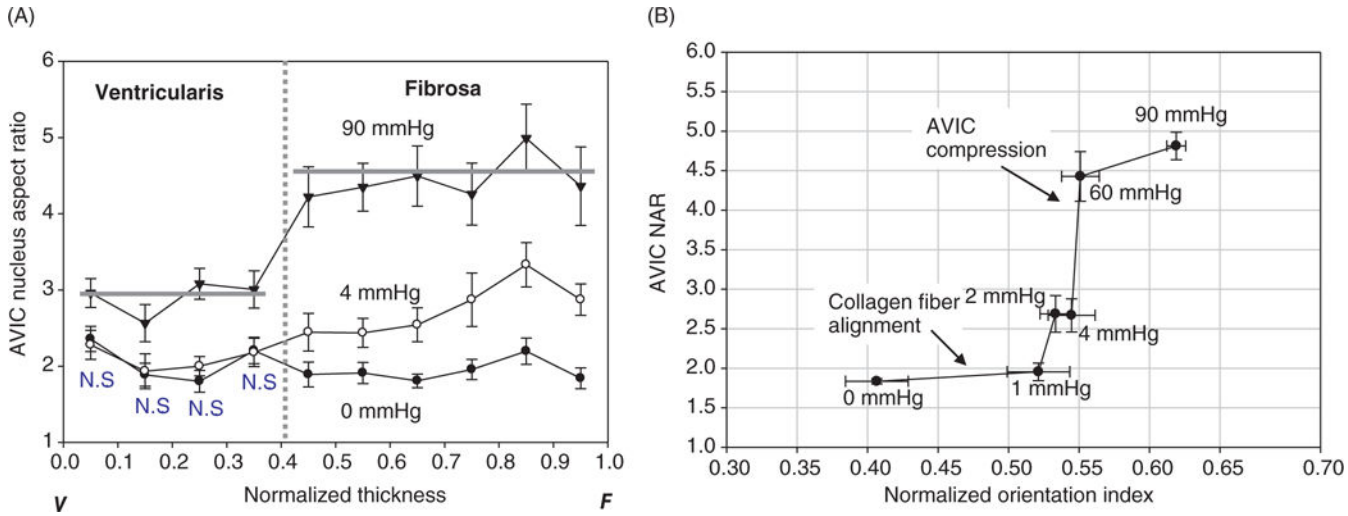

Figure 13.

(A) The relation between AVIC NAR and TVP loading, with values reported over normalized leaflet thickness. (B) AVIC NAR versus the normalized collagen fiber orientation index (NOI) at different TVP levels. These results suggest that AVICs are not appreciably loaded until the collagen fibers fully straighten at TVPs more than ~4 mmHg.

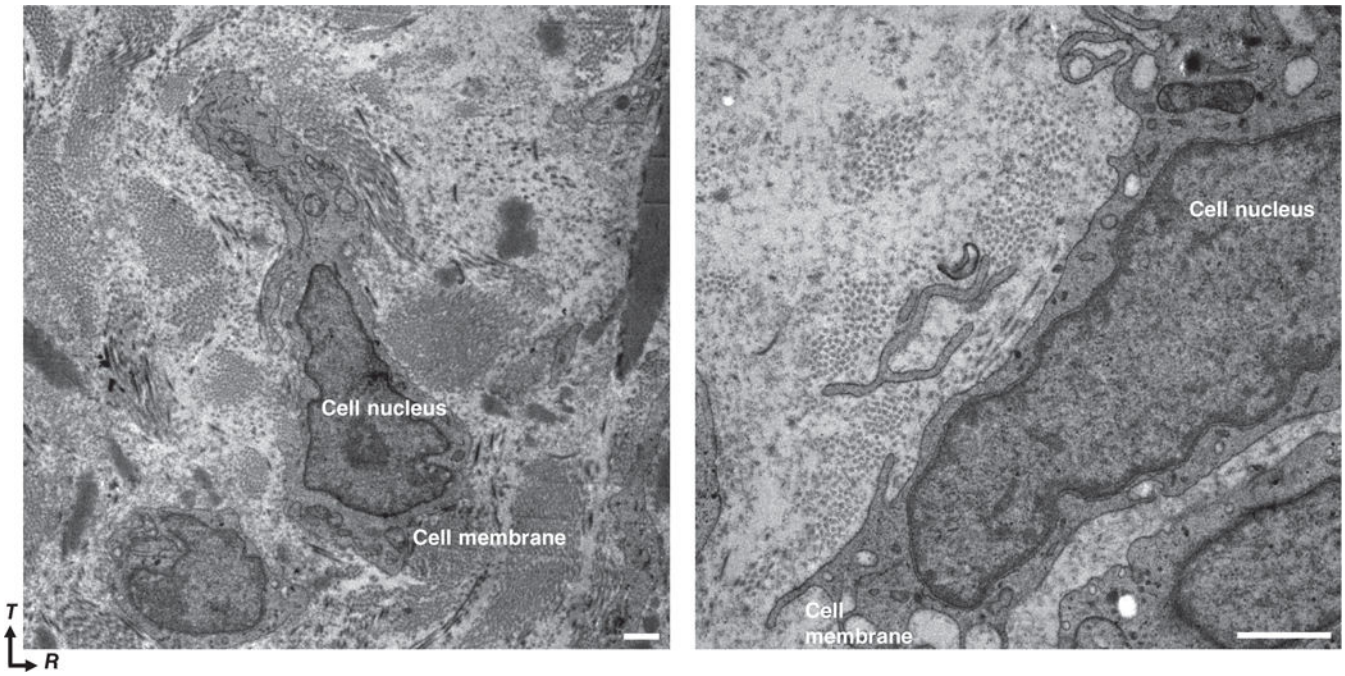

Figure 14.

Transmission electron micrograph of an MVIC from the fibrosa layer of the MV anterior leaflet highlighting the cellular microenvironment, particularly collagen fibril circumferential orientation and close interaction and alignment with the MVIC. Scale bar, 1 μm. (T: transmural, R: radial, C: circumferential.)

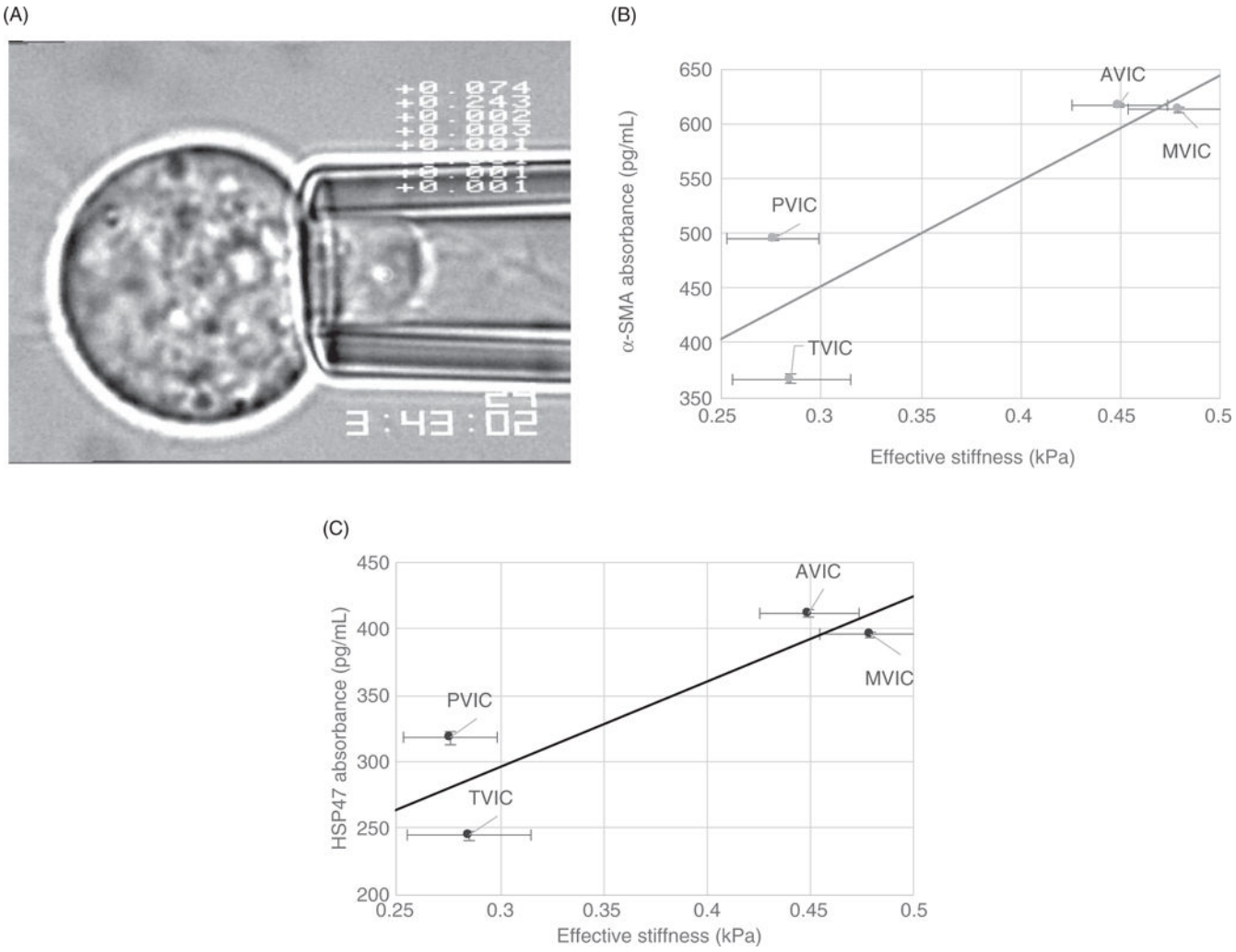

Figure 15.

(A) A VIC under MA—the vertical bar represents the aspiration length. (B) Functional correlations of effective cell stiffness E versus TVP. (C) Linear correlation between Hsp47 versus α-SMA, showing a strong correlation between the two proteins ($r = 0.996$) as the one progresses from the right to the left side of the heart.

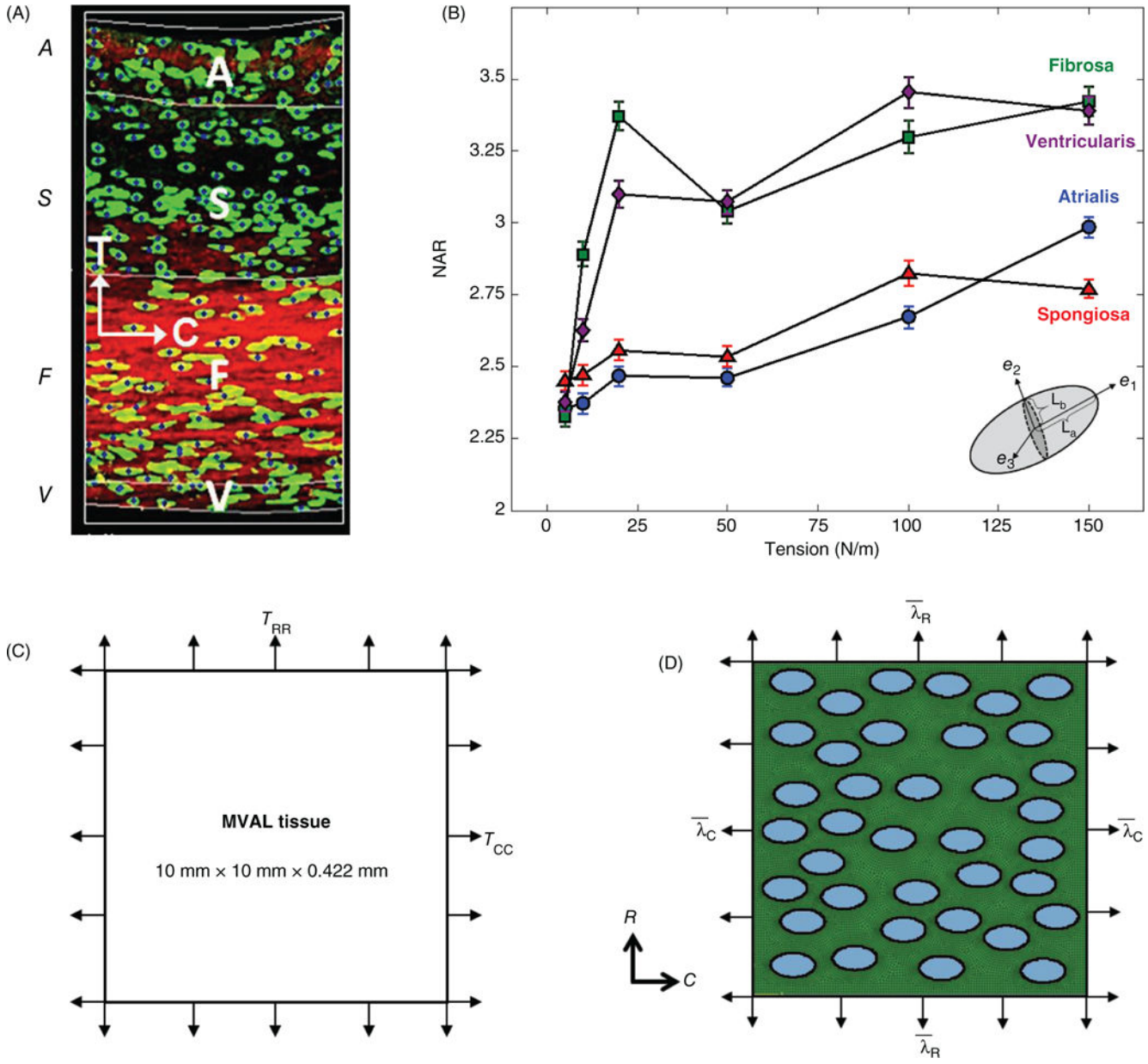

Figure 16.

(A and B) Transmural MVIC distribution and deformation in the MV anterior leaflet under controlled biaxial loading. (A) Stack of two-photon excited fluorescence images. Red represents collagen fibers and green represents cell nuclei stained with Cytox Green. Image stacks were processed and used to quantify cellular deformation by measuring the NAR. (B) Measured layer-specific NAR as a function of membrane tension. (A: atrialis, S: spongiosa, F: fibrosa, V: ventricularis.) (C and D) The macro-micro finite element (FE) model used to investigate MVIC deformation. (C) Schematic diagram of the tissue-level model: the region of interest of the MVAL tissue under equibiaxial tension loading. (D) Diagram of the cell-level microenvironment model, which consists of 37 uniformly distributed MVICs embedded in the layer-specific representative volume element. The tissue-level deformations

are used to prescribe boundary displacements. Adapted, with permission, from Lee et al. (134).

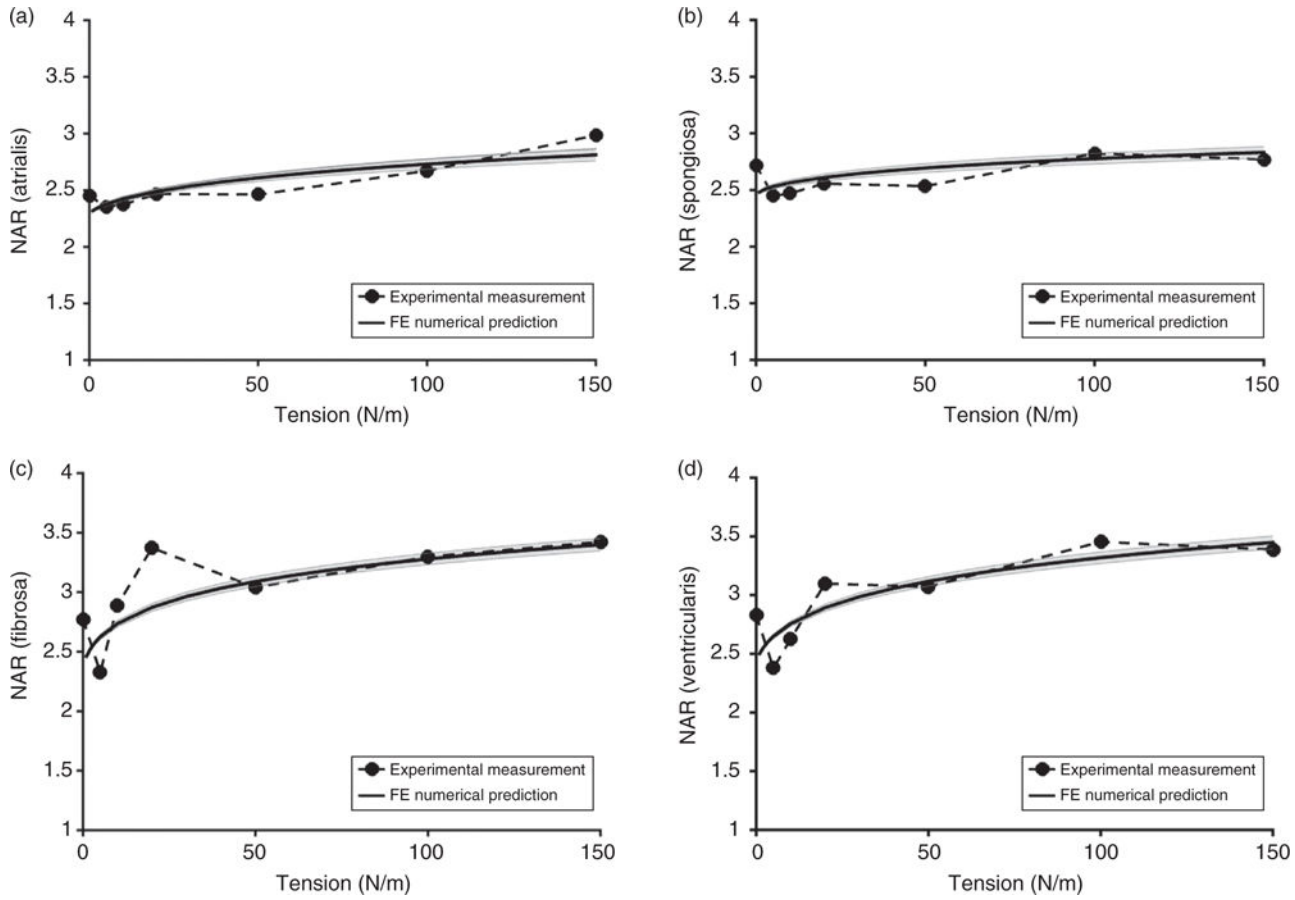

Figure 17.

Comparisons of the experimentally measured and numerically predicted NARs as a function of tissue-level tension: (A) atrialis layer (r^2 = 0.8403), (B) spongiosa layer (r^2 = 0.9166), (C) fibrosa layer (r^2 = 0.8906), and (D) ventricularis layer (r^2 = 0.9373). Adapted, with permission, from Lee et al. (134).

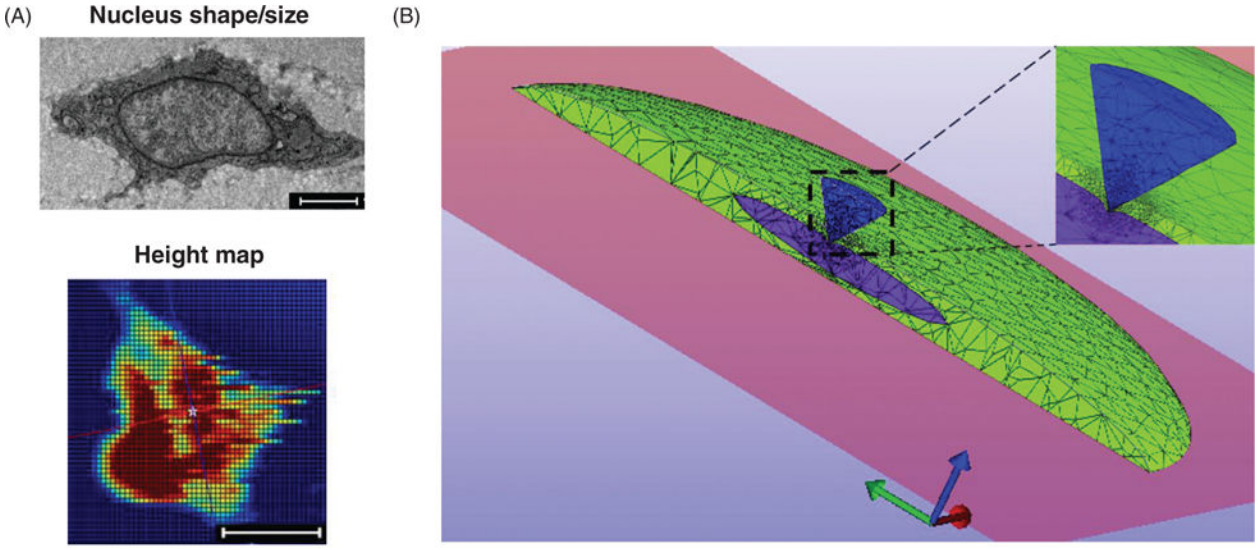

Figure 18.

AFM simulation setup with finite element mesh. (A) The volume ratio of the nucleus was acquired from electron micrographs of *in situ* VICs. Scale bar = 1 μm. VIC dimensions were acquired from height maps from AFM experiments. The colors represent the height of each point in μm. Scale bar = 10 μm. (B) The mesh was refined around the indentation region, with typically 10,000~50,000 linear tetrahedron elements.

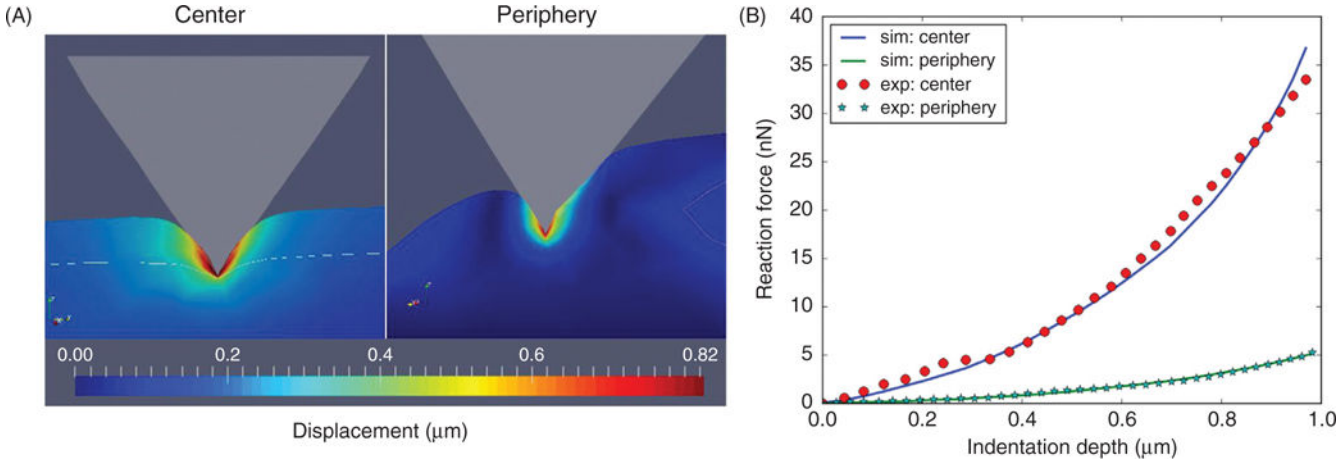

Figure 19.

(A) Deformation contours central and peripheral indentations highlight that VIC deformation is localized around the indentation region. The simulations show that indentations in the central region deform the nucleus more than those at the periphery. (B) Simulated and experimental indentation data at the center can be used to analyze VIC nucleus mechanical properties.

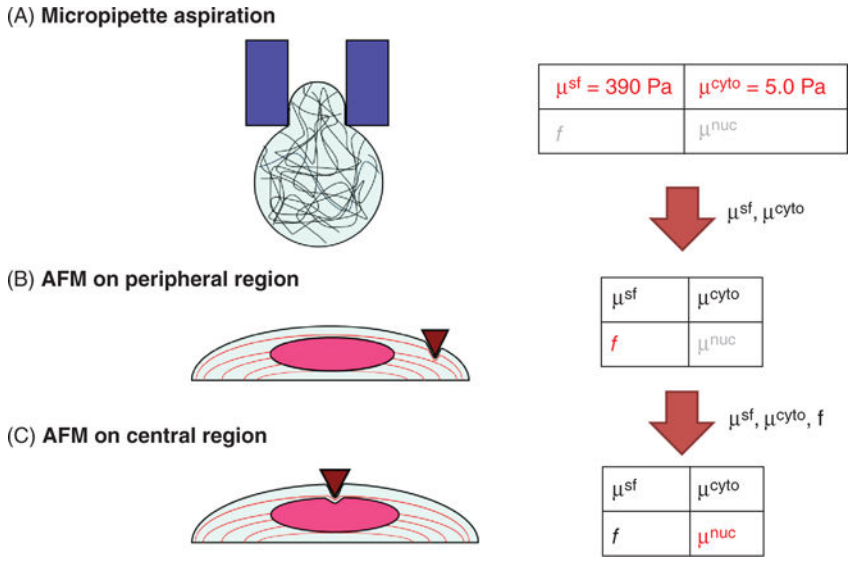

Figure 20.

The step-by-step calibration process. (A) The cytoskeletal shear modulus (μ_{cyto}) and α-SMA fiber shear modulus (μ_{sf}) were calibrated using the MA data for different types of VICs with different expression levels of α-SMA fibers. (B) Using the AFM indentation data on the cell peripheral regions, the fiber active contraction strength (*f*) was calibrated for AVICs and PVICs. (C) Using the AFM indentation data on the cell central region, the shear modulus of nucleus (μ_{nuc}) was calibrated for AVICs and PVICs. The parameters in red represents the ones that are being calibrated in the step, the parameters in gray represents the ones that are assumed not contribute to the mechanical response of the VICs (hence ignored) in the step, and the parameters in black represents the ones that are already calibrated from the previous steps and integrated into the model. Adapted, with permission, from Sakamoto et al. (221).

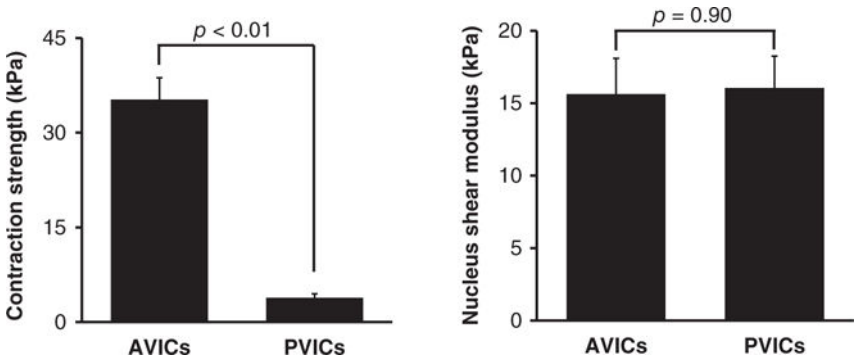

Figure 21.

(A) Contraction strength of the α-SMA fibers in the AVICs and PVICs. About 9:1 ratio in the contraction strength was observed from AVICs to PVICs. (B) Shear moduli of the AVICs and PVICs nuclei, which exhibited no differences. Adapted, with permission, from Sakamoto et al. (221).

Table 1

Abbreviations

AVV	Atrioventricular valve
SLV	Semilunar valve
MV	Mitral valve
TV	Tricuspid valve
AV	Aortic valve
PV	Pulmonary valve
ECM	Extracellular matrix
PGs	Proteoglycans
GAGs	Glycosaminoglycans
MMPs	Matrix metalloproteinases
TIMPs	Tissue inhibitor of matrix metalloproteinases
VIC	Valve interstitial cell
OFT	Outflow tract
EMT	Endothelial-mesenchymal transformation
TIC	Tachycardia-induced cardiomyopathy
MR	Mitral regurgitation
CAVD	Calcified aortic valve disease
AVSc	Aortic valve sclerosis
CAVS	Calcified aortic valve stenosis
CHF	Chronic heart failure
MI	Myocardial infarction
AS	Aortic valve stenosis
MA	Micropipette aspiration
SALS	Small angle light scattering
NOI	Normalized orientation index
HSP47	Heat shock protein 47
NAR	Nuclear aspect ratio
α-SMA	α-Smooth muscle actin
MVAL	Mitral valve anterior leaflet
MVPL	Mitral valve posterior leaflet
SMC	Smooth muscle cells
aVIC	Activated VIC
qVIC	Quiescent VIC
OPN	Osteopontin
ON	Osteonectin
RUNX2	Run-related transcription factor 2
OCN	Osteocalcin
ALP	Alkaline phosphatase
FN	Fibronectin
BMP	Bone morphogenic factor

MSM	Multiscale modeling
TEM	Transmission electron microscopy